

©Copyright 2007
Kenneth Hart Williford

Biogeochemistry of the Triassic–Jurassic Boundary

Kenneth Hart Williford

A dissertation submitted in partial fulfillment
of the requirements for the degree of

Doctor of Philosophy

University of Washington

2007

Program Authorized to Offer Degree: Department of Earth and Space Sciences

UMI Number: 3290618

Copyright 2007 by
Williford, Kenneth Hart

All rights reserved.

INFORMATION TO USERS

The quality of this reproduction is dependent upon the quality of the copy submitted. Broken or indistinct print, colored or poor quality illustrations and photographs, print bleed-through, substandard margins, and improper alignment can adversely affect reproduction.

In the unlikely event that the author did not send a complete manuscript and there are missing pages, these will be noted. Also, if unauthorized copyright material had to be removed, a note will indicate the deletion.

UMI[®]

UMI Microform 3290618

Copyright 2008 by ProQuest Information and Learning Company.

All rights reserved. This microform edition is protected against
unauthorized copying under Title 17, United States Code.

ProQuest Information and Learning Company
300 North Zeeb Road
P.O. Box 1346
Ann Arbor, MI 48106-1346

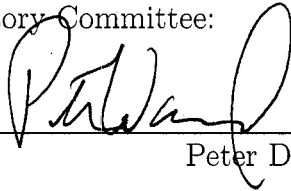
University of Washington
Graduate School

This is to certify that I have examined this copy of a doctoral dissertation by

Kenneth Hart Williford

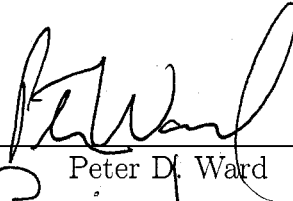
and have found that it is complete and satisfactory in all respects,
and that any and all revisions required by the final
examining committee have been made.

Chair of the Supervisory Committee:



Peter D. Ward

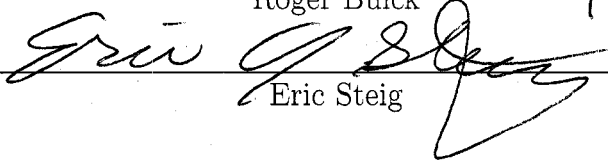
Reading Committee:



Peter D. Ward



Roger Buick



Eric Steig

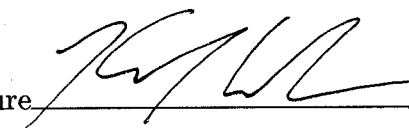
Date:

9/24/07

In presenting this dissertation in partial fulfillment of the requirements for the doctoral degree at the University of Washington, I agree that the Library shall make its copies freely available for inspection. I further agree that extensive copying of this dissertation is allowable only for scholarly purposes, consistent with "fair use" as prescribed in the U.S. Copyright Law. Requests for copying or reproduction of this dissertation may be referred to Proquest Information and Learning, 300 North Zeeb Road, Ann Arbor, MI 48106-1346, 1-800-521-0600, to whom the author has granted "the right to reproduce and sell (a) copies of the manuscript in microform and/or (b) printed copies of the manuscript made from microform."

Signature

Date

A handwritten signature in black ink, appearing to be 'J. W. L.', written over a horizontal line.

9/25/07

University of Washington

Abstract

Biogeochemistry of the Triassic–Jurassic Boundary

Kenneth Hart Williford

Chair of the Supervisory Committee:

Professor Peter D. Ward

Department of Biology, Department of Earth and Space Sciences

New lithologic, biostratigraphic, and stable organic carbon isotope data are presented from three Triassic–Jurassic (Tr–J) boundary sections in New Zealand and the Tr–J section at Kennecott Point, Queen Charlotte Islands (QCI), British Columbia, Canada. New stable stable organic and pyrite sulfur isotope and lipid biomarker data are presented from the QCI section.

The stable carbon isotope data from New Zealand are ambiguous, likely due to low organic matter content and variability in source, and these data alone do not significantly improve correlations with other Tr–J sections around the world. A rare Late Hettangian ammonite (*Eolytoceras tasekoi*) (Stevens, 2004) was discovered at the Marokopa Beach section, near the Tr–J boundary as defined by MacFarlan (1998), supporting the conclusion that the Otapirian–Aratauran stage boundary is above the Tr–J boundary as recognized internationally.

An extended record of $\delta^{13}\text{C}_{org}$ from the QCI section shows a long term trend of isotopic lightening attributed to an increase in atmospheric CO_2 due to volcanism associated with the opening of the Atlantic Ocean, including the Central Atlantic Magmatic Province. This trend is interrupted by a negative excursion of 2‰ (Ward

et al., 2001, 2004) and a newly discovered 5‰ positive excursion. A record of stable organic and pyrite sulfur isotopes ($\delta^{34}\text{S}_{org+pyrite}$) from this section shows a large positive excursion coincident with the excursion in carbon. $\delta^{34}\text{S}_{org+pyrite}$ values shift from -30‰ to 20‰ over 3 m of section, suggesting that isotopic fractionation associated with bacterial sulfate reduction (BSR) was reduced or eliminated due to a rapid drawdown of seawater sulfate, perhaps via increased BSR or increased evaporite flux.

A record of lipid biomarkers from the QCI section shows that organic material is of low to moderate thermal maturity and highly biodegraded. Abundant C₂₉ steranes are indicative of a significant terrigenous component. Samples from strata containing the positive excursion in $\delta^{13}\text{C}_{org}$ and $\delta^{34}\text{S}_{org+pyrite}$ are much less biodegraded and contain few hopanes and steranes but abundant *n*-alkanes with a clear odd over even predominance. There is a spike in hopane abundance just before the Tr–J boundary, coincident with the negative excursion in $\delta^{13}\text{C}_{org}$ and a major radiolarian extinction (Carter and Hori, 2005). This could represent a decline in net primary production as bacterial heterotrophy outstripped primary productivity in the wake of the Tr–J event, contributing to the negative excursion in $\delta^{13}\text{C}_{org}$.

These findings demonstrate that the Tr–J mass extinction was accompanied by perturbations in carbon and sulfur cycling, and a microbial response to boundary events is also evident. Processes associated with the early rifting of the Pangean supercontinent, including sea level change, evaporite deposition and Central Atlantic Magmatic Province volcanism, are the most likely primary causes for the global biogeochemical perturbations, and volcanically induced warming remains the most likely cause for the Tr–J extinctions.

TABLE OF CONTENTS

	Page
List of Figures	iv
List of Tables	vi
Chapter 1: Introduction	1
1.1 Motivation	1
1.2 Driving questions	4
1.3 Mass extinctions	5
1.3.1 The Late Ordovician	7
1.3.2 The Late Devonian	8
1.3.3 The Permian–Triassic boundary	9
1.4 The Triassic–Jurassic boundary	10
1.4.1 The Cretaceous–Paleogene boundary	14
1.5 Stable isotopes and mass extinctions	15
1.6 Biomarkers and mass extinctions	17
1.6.1 Permian–Triassic biomarkers	18
1.6.2 Cretaceous–Tertiary biomarkers	18
1.6.3 Biomarkers and methane	19
1.7 Key Tr–J boundary sections	19
1.7.1 North America	20
1.7.2 Europe	22
1.7.3 New Zealand	22
1.8 Structure of the dissertation	23

Chapter 2:	Records of stable organic carbon isotopes from three Triassic–Jurassic boundary sections in New Zealand	25
2.1	Introduction	25
2.2	Methods	28
2.3	Results	29
2.3.1	Nugget Point	29
2.3.2	Awakino River	35
2.3.3	Marokopa Beach	39
2.4	Discussion and Implications for Global Correlation	43
2.5	Acknowledgements	48
Chapter 3:	An extended organic carbon-isotope record across the Triassic/Jurassic boundary in the Queen Charlotte Islands, British Columbia, Canada	49
3.1	Introduction	49
3.2	Materials and Methods	50
3.3	Results	52
3.4	Discussion	52
3.5	Relationship of the new results to the causes of the Late Triassic extinctions	55
3.6	Acknowledgements	58
Chapter 4:	A record of sulfide and organic sulfur isotopes across the Triassic–Jurassic boundary in the Queen Charlotte Islands, British Columbia, Canada	60
4.1	Introduction	60
4.2	Materials and Methods	63
4.3	Results	65
4.4	Discussion	69
4.4.1	Isotopic composition of Triassic–Jurassic seawater sulfate	71
4.4.2	Triassic–Jurassic rifting and evaporite deposition	74
4.4.3	Mass balance calculations	74
4.5	Conclusions	75

4.6	Acknowledgements	76
Chapter 5:	Organic geochemistry of a Triassic–Jurassic boundary section in the Queen Charlotte Islands, British Columbia, Canada	77
5.1	Introduction	77
5.2	Materials and Methods	79
5.3	Results	81
5.3.1	Source Integrity	82
5.3.2	Aliphatic Fractions	84
5.3.3	<i>n</i> -alkanes and acyclic isoprenoids	84
5.3.4	Hopanoids	87
5.3.5	Steranes	91
5.3.6	Aromatic Fractions	93
5.3.7	Phenanthrene and alkyl phenanthrenes	93
5.4	Discussion	93
5.4.1	Maturity	93
5.4.2	Source Indicators	93
5.5	Conclusions	103
5.6	Acknowledgements	104
Chapter 6:	Conclusions	105
6.1	Implications for the Triassic–Jurassic boundary record	105
6.1.1	Causes and consequences of Tr–J boundary events	105
6.1.2	CAMP	106
6.1.3	Triassic–Jurassic carbon and sulfur cycling	107
6.2	General implications for mass extinctions	108
6.3	Implications for planetary habitability and Astrobiology	110
	Bibliography	113
Appendix A:	Summary of $\delta^{13}\text{C}_{org}$ data for Kennecott Point section	137
Appendix B:	Summary of $\delta^{34}\text{S}_{org+pyrite}$ data for Kennecott Point section	146

LIST OF FIGURES

Figure Number	Page
1.1 Publication frequency on the “big five” mass extinctions	2
2.1 Late Triassic-Early Jurassic interval of the New Zealand Geological Timescale	26
2.2 Overview map showing New Zealand study areas	27
2.3 Nugget Point study area detail	30
2.4 Nugget Point section from above	31
2.5 Nugget Point boundary section, looking west	32
2.6 Stack just offshore from Nugget Point section, looking east	33
2.7 <i>Macrogrammites grammicus</i> in a float boulder at fossil locality 640 of Speden and McKellar (1958)	34
2.8 <i>Otapiria sp.</i> from top of Nugget Point section	35
2.9 $\delta^{13}\text{C}_{org}$ record for Tr–J boundary strata in an unnamed bay near Nugget Point, New Zealand	36
2.10 Awakino River study area detail	37
2.11 Tr–J section at Awakino River, looking south	38
2.12 $\delta^{13}\text{C}_{org}$ record for the Awakino River Otapirian–Aratauran boundary section	40
2.13 Marokopa Beach study area detail	41
2.14 Marokopa Beach section	42
2.15 <i>Eolytoceras tasekoi</i> recovered from Marokopa Beach section	43
2.16 $\delta^{13}\text{C}_{org}$ record for the Marokopa Beach Tr–J boundary section	44
2.17 $\delta^{13}\text{C}_{org}$ record for Otapirian–Aratauran boundary sections at Marokopa Beach, Awakino Gorge, and Nugget Point, New Zealand	46
3.1 $\delta^{13}\text{C}_{org}$ record for Norian to Sinemurian strata on Kennecott Point, Queen Charlotte Islands, British Columbia, Canada.	53

3.2	Stable organic carbon isotope data from Kennecott Point showing the results of least-squares regressions on the Rhaetian and Hettangian intervals	56
3.3	Comparison of $\delta^{13}\text{C}_{org}$ entire record from Muller Canyon and partial record from Kennecott Point	59
4.1	$\delta^{13}\text{C}_{org}$ and $\delta^{34}\text{S}_{org+pyrite}$ record for Norian to Sinemurian strata on Kennecott Point, Queen Charlotte Islands, British Columbia, Canada.	66
4.2	$\delta^{34}\text{S}_{org+pyrite}$ and weight percent sulfur for Norian to Sinemurian strata	69
4.3	TOC vs. weight percent sulfur	70
5.1	Aliphatic fraction total ion chromatograms for all samples	85
5.2	m/z 57 fragmentogram from sample QCIJ 99.5, showing alkanes and acyclic isoprenoids	86
5.3	m/z 57 fragmentogram from sample QCI99 27.3	87
5.4	m/z 57 chromatograms from all samples	88
5.5	m/z 191 fragmentogram from sample QCI99 27.3, showing hopanoids	89
5.6	m/z 191 chromatograms from all samples	90
5.7	m/z 217 fragmentogram from latest Rhaetian sample QCI99 27.3, showing steranes	91
5.8	m/z 217 chromatograms from all samples	92
5.9	Aromatic fraction total ion chromatograms from all samples	94
5.10	m/z 178, 192, 206, 220, and 234 from sample QCIJ 99.5 showing phenanthrenes	95
5.11	Pr/ n -C ₁₇ vs. Ph/ n -C ₁₈	97
5.12	Ternary diagram showing the relative distributions of regular C ₂₇ , C ₂₈ , and C ₂₉ steranes	98
5.13	Bulk $\delta^{13}\text{C}_{org}$, Pr/Ph, and H30:nC ₂₉ across the Tr-J boundary	99
5.14	Total amount of nC ₂₂ to nC ₂₇ alkanes and C ₃₀ hopanes in Rhaetian to Sinemurian samples	101
5.15	Total amount of nC ₂₂ to nC ₂₇ alkanes and C ₃₀ hopanes in Rhaetian to Sinemurian samples	102

LIST OF TABLES

Table Number	Page
4.1 Statistical distribution of stable sulfur isotope data	67
5.1 Summary of organic geochemical data	83
5.2 $\delta^{13}\text{C}$ of bulk organic matter, kerogen, and bitumen	84
A.1 Summary of $\delta^{13}\text{C}_{org}$ data for Kennecott Point section	137
B.1 Summary of $\delta^{34}\text{S}_{org+pyrite}$ data for Kennecott Point section	147

ACKNOWLEDGMENTS

The author wishes to express sincere appreciation to the following individuals: Peter Ward, Roger Buick, Eric Steig, Anitra Ingalls, Geoff Garrison, Jack Grant-Mackie, Hamish Campbell, Stuart Wakeham, Julian Sachs, Julien Foriel, Valerie Schwab, Jack Grant-Mackie, Hamish Campbell, Mike Orchard, Jean Paul Zonneveld, Kliti Grice, Rienk Smittenberg, Hugh Willa, Gwenna Smith, Loren Ballanti, Brett Sundloff, David Huber, and Scobie Puchtler.

DEDICATION

To Dee, Hart, Katie, and Raga, with love.

Chapter 1

INTRODUCTION

1.1 Motivation

The Triassic Period, from 251.0 ± 0.4 (Gradstein *et al.*, 2004; Bowring *et al.*, 1998) to 199.6 ± 0.3 (Gradstein *et al.*, 2004; Pálffy *et al.*, 2000) million years ago, is bounded by major mass extinctions (Raup and Sepkoski, 1982). The Permian–Triassic extinction was the most catastrophic of the Phanerozoic mass extinctions, eliminating over 90% of marine species and 70% of terrestrial vertebrate families (Erwin, 1994). Species level biodiversity was reduced by three quarters during the Late Triassic (Jablonski, 1991), but the Tr–J mass extinction has received relatively little attention. Fig. 1.1 shows the results of five searches of the GeoRef database for which the term “mass extinction*” was combined with each of the following: “ordovician,” “devonian,” “permian AND triassic,” “triassic AND jurassic,” and “cretaceous AND tertiary.” The number of peer-reviewed journal articles returned for each search is shown, and the results suggest that the Tr–J mass extinction is the least studied of the “big five.”

This study of mass extinctions has focused on the biostratigraphic record of the readily collectible and identifiable fossils of marine invertebrate animals with mineral skeletons (e.g. Raup and Sepkoski, 1982), as these organisms are common enough to make paleoecological studies feasible, and far more likely than other groups to be rapidly buried and thus preserved as fossils (Clarkson, 1996). Marine invertebrates do not tell the full story, however. Advances in micropaleontology and stable isotope

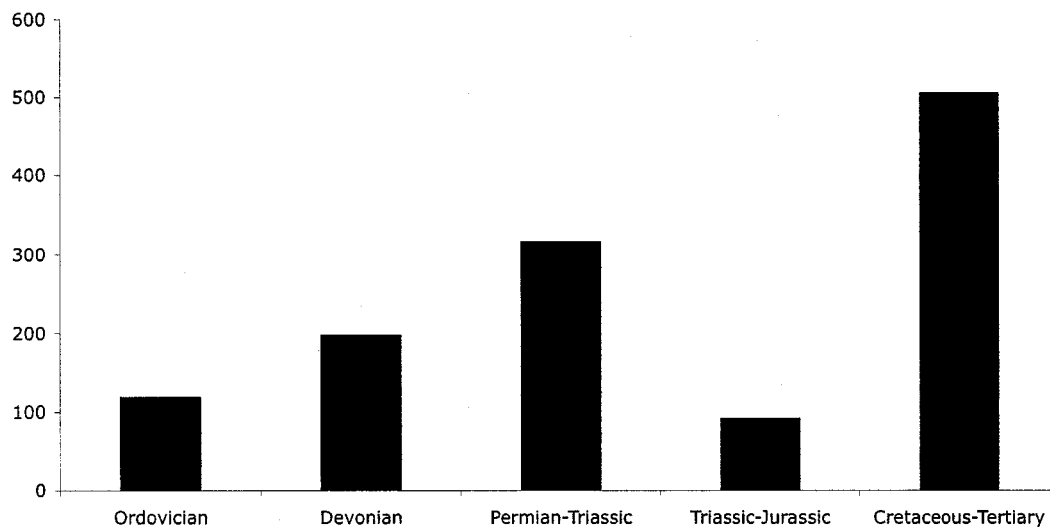


Figure 1.1: Publication frequency on the “big five” mass extinctions. Number of peer-reviewed journal articles returned from five searches of the GeoRef database using the terms “mass extinction*” (in every search) AND “ordovician,” “devonian,” “permian AND triassic,” “triassic AND jurassic,” and “cretaceous AND tertiary” (in individual searches) are shown.

geochemistry increased the resolution with which mass extinction intervals could be examined and began to address questions about the relationship of biogeochemical cycling to mass extinction (e.g. Romein and J., 1981; D’Hondt *et al.*, 1998). More recently, it has become possible to further increase the resolution by using records of molecular fossils, or biomarkers, to focus the lens of inquiry on microbial communities (e.g. Grice *et al.*, 2005; Xie *et al.*, 2005). Bacteria and archaea are the dominant organisms on Earth in terms of numbers, biomass, and genetic diversity (Whitman *et al.*, 1998), and together with the unicellular eukarya (e.g. Lovelock *et al.*, 1972), these organisms provide the primary controls on the global biogeochemical cycles of the planet (Pace, 1997). The record of microbial communities in ancient Earth envi-

ronments is thus a powerful window into the most fundamental connections between the living and nonliving Earth during times of great environmental change.

Understanding the response and relationship of planetary ecosystems to extreme environmental change is vital to Astrobiology: the study of the origin, distribution and future of life in the Universe. The first life on Earth was microbial, Earth life remained microbial for most of its history, and most existing life on this planet is microbial (Pace, 1997). Compared to multicellular organisms, the vastly expanded range of environmental tolerance and metabolic diversity known for microbes on Earth (e.g. Alpert, 2006) makes it likely that most past, present and future life in the Universe was, is and will be microbial. Indeed, the statistically improbable set of planetary, orbital, and even galactic circumstances necessary to support complex, multicellular life on Earth implies that such life is rare in the Universe (Ward and Brownlee, 2000). For these reasons, the study of microbial life on Earth will be a primary driver in the search for evidence of life elsewhere in the Universe. Some of our best tools for finding evidence of life on other planets will be those that we use to reveal the nature and history of life in deep time on our own planet.

The study of mass extinctions has important implications for the welfare of the human species because we depend on stable ecosystems to produce food, provide renewable resources and assimilate waste. Human communities over the last several thousand (and especially the last 200) years have wrought environmental change with a magnitude and pace rarely seen in the last several million years (e.g. Houghton *et al.*, 2001; Crutzen, 2003). Human hunting, agriculture and industry have changed the face of the planet to such a degree that some have considered erecting a new epoch in the history of the planet called the Anthropocene (Crutzen, 2005). In fact, we may be in the midst of what some have called “the sixth extinction” (e.g. Leakey and Lewin, 1996), beginning with the eradication of mammalian megafaunas in the Pleistocene

(Martin and Wright, 1967). The implications of such a scenario for human communities in the near and distant future are uncertain, but inasmuch as they provide insight into the behavior of planetary systems in perturbation, the biogeochemical records of the past are among the most powerful predictive tools we have at our disposal.

1.2 *Driving questions*

1. What were the magnitude and duration of perturbations to the global carbon cycle across the Triassic–Jurassic (Tr–J) boundary as revealed by stable isotopes, and when did they occur in relation to biotic changes?

This question was the fundamental driver for this research effort. As is so often the case, results obtained in search of answers raised further questions and suggested new methods of inquiry. Some of the questions that arose along the way, and which inspired the final two chapters of this work, are listed below:

2. What were the magnitude and duration of perturbations to the global sulfur cycle across the Tr–J boundary, and when did they occur in relation to biotic changes?
3. Are the latest Triassic negative excursion and/or the earliest Jurassic positive excursion in bulk $\delta^{13}\text{C}_{org}$ related to a change in microbial ecology?
4. Is the earliest Jurassic positive excursion in bulk $\delta^{13}\text{C}_{org}$ related to changes in the relative input of terrestrial and marine organic matter to marine sediments?

There has been little to no work published to date that addresses these final three questions for the Tr–J boundary. The rest of this introductory chapter is focused on previous work that has sought to address similar questions for other intervals of Earth history.

1.3 Mass extinctions

Molecular fossils of indisputably biological origin occurring in Western Australian shales extend the record of microbial life on Earth to at least 2.7 Ga (Brocks *et al.*, 1999). There is other, less certain evidence for microbial life on Earth that extends the record far further. The c. 3.5 Ga stromatolites of the Warrawoona Group in Western Australia are the oldest putative fossils on the planet (Schopf, 2006), but their biogenicity is disputed (Brasier *et al.*, 2006). Carbon isotope ratios in graphite from the Isua supracrustal belt in West Greenland offer possible evidence for life in the oldest sedimentary rocks on Earth (Mojzsis *et al.*, 1996), though this interpretation is controversial and uncertain (Fedó *et al.*, 2006).

While the Phanerozoic Eon represents only about twelve percent of Earth history, it is only this most recent interval that contains the rich and accessible record of fossilized multicellular organisms such as animals and plants. Of these multicellular organisms, the most likely to fossilize are marine animals that build mineral skeletons, as organisms without hard parts, especially those above sea level, are more likely to disintegrate and decay prior to burial and preservation (Clarkson, 1996).

The initial recognition of a stratigraphic order to sedimentary rocks on Earth was dependent upon the macrofossil record of origination and extinction of species (Smith, 1816, 1835). The establishment of a geologic timescale was made possible by the recognition that patterns of origination and extinction can be reliably documented across the globe (Lyell, 1830). These principles were first formalized by English geologist William Smith (1769–1839), and it was his nephew John Phillips (1800–1874) who divided the Phanerozoic Eon into its three Eras based upon what early geologist had recognized as the two intervals of greatest fossil turnover (Phillips, 1840a,b, 1841), now known as the Permian–Triassic and Cretaceous–Tertiary boundaries. Not until 120 years later did the term “mass extinction” began to enter common pale-

ontological parlance (e.g. Nicol, 1961; Newell, 1962) as a way to describe these and other outstanding intervals of change in the fossil record.

Raup and Sepkoski (1982) used Sepkoski's database of Phanerozoic marine invertebrate diversity to investigate extinction rates for each of 76 Phanerozoic stages, finding that "background" extinction rates clustered around a generally decreasing linear trend at less than 8 families extinct per million years. "Mass" extinction rates exceeded this measure, ranging from 10 families per million years at the end of the Frasnian (Late Devonian) to 19.3 families per million years at the end of the Ashgillian (Late Ordovician). Four stages exceeded the 99% confidence interval for a linear regression performed on all 76 stages, and were identified as highly significant: Ashgillian (end-Ordovician), Guadalupian and Dzulfian (Late Permian), and Maestrichtian (end-Cretaceous). The extinction rate for the Norian stage (Late Triassic) was significant at the 95% confidence level. The Givetian, Frasnian, and Fennanian stages (Late Devonian) all had extinction rates that exceeded background values, but were not statistically significant at the 95% confidence level; the authors suggested that the Late Devonian may represent a protracted mass extinction event. Raup and Sepkoski (1982) thus identified five mass extinctions in the marine fossil record: end-Ordovician, Late Devonian, end-Permian, Late Triassic, and end-Cretaceous. These intervals became known as the "big five" mass extinctions, and an entire subdiscipline of paleontology was set into motion to study the dynamics of mass extinction (Bambach, 2006).

Jablonski (1991) computed extinction intensities at the genus and species level for the marine fossil record of the Phanerozoic and found that seven events resulted in over 50% species loss: the "big five" events, as well as the Cenomanian (Middle Cretaceous) and the Pliensbachian (Early Jurassic). Using updated genus diversity data and a statistical approach sensitive to time, origination rate, and extinction rate, Bambach

et al. (2004) undertook a critical analysis of the mass extinction concept from first principles, finding that only the end-Ordovician, end-Permian, and end-Cretaceous events stood apart as being driven primarily by elevated extinction rates, and labelling other events historically considered mass extinctions as “mass depletions.”

The aim of this work is to explore the interaction of living and nonliving systems during an interval of profound global change, not to weigh in on the debate about which events should and should not be considered “mass extinctions.” As such, a liberal interpretation of the term is applied. For the purposes of this study a mass extinction is defined as an interval of time of a few million years or less during which apparent global biodiversity at the species level is reduced by more than half. Each of the “big five” events meets these criteria, and the causes and consequences of these events are briefly discussed below.

1.3.1 *The Late Ordovician*

The Late Ordovician event was the first major mass extinction of the Phanerozoic Eon (Raup and Sepkoski, 1982). These extinctions eliminated 85% of marine species (Jablonski, 1991), but seems to have had little macroecological consequence, as post-extinction faunas were highly similar to preextinction faunas (Bottjer *et al.*, 2001). The event occurred in two pulses (Sheehan, 2001), corresponding to the beginning and the end of glaciation in the final stage of the Ordovician, the Hirnantian, dated from 445.6 ± 1.5 to 443.7 ± 1.5 Ma (Gradstein *et al.*, 2004). Given that the Ordovician is thought to have been a time of high atmospheric CO₂ (7 to 17 × present atmospheric level) (Berner, 2006), glaciation during this period seems paradoxical. Brenchley *et al.* (1994) demonstrate that the glaciation was shortlived (< 0.5 million years), and they offer support for the energy balance model-based interpretation advanced by Crowley and Baum (1991) that glaciation was made possible by the poleward migration

of Gondwanaland at this time. Brenchley *et al.* (1994) also report oxygen isotopic evidence for 10°C global cooling and offer a mechanism involving changes to oceanic circulation leading to upwelling, a productivity spike, and temporary drawdown of atmospheric CO₂.

1.3.2 *The Late Devonian*

There are multiple extinction events over the course of the Devonian, but the largest occurred at Frasnian–Famennian boundary (McGhee, 1996), dated at 374.5 ± 2.6 Ma (Gradstein *et al.*, 2004). This extinction is also known as the “Kellwasser Event,” after the so called “Kellwasser horizons,” two Late Frasnian units of dark, organic rich rock that occur across Europe and the Americas (Buggisch, 1991). Joachimski and Buggisch (1993) report positive excursions in stable carbon isotopes correlating with the Kellwasser horizons, which they interpret as evidence for an increase in organic carbon burial due to global transgression and anoxia, and they favor the climatic change that resulted as the primary extinction mechanism. Pujol *et al.* (2006) offer support for this scenario based upon their analyses of metals, P₂O₅ and Ba, and C_{org} in several European F–F sections, suggesting that volcanically driven eustatic sea level change along with eutrophication and toxicity due to high nutrient and metal inputs during Kellwasser events were responsible for the extinctions. Interestingly, George and Chow (2002) find no evidence of anoxia associated with F–F extinctions in the Canning Basin of Western Australia, where stromatoporoid reefs give way to microbial, stromatolitic bioherms; instead the authors implicate tectonically driven sea level fluctuations and an increased input of siliclastic debris. Another extinction mechanism that has been proposed is eutrophication of the oceans due to the rise of rooted land plants and the increased erosional export of nutrients from the continents (Algeo *et al.*, 1995). An estimated 82% of marine species were eliminated in the Late

Devonian (Jablonski, 1991).

1.3.3 *The Permian–Triassic boundary*

The largest mass extinction of the Phanerozoic occurred at the boundary between the Permian and Triassic (P–T) periods and eliminated over 90% of Earth’s species (Benton and Twitchett, 2003). The most commonly cited date for the boundary is 251.0 ± 0.4 Ma, based on U/Pb zircon geochronology combined with bio- and chemostratigraphic controls (Gradstein *et al.*, 2004; Bowring *et al.*, 1998). A more recent study using the U/Pb system and taking into account the effects of postdepositional Pb loss assigns an age of 252.6 ± 0.2 Ma (Mundil *et al.*, 2004). Becker *et al.* (2004) summarize evidence for bolide impact at the P–T boundary and suggest that the Bedout High, a submarine structure off the coast of northwest Australia, is a remnant of the impact crater. The evidence offered by Becker *et al.* (2004) is widely criticized (Farley and Mukhopadhyay, 2001; Wignall *et al.*, 2004; Renne *et al.*, 2004), however, and the kind of unambiguous, globally distributed evidence for impact that exists at the K–Pg boundary has not been discovered at the P–T boundary (Twitchett, 2006).

The biostratigraphic and biogeochemical record across the P–T boundary suggests instead that the extinction mechanism was “intrinsic,” or related solely to changes in the Earth system (Ward *et al.*, 2005; Huey and Ward, 2005). Historically, the P–T extinction was thought to be the result of declining numbers of marine provinces due to the final assemblage of the Pangaeon supercontinent in the Permian (Valentine and Moores, 1970), though this explanation alone cannot account for the magnitude of the extinction (Erwin, 1993). There is widespread evidence for anoxia during the P–T transition, with many marine sections changing from bioturbated to laminated at the boundary, and this has been implicated in the extinction (Wignall and Hallam, 1992).

Stable isotope evidence make it clear that there was an extended interval of carbon cycle perturbation at the P–T boundary (Payne *et al.*, 2004). An estimated 2 to 3 $\times 10^6$ km³ of basalt were erupted in the Siberian Traps coincident with the P–T boundary (Renne *et al.*, 1995), releasing from 2000 to 13000 Gt CO₂ (Berner, 2002). Such a large increase in atmospheric CO₂ would have been accompanied by an increase in global temperatures. Kidder and Worsley (2004) find evidence for and discuss the catastrophic implications of a 15°C average rise in global temperatures across the P–T transition based on earlier studies of Permian pollen (Taylor *et al.*, 1992) and Triassic paleosols (Retallack, 1999).

1.4 The Triassic–Jurassic boundary

Another of the big five mass extinctions, and the subject of the work presented here, occurred roughly 200 million years ago at the Triassic–Jurassic boundary. The Tr–J extinction was equivalent in magnitude to the K–T extinction, as over 70% of marine invertebrate species were lost (Raup and Sepkoski, 1982). The Tr–J extinction has received less attention than other mass extinctions primarily due to the relative lack of exposed, continuous and accessible sections (Hallam and Wignall, 2000). One recent study has suggested that the Tr–J event was a “mass depletion” rather than a mass extinction, claiming that low levels of speciation were more important than high levels of extinction during this event (Bambach *et al.*, 2004). These data still indicate, however, that the Tr–J boundary represents one of the five intervals of greatest biodiversity loss in the Phanerozoic. The currently accepted date for the Tr–J boundary is 199.6 ± 0.3 Ma, based on U/Pb from zircons in a volcanic ash deposited 5 meters below the radiolarian extinction in the Queen Charlotte Islands (Pálfy *et al.*, 2000). The same work suggests that extinctions on land may have preceded the marine extinctions. There are also major extinctions at the Norian–

Rhaetian boundary, the stage boundary immediately preceding the Tr–J boundary (Rhaetian–Hettangian), and 41% of all meso- and macrobenthic genera crossing the Norian–Rhaetian are extinct by the Hettangian (Kiessling *et al.*, 2007). Recent studies suggest that the Rhaetian and Hettangian stages each represent close to 2 million years (Gallet *et al.*, 2003; Mundil and Palfy, 2005), and it has been suggested that the Tr–J mass extinction is actually a protracted event that encompasses the entire Rhaetian (Hallam, 2002).

There is considerable debate about the effect of the Tr–J event on different groups of organisms. Leaf fossil collections indicate that there was a 95% turnover in terrestrial megafloora across the Tr–J boundary (McElwain *et al.*, 1999). The effect of the Tr–J event on the terrestrial vertebrates is controversial; some studies suggest that up to 11 families went extinct (Benton, 1993), though others find no evidence of significant terrestrial tetrapod extinctions (Cuny, 1996). Marine reptiles suffered minor extinctions (Benton, 1993), while fish were apparently unaffected (McCune and Schaeffer, 1986).

The records of marine invertebrate extinctions and microfossils across the Tr–J boundary are also uncertain. The Tr–J boundary has traditionally been defined on the basis of ammonite turnover, and the interpretations of this turnover are varied. Some claim that only one ammonite genus survived across the Tr–J boundary (Hallam, 1981), but there is evidence that the greatest ammonite extinctions took place at the Norian–Rhaetian rather than the Tr–J boundary (Teichert, 1988). Bivalves suffer a greater than 90% extinction from the Norian to the Hettangian (Hallam, 1981), but this figure must be viewed in the context of a Norian stage that lasts several million years. 17 families of brachiopods go extinct at the Tr–J boundary (Harper *et al.*, 1993). There is a comprehensive extinction among radiolaria at the Tr–J boundary in the Queen Charlotte Islands and Inuyama, Japan (Carter and Hori,

2005), but collections from other localities have led some to suggest that these may have been local events (Kidder and Erwin, 2001). 3 of 17 families of foraminifera go extinct at the Tr–J boundary (Hart and Williams, 1993). It was long thought that the conodonts were completely extinct by the Hettangian, with the most extreme extinction occurring at the Norian-Rhaetian boundary (Aldridge and Smith, 1993). Recently, however, rare individuals have been reported from the earliest Hettangian (e.g. Pálffy *et al.*, 2007). The preliminary GC-MS results shown here (Fig. 5.1) represent the only known record of changes in microbial ecology across the Tr–J boundary.

Several extinction mechanisms have been proposed for the Tr–J (Tanner *et al.*, 2004), and it is likely that some or all of the proposed mechanisms had significant effects on the late Triassic biosphere. Multiple Tr–J boundary sections show evidence for marine regression followed by transgression across the boundary, and this sea level change has been implicated in the extinctions (Newell, 1967; Barattolo and Romano, 2005). There is an isolated iridium anomaly near the Tr–J boundary in the Newark Supergroup of eastern North America that has been interpreted as evidence for a bolide impact (Olsen *et al.*, 2002), but converging lines of globally distributed evidence for impact are lacking. The 100 km diameter Manicouagan crater in northern Canada has been dated at 214 ± 1 Ma (Hodych and Dunning, 1992), and this impact may have contributed to a degraded Rhaetian environment without acting as a catastrophic Tr–J boundary kill mechanism.

The largest known flood basalt eruption in Earth history in terms of aerial extent, the Central Atlantic Magmatic Province (CAMP), was coincident with the Tr–J boundary (Marzoli *et al.*, 1999, 2004). Flood basalt eruptions appear to have played a part in the P–T and K–T extinctions, and CAMP must have had a significant impact on the Tr–J biosphere as well (White and Saunders, 2005). A study of stomatal in-

dices from fossil *Ginkgo* leaves across the Tr–J points to an atmospheric CO₂ increase of 600 to 2400 ppm, attributed to the increased volcanism (McElwain *et al.*, 1999).

So far, excursions in bulk $\delta^{13}\text{C}$ coincident with the Tr–J boundary have been discovered from Tr–J boundary sections in British Columbia (Ward *et al.*, 2001, 2004; Williford *et al.*, 2007) (Fig. 3.1), Hungary (Pálffy *et al.*, 2001), England (Hesselbo *et al.*, 2002), Nevada (Guex *et al.*, 2004; Ward *et al.*, 2007), Italy (Galli *et al.*, 2005), and New Zealand (this study). The isotope records from British Columbia and Nevada show an intriguing similarity (Williford *et al.*, 2007) (Fig. 3.3), with a negative excursion at the boundary followed by a positive excursion in the earliest Hettangian.

Pálffy *et al.* (2001) proposed that warming due to CAMP-driven atmospheric CO₂ increase along with depressurization due to marine regression could have caused destabilization of seafloor methane hydrates (clathrates), leading to runaway greenhouse conditions, a scenario proposed by Dickens *et al.* (1995) to explain the -3‰ excursion in $\delta^{13}\text{C}$ during the Late Paleocene. Clathrate destabilization has become a common explanation for negative excursions in $\delta^{13}\text{C}$, as the characteristic isotopic composition of methane is so light (\sim -65‰) that the introduction of a relatively small quantity can have a large effect on the isotopic composition of the atmosphere in comparison to volcanogenic (-5‰) or heterotrophically respired (\sim -28‰) CO₂ (e.g. Dickens *et al.*, 1995). This hypothesis has its weaknesses, however. Clathrates form on continental slopes under a limited range of temperatures and pressures that define the “Gas Hydrate Stability Zone” (Milkov, 2004). At higher temperatures and lower sea level, the Gas Hydrate Stability Zone is smaller (e.g. Milkov and Sassen, 2003). Due to the existence of the supercontinent Pangea, continental slope length was significantly less than it is under today’s distributed continental configuration (Golonka, 2007). This would suggest that the global volume of the Gas Hydrate Stability Zone, and by extension, the total methane hydrate reservoir, was smaller in the Triassic than

in modern times. A recent study constrained by DSDP/ODP drilling data estimated the modern gas hydrate reservoir at 500 to 2500 Gt methane (Milkov, 2004). Dickens *et al.* (1995) finds that 1600 to 2000 Gt methane would be required to cause a -2‰ excursion in $\delta^{13}\text{C}$. The discovery of an increase in isotopically depleted biomarkers for methane oxidizing bacteria or archaea (e.g. pentamethylcosane) associated with the negative excursions in bulk $\delta^{13}\text{C}$ would provide supporting evidence for the clathrate destabilization hypothesis.

The extended record of $\delta^{13}\text{C}_{org}$ from Kennecott Point shown by Williford *et al.* (2007) reveals a negative offset in bulk carbon isotope values during the boundary interval as well as a statistically significant long-term negative trend in isotope values during the Hettangian (Fig. 3.2). The authors attribute these features to the gradual addition (over the course of 2 million years or more) of moderately light CO_2 from volcanism associated with the opening of the Atlantic basin, including CAMP.

1.4.1 *The Cretaceous–Paleogene boundary*

The most infamous mass extinction, known as the Cretaceous–Paleogene (K–Pg) (formerly as the Cretaceous–Tertiary), occurred 65.5 ± 0.3 million years ago (Gradstein *et al.*, 2004; Sharpton *et al.*, 1992; Swisher *et al.*, 1992) and led to the elimination of 75% of marine species (Jablonski, 1991) and 100 continental families (Benton, 1995). The story that has emerged over the last several decades to explain the K–Pg extinction implicates an asteroid or comet that impacted the Earth (Alvarez *et al.*, 1980), leaving behind the Chicxulub crater, ~ 180 km in diameter (Hildebrand *et al.*, 1991). Dust and ash ejecta from this impact event likely filled the atmosphere and reduced solar irradiance, leading to a precipitous decline in primary productivity (Alvarez *et al.*, 1980; Hsü and McKenzie, 1985). Abnormally low stomatal indices from fern leaves deposited at the K–Pg boundary in Colorado suggest an increase in atmo-

spheric CO₂ from around 350 ppm to >2300 ppm (Beerling *et al.*, 2002). Assuming the increase was real, Beerling *et al.* (2002) attribute it to the generation of at least 6400 Gt CO₂ as the boundary impactor struck carbonate rocks on the continental shelf, and they find that such an event would have led to 10-12°C of global warming.

An intriguing factor that unites the last three of the big five Phanerozoic mass extinctions is that they occur in close temporal association with large flood basalt provinces (White and Saunders, 2005). Flood basalts were emplaced in the Deccan Traps of India during the K–Pg transition (Courtilot *et al.*, 1986) and would have contributed to the increase in atmospheric CO₂, though Beerling *et al.* (2002) suggest this input was greatly exceeded by that of the bolide impact.

Keller (2003, 2005) argues based upon her reading of the micropaleontological and geochronological evidence that the Chicxulub crater predates the K–Pg boundary by c. 300 kyr and is associated, along with episodes of intense Deccan volcanism, with environmental stress but no major extinctions. This view is refuted by Arenillas *et al.* (2006), who find that earliest Paleogene foraminiferal assemblages appear in direct stratigraphic association with material that they interpret as Chicxulub impact ejecta. This controversy raises an important question, however, about whether impacts and their downstream effects alone are sufficient to cause mass extinctions, or whether they can only act as one of a series of synergistic extinction mechanisms (e.g. Keller, 2003; Twitchett, 2006).

1.5 Stable isotopes and mass extinctions

The application of stable isotope geochemistry to intervals of mass extinction was part of the increasing interest in these events in the wake of the Alvarez *et al.* (1980) impact hypothesis (e.g. Keith, 1982; Margolis *et al.*, 1985; Orth *et al.*, 1986; McGhee *et al.*, 1986; Holser and Magaritz, 1987; Geldsetzer *et al.*, 1987). Keith (1982) used stable

isotopes to argue against the impact hypothesis, favoring a volcanically driven model of high CO₂, warming, ocean stagnation, bacterial expansion, and sulfide toxicity due to chemocline upward excursion. The impact hypothesis for the K–Pg event has since been strengthened by the discovery of independent geological evidence, but the particulars of Keith’s volcanic model remain among the favored mechanisms to explain the P–T and Tr–J events, and it may be that the K–Pg impact was simply the coup de grâce in what was a primarily volcanic mass extinction.

Carbon isotope stratigraphy at geologic time boundaries became widespread in the 1990’s. Kump and Arthur (1999) provided an excellent model for the interpretation of carbon isotope excursions, arguing that organic and inorganic carbon isotope data are needed to constrain the various forcing factors on the isotopic compositions of the ocean, atmosphere and biosphere, including the effects of elevated atmospheric CO₂ on the photosynthetic isotope effect. D’Hondt *et al.* (1998) used carbon isotope ratios in benthic and planktonic foraminifera to show a decrease in the biological pump as well as 3 million year recovery time associated with the K–Pg extinction. Carbon isotopes from the P–T boundary in the Southern Alps were used to argue for a complex, gradual event, spanning several million years (Magaritz *et al.*, 1994). Payne *et al.* (2004) documented large scale, repeated perturbations in the global carbon cycle over 5 million years of the Early Triassic, suggesting that the delayed biologic recovery from the P–T event may have been related to disturbances in global biogeochemical cycling. The first reliable demonstrations of a negative carbon isotope anomaly at the Tr–J boundary were documented in 2001 from the Queen Charlotte Islands (Ward *et al.*, 2001) and Hungary (Pálffy *et al.*, 2001) and confirmed in other Tr–J sections of the world over the next several years (Hesselbo *et al.*, 2002; Guex *et al.*, 2004; Galli *et al.*, 2005; Ward *et al.*, 2007; Williford *et al.*, 2007).

Perturbations in sulfur cycling have been identified for the Devonian (Geldsetzer

et al., 1987), Permian (Kajiwara *et al.*, 1994; Worden *et al.*, 1997; Kaiho *et al.*, 2001; Maruoka *et al.*, 2003; Newton *et al.*, 2004; Korte *et al.*, 2004; Grice *et al.*, 2005; Kaiho *et al.*, 2006b,a), and Cretaceous (Kajiwara and Kaiho, 1992) extinction events. The sulfur isotope excursions at the P–T boundary have recently been attributed to a massive release of hydrogen sulfide into the surface oceans due to superanoxia, expanded sulfate reduction in sediments, chemocline upward excursion, and photic zone euxinia (Kump *et al.*, 2005; Grice *et al.*, 2005; Kaiho *et al.*, 2006b,a). Sulfide toxicity and ozone depletion that would have resulted from this scenario is now considered to be a potential secondary mechanism for the P–T extinction.

1.6 Biomarkers and mass extinctions

In recent years it has become possible to isolate organic compounds diagnostic of particular organisms, including those that do not otherwise fossilize readily (such as bacteria and archaea), from ancient sedimentary rocks. These “molecular fossils, or biomarkers, can provide information about the environment of deposition when the parent organism has strict environmental requirements (e.g. the presence of compounds produced only by halophilic archaea suggest an environment with high salinity)(Hayes, 2002).

Bulk $\delta^{13}\text{C}$ records, whether from organic matter ($\delta^{13}\text{C}_{org}$) or carbonates ($\delta^{13}\text{C}_{carb}$), can be confounded by uncertainty in the source of the carbon. Excursions in the organic record can be driven by biological productivity or changes in atmosphere/ocean chemistry as discussed above, but they can also be driven by changes in the ratio of terrestrial to marine organic input, as marine and terrestrial organic matter tend to fractionate carbon isotopes differently (Arthur *et al.*, 1988). One way to confront this problem is to analyze the isotopic composition of individual organic compounds by coupling gas chromatography mass spectrometry (GC-MS) and isotope ratio mass

spectrometry (IRMS), or “compound specific isotope analyses” (Hayes *et al.*, 1989). The isotopic composition of specific biomolecules can also provide information about the metabolism of the parent organism. For example, highly depleted ($\delta^{13}\text{C} < -40\text{‰}$) 3β -methylhopanes imply the presence of methanotrophic bacteria (Summons *et al.*, 1994).

1.6.1 Permian–Triassic biomarkers

In several P–T boundary sections around the world, diverse reef assemblages give way to microbialites – a rock type characteristic of deposition in a biofilm setting (Baud *et al.*, 1997; Kershaw *et al.*, 1999; Ezaki *et al.*, 2003). This suggests that the near complete reduction of marine invertebrate animal diversity after the extinction left extensive areas open to colonization by microbes. Changes in the 2α -methylhopane index (2-MHP) across a PTB section in Meishan, China suggest that invertebrate extinctions were preceded by a decrease in the proportion of cyanobacteria and followed by an expansion in the cyanobacteria (Xie *et al.*, 2005).

Another recent study shows evidence for photic zone euxinia (PZE) coeval with the PTB. Increasing $\delta^{34}\text{S}$ values across the boundary indicate an increase in the export of isotopically light biogenic sulfides to marine sediments, and the appearance of abundant aryl-isoprenoids and the carotenoid pigment isorenieratane imply the presence of the anoxygenic photosynthetic green sulfur bacteria of the Chlorobiaceae (Grice *et al.*, 2005).

1.6.2 Cretaceous–Tertiary biomarkers

A good deal of work has been done on the biomarker record of K–T rocks from Hokkaido, Japan. A decrease in the concentration of long chain *n*-alkanes in the boundary claystone compared with the rocks deposited before and after the event bed

suggests a sudden decrease the abundance of terrestrial plants that lasted for 7,000 years, with a recovery phase of 2000 years (Mita and Shimoyama, 1999). A similar trend was found in cyclic alkanes (Shimoyama and Yabuta, 2002) and in highly-branched isoprenoidal molecules, probably due to extinctions among the diatoms (Katsumata and Shimoyama, 2001).

1.6.3 Biomarkers and methane

Several studies have sought to link biomarkers to the presence of methane in marine environments, typically finding that molecules produced by organisms that produce or oxidize methane are depleted in ^{13}C relative to the substrate and the total biomass. 3β -methylhopane is a biomarker for methanotrophic bacteria like *Methylococcus* and *Methylomonas* (Summons *et al.*, 1994). C_{20} -isoprenoid 2,6,11,15-tetramethylhexadecane (crocetane) and C_{25} -isoprenoid 2,6,10,15,19-pentamethylcosane with $\delta^{13}\text{C}$ values ranging from -70‰ to -130‰ were found in association with authigenic carbonates deposited during anaerobic methane oxidation around cold seeps in the Black Sea (Thiel *et al.*, 2001). Pleistocene sediments from the last interstadial in the Santa Barbara Basin show elevated levels of isotopically depleted diplopterol and archaeol, biomarkers for aerobic and anaerobic methane oxidation, together with decreases in the $\delta^{13}\text{C}$ of planktonic foraminifera. These three lines of evidence strongly imply a significant concentration of methane throughout the entire water column, suggesting intermittent clathrate destabilization (Hinrichs *et al.*, 2003).

1.7 Key Tr–J boundary sections

The Triassic–Jurassic boundary was less studied than the other Phanerozoic mass extinctions, perhaps due to the relative lack of marine sections showing continuous deposition (Morante and Hallam, 1996). This has changed in recent years primar-

ily as a result of the UNESCO International Geoscience Programme (IGCP) 458 project entitled, “Triassic/Jurassic boundary events: Mass extinction, global environmental change, and driving forces,” and led by József Pálffy, Stephen Hesselbo, and Christopher McRoberts. This project culminated in the publication of a volume in *Palaeogeography, Palaeoclimatology, Palaeoecology* (v.244, issues 1-4): *Triassic–Jurassic boundary events: problems, progress, possibilities*, and generated a significant amount of new work and interest around the Tr–J boundary. Some of the most important Tr–J sections in the world, as well as basic geologic descriptions of the sections chosen for this study are indicated below.

1.7.1 North America

The Tr–J sections at Kunga Island and Kennecott Point in the Queen Charlotte Islands, British Columbia, Canada show evidence for significant extinctions among the radiolaria (E.S. and Hori, 1993; Carter and Hori, 2005) and have provided a good biostratigraphic record of ammonoids (e.g. Tipper *et al.*, 1991; Longridge *et al.*, 2007). The Kunga Island section is the site of the currently accepted date for the Tr–J boundary (Pálffy *et al.*, 2000). The Kennecott Point section has produced some of the best stable isotope data for the Tr–J boundary (Ward *et al.*, 2001, 2004; Williford *et al.*, 2007, this study) due to its apparently continuous exposure of organic rich shales, siltstones and sandstones from the Norian into the Late Sinemurian. There are intermittent turbidites and rare hummocky cross stratification, and these rocks appear to have been deposited at outer shelf to upper slope depths (Haggart *et al.*, 2001; Ward *et al.*, 2004). The Kennecott Point section is cut by numerous small scale offsets, which can generally be traced and deconstructed on the outcrop during sampling (Ward *et al.*, 2004).

The Global Stratotype Section and Point has not been determined for the base of

the Hettangian stage, or the Tr–J boundary, but a leading candidate at this time is the section at New York Canyon, Nevada, USA. This section was first described by Muller and Ferguson (1936), and a more recent, detailed analysis is offered by Hallam and Wignall (2000). The New York Canyon section contains the most complete record of ammonites across the Tr–J boundary (Guex *et al.*, 2004), and it has produced a stable carbon isotope curve that correlates well with that observed in the Queen Charlotte Islands (Guex *et al.*, 2004; Ward *et al.*, 2007). The section proceeds from the bedded limestones of the Mount Hyatt Member of the Gabbs Formation, into the silty marls of the boundary-crossing Muller Canyon Member, and finally into the limestones of the overlying Sunrise Formation, showing evidence for regression around the Tr–J boundary, followed by a Hettangian transgression (Hallam and Wignall, 2000).

The Newark Supergroup in northeastern USA contains key Tr–J terrestrial sections that have produced high resolution palynology (Olsen *et al.*, 1996), tetrapod biostratigraphy (Olsen *et al.*, 1987), cyclostratigraphy (Olsen and Kent, 1996), magnetostratigraphy (Kent *et al.*, 1995), and an iridium anomaly (Olsen *et al.*, 2002). Much of the controversy surrounding the timing of the CAMP eruptions involves work done on the Orange Mountain Basalt in this area, where it has been suggested that the oldest volcanics postdate the Tr–J extinctions (Whiteside *et al.*, 2007). Other important terrestrial Tr–J boundary sections containing the record of vertebrate evolution including the major radiation of the dinosaurs are found in the southwestern United States: the Chinle and Glen Canyon Groups of the Colorado Plateau (Lucas and Tanner, 2007) and the Moenave Formation in the Four Corners region (Tanner and Lucas, 2007).

1.7.2 Europe

The Tr–J section at St. Audrie’s Bay on the Somerset coast of England has been the focus of a great amount of detailed stratigraphic work in the last decade, including important records of paleomagnetism (Hounslow *et al.*, 2004), palynology (Hesselbo *et al.*, 2002; van de Schootbrugge *et al.*, 2007), carbon isotopes (Hesselbo *et al.*, 2002), and facies change (Hesselbo *et al.*, 2004). The base of the Hettangian stage, and thus the Jurassic system, was historically defined at the St. Audrie’s Bay section by the lowest occurrence of the ammonite *Psiloceras planorbis* (Maubeuge, 1964). Other key European sections include those at Kendelbachgraben (Morbey, 1975) and Tiefengraben (Kuerschner *et al.*, 2007), both providing excellent palynological records, the Lombardian Alps of Italy (McRoberts, 1994; Galli *et al.*, 2005), and the Csövár section, Hungary, which has been the site of more recent integrated litho-, bio- and isotope stratigraphy (Pálffy *et al.*, 2001, 2007).

1.7.3 New Zealand

The Triassic–Jurassic (Tr–J) boundary in New Zealand occurs on the west coast of the North Island and the Catlins region of Southland as part of the Murihiku Supergroup, a Late Permian to Late Jurassic accreted terrane deposited in a forearc basin, east of an andesitic to dacitic volcanic arc on the active eastern edge of Gondwana (Campbell *et al.*, 2003; Briggs *et al.*, 2004). The rocks are volcanoclastic sandstones and siltstones with intermittent turbidites. New Zealand geologists use a set of local stages (Crampton *et al.*, 1995), according to which the final stage of the Triassic is the Otapirian, and the first stage of the Jurassic is the Aratauran. The most recent New Zealand geological time scale (Cooper, 2004) places the Otapirian–Aratauran boundary at the Tr–J boundary, using the date of 199.6 ± 0.3 Ma (Pálffy *et al.*, 2000). The New Zealand sections were chosen for stable isotope research in order to test whether the

Otapirian–Aratauran boundary is equivalent to the Rhaetian–Hettangian boundary as internationally recognized and thus help determine how the New Zealand sections correlate with other Tr–J sections around the world.

1.8 Structure of the dissertation

This dissertation is organized into six chapters: introductory and concluding chapters, and four core chapters containing new research on the biogeochemistry of the Tr–J boundary. An overview of the collaborators and their contributions to the work follows.

Chapter II, entitled, “An extended organic carbon-isotope record across the Triassic/Jurassic boundary in the Queen Charlotte Islands, British Columbia, Canada,” was previously published as:

Williford, K.H., Ward, P.D., Garrison, G.H., Buick, R., 2007. An extended stable organic carbon isotope record across the Triassic–Jurassic boundary in the Queen Charlotte Islands, British Columbia, Canada. *Palaeogeography Palaeoclimatology Palaeoecology* 244(1-4): 290-296.

Samples and lithologic data were collected by Peter Ward in 2001. Ken Williford and Geoff Garrison prepared the samples and performed the stable isotope analyses. Data were compiled and analyzed by Williford. Roger Buick contributed to the manuscript.

Chapter III, entitled, “Records of stable organic carbon isotopes from three Triassic–Jurassic boundary sections in New Zealand” will be submitted to the *New Zealand Journal of Geology and Geophysics* for publication as follows:

Williford, K.H., Ward, P.D. Records of stable organic carbon isotopes from three Triassic–Jurassic boundary sections in New Zealand.

Samples and lithologic data were collected by Williford and Ward in 2004. Sample

preparation, stable isotope analysis, and data analysis were undertaken by Williford.

Chapter IV, entitled, "A record of sulfide and organic sulfur isotopes across the Triassic–Jurassic boundary in the Queen Charlotte Islands, British Columbia, Canada" will be submitted to *Geology* for publication as follows:

Williford, K.H., Foriel, J., Ward, P.D. A record of sulfide and organic sulfur isotopes across the Triassic–Jurassic boundary in the Queen Charlotte Islands, British Columbia, Canada.

Samples and lithologic data were collected by Ward and Williford. Stable sulfur isotope analyses and sulfur methods were provided by Julien Foriel.

Chapter V, entitled, "Organic geochemistry of a Triassic–Jurassic boundary section in the Queen Charlotte Islands, British Columbia, Canada," will be submitted to *Organic Geochemistry* for publication as follows:

Williford, K.H., Ward, P.D., Kring, D., Schwab, V., Sachs, J., Ingalls, A., Wakeham, S.G., Grice, K. A record of biomarkers and stable sulfur isotopes across the Triassic–Jurassic boundary in the Queen Charlotte Islands, British Columbia, Canada.

Organic geochemical analyses were conducted by Williford in the laboratories of Anita Ingalls, Stuart Wakeham, and Julian Sachs, all of whom also provided valuable training and expertise in organic geochemical techniques. Additional training and vital contributions to the data analysis were provided by Valerie Schwab. Grice provided helpful comments on the manuscript.

Chapter 2

RECORDS OF STABLE ORGANIC CARBON ISOTOPES FROM THREE TRIASSIC–JURASSIC BOUNDARY SECTIONS IN NEW ZEALAND

2.1 Introduction

When a pattern of geochemical change is recognized at many localities around the world, chemostratigraphy can be used to supplement biostratigraphy in the effort to correlate rock sections of the same general age. Accurate correlation is fundamental to the ability to understand the nature and timing of events that occurred during intervals of great global change, such as mass extinctions. In locations where fossils are rare, correlation is especially difficult, and records of geochemical change all the more valuable. This situation exists for the Triassic–Jurassic boundary of New Zealand, where the biostratigraphic record is sufficiently different from the rest of the world that a system of local stages has supplanted the international stratigraphic system (Cooper, 2004).

In the system of international stages, the Tr–J boundary is defined as the boundary between the Rhaetian (final stage of the Triassic) and the Hettangian (first stage of the Jurassic). Based on the argument that the fossil succession in New Zealand is fundamentally different from that of other regions due to the isolation in which that record developed, New Zealand geologists subdivided the periods of the Phanerozoic into their own set of stages (Fig. 2.1) (Crampton *et al.*, 1995). The final stage of the Triassic in New Zealand is the Otapirian, and the first stage of the Jurassic is the Aratauran. The most recent New Zealand geological time scale (Cooper, 2004)

Age (Ma)			International	New Zealand		
175.6 -	Jurassic	Early	Toarcian	Herangi	Ururoan	Hu
			Pliensbachian		Aratauran	Ha
			Sinemurian			
			Hettangian			
199.6 -	Triassic	Late	Rhaetian	Balfour	Otapirian	Bo
			Norian		Warepan	Bw
					Otamitan	Bm
					Oretian	Br
237 -			Carnian		Gore	Kaihikuan

Figure 2.1: Late Triassic–Early Jurassic interval of the New Zealand Geological Timescale (Cooper, 2004)

places the Otapirian–Aratauran boundary at the Tr–J boundary, using the date of 199.6 ± 0.3 Ma (Pálffy *et al.*, 2000).

We wished to test the hypothesis that the Otapirian–Aratauran boundary as currently defined in New Zealand correlated with the internationally recognized Tr–J (Rhaetian–Hettangian) boundary. Since 2001, a relatively consistent pattern of carbon isotopic change across the Tr–J boundary has been identified at sections around the world (Ward *et al.*, 2001; Pálffy *et al.*, 2001; Hesselbo *et al.*, 2002; Guex *et al.*, 2004; Galli *et al.*, 2005; Ward *et al.*, 2007; Williford *et al.*, 2007), including a short negative excursion of about 2‰ in the latest Rhaetian followed by a larger, positive excursion encompassing most of the Hettangian, and a return to baseline values in the latest Hettangian. To determine how the Tr–J boundary sections in New Zealand correlate with others in the world, three Otapirian–Aratauran boundary sections within the Murihiku Terrane were sampled for stable organic carbon isotopes in March of 2004 (Fig. 2.2). On the west coast of the North Island, sections in the Awakino River

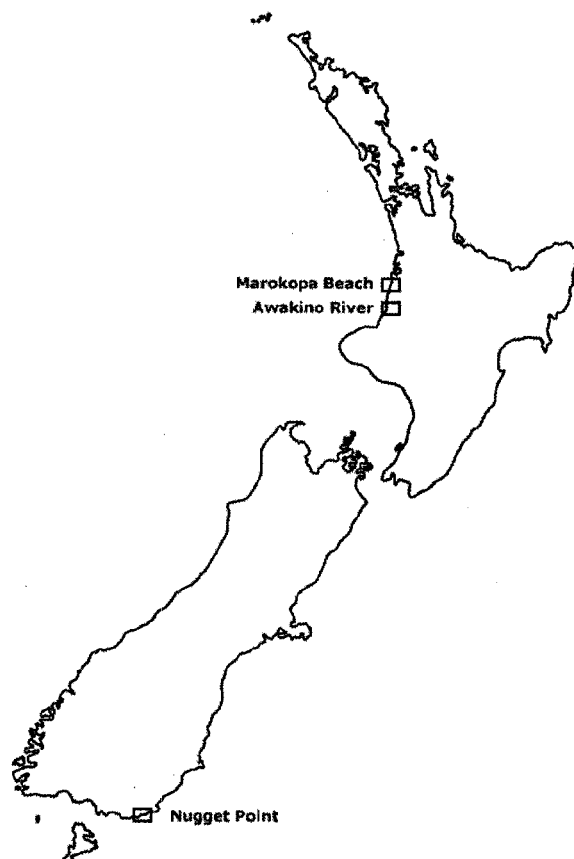


Figure 2.2: Overview map showing New Zealand study areas

Gorge (Zhang and Grant-Mackie, 2001) and Marokopa Beach (MacFarlan, 1998) were chosen, as they contained published biostratigraphic control. Akikuni *et al.* (2006) have reported finding negative excursions in $\delta^{13}\text{C}_{org}$ above the palynologically defined Tr-J boundary from the Awakino River and Kawhia Harbour sections, though these findings are as yet unpublished. In Southland, the Nugget Point section (Speden and McKellar, 1958) was chosen.

The Triassic–Jurassic (Tr–J) boundary in New Zealand occurs on the west coast of the North Island and the Catlins region of Southland as part of the Murihiku Supergroup. The Murihiku Supergroup was originally defined as Early Triassic to

Late Jurassic by Campbell and Coombs (1966), but was redefined by Campbell *et al.* (2003) to include Late Permian carbonate sequences of the Kuriwao Group (Waterhouse, 1964). This unit is generally considered to represent an accreted terrane deposited in a forearc basin, east of an andesitic to dacitic volcanic arc on the active eastern edge of Gondwana (Briggs *et al.*, 2004). The forearc basin was filled with volcanoclastic sandstones and siltstones, with intermittent turbiditic deposition and occasional conglomerates and shellbeds, resulting in a continuous, fault-bounded package now recognized to be 13.5 km thick. Murihiku rocks outcrop on the west coast of the North Island and in the Catlins region of Southland. Sedimentation rate during the latest Triassic in the Murihiku Basin was quite high: the final stage of the Triassic (when defined as the interval between the last appearance of *Monotis* and the first appearance of a Psiloceratid ammonite) at the Marokopa Beach section is roughly 1300 m thick (MacFarlan, 1998), whereas the equivalent interval in the Queen Charlotte Islands, British Columbia is 100 m thick (Ward *et al.*, 2001).

2.2 Methods

In the field, the Otapirian–Aratauran boundary as defined by previous workers was located using maps and measured sections. Due to the apparently expanded nature of the New Zealand sections in comparison with others around the world, we elected to sample more total section (200–300 m) with a wider sample spacing (2–3 m) than we have used at other field sites (1 m) (e.g. Williford *et al.*, 2007).

The ratio of stable carbon isotopes ($^{13}\text{C}/^{12}\text{C}$) in sedimentary bulk organic matter (i.e. $\delta^{13}\text{C}_{org}$) was analyzed via elemental analyzercontinuous-flow isotope ratio mass spectrometry (EA-CFIRMS) at ISOLAB, operated jointly by the Quaternary Research Center and the Astrobiology Program at the University of Washington.

Surface debris was removed from samples by sonicating for one hour in deionized

(DI) water. Clean samples were split and ground to a fine powder in a rock-crushing mill. Glassware was baked overnight at 500°C to remove organic carbon. All equipment was washed with methanol between each sample to avoid organic contamination. Approximately one gram of each powdered sample was acidified with an excess of 10% HCl and allowed to react at 40°C for at least 12 hr to remove inorganic carbonate material, especially recalcitrant mineral phases such as siderite (FeCO₃). Samples were then triple rinsed with ultrapure (>18 MΩ) DI water and oven dried at 40° C. Isotope analyses were made with a Costech ECS 4010 Elemental Analyzer coupled to a ThermoFinnigan MAT 253 mass spectrometer via a ThermoFinnigan CONFLO III gas interface. Isotope ratios are reported in standard delta (δ) notation relative to Vienna Pee Dee Belemnite (VPDB), where $\delta^{13}\text{C} = [((^{13}\text{C}/^{12}\text{C})_{\text{sample}}/({}^{13}\text{C}/^{12}\text{C})_{\text{VPDB}}) - 1] * 1000$. Average standard deviation of sample replicates was 0.18‰ for $\delta^{13}\text{C}_{\text{org}}$ (1σ ; n = 181). Average analytical precision based on routine analyses of internal laboratory reference materials was 0.15‰ for $\delta^{13}\text{C}_{\text{org}}$ (1σ).

2.3 Results

2.3.1 Nugget Point

The Otapirian–Aratauran boundary near Nugget Point occurs in an unnamed bay between Roaring Bay and Sandy Bay (Fig. 2.3). The Late Triassic and Early Jurassic rocks of the Catlins coast in Southland were first studied by McKay (1877), but the rugged nature of the rocks bracketing the unnamed bay between Roaring and Sandy Bays precluded the study of the boundary beds for nearly a century. Speden and McKellar (1958) first reported on this sequence of rocks, identifying the Otapirian–Aratauran boundary on the basis of the discovery by J.D. Campbell and D.S. Coombs of psiloceratid ammonites associated with *Otapiria marshalli* (Trechmann) in a siltstone bed (S179/640) on the north side of a large stack and in the cliff at the back

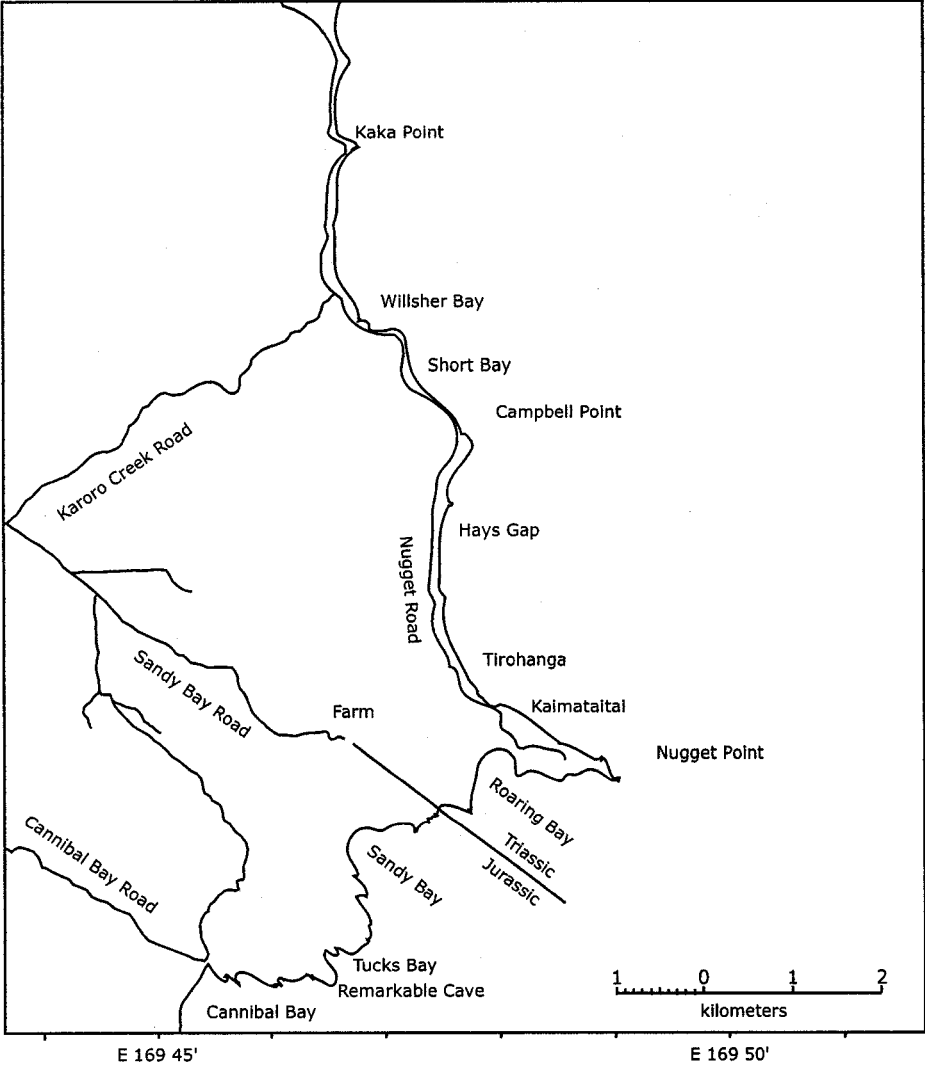


Figure 2.3: Nugget Point study area detail

of the boulder beach. Detail of the Nugget Point study area is given in Fig. 2.3. To access the section, it was necessary to cross a sheep ranch located at the end of Sandy Bay Road, and the property owners cooperation is gratefully acknowledged.

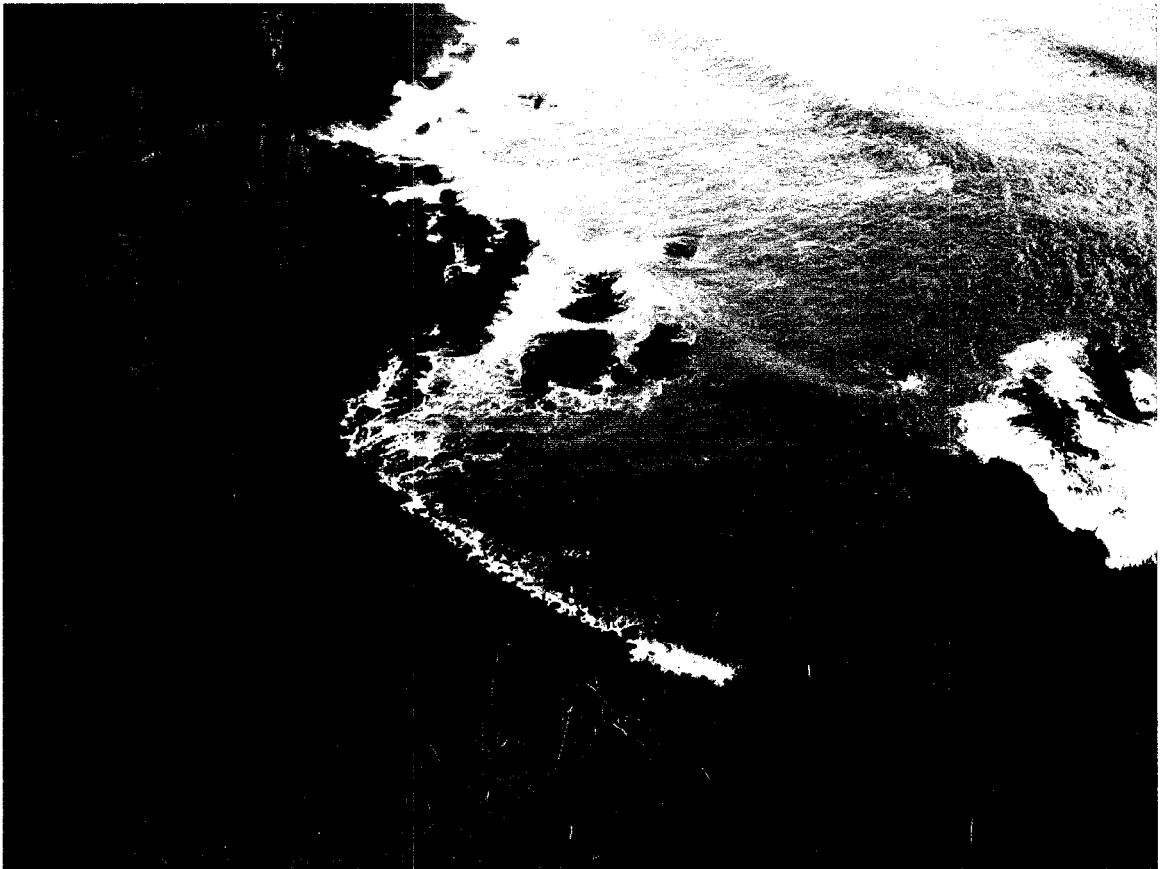


Figure 2.4: Nugget Point section from above, looking southeast. Rocks are younging to the right

The section was accessed by descending a steep slope into an unnamed bay about 1.5 km from the entrance to the farm at the end of Sandy Bay Road (Fig. 2.4). Fig. 8 shows the slope and the approximate location of the Otapirian–Aratauran boundary.

Upon descending into the boundary bay, the stack containing the Psiloceratid bed was located (Fig. 2.6), and an ammonite was discovered in a float boulder near the cliff, along strike from the northern edge of the stack (2.7). This ammonite is identified as *Macrogrammites grammicus* based upon the images of specimens recovered from this locality published in Stevens (2004).

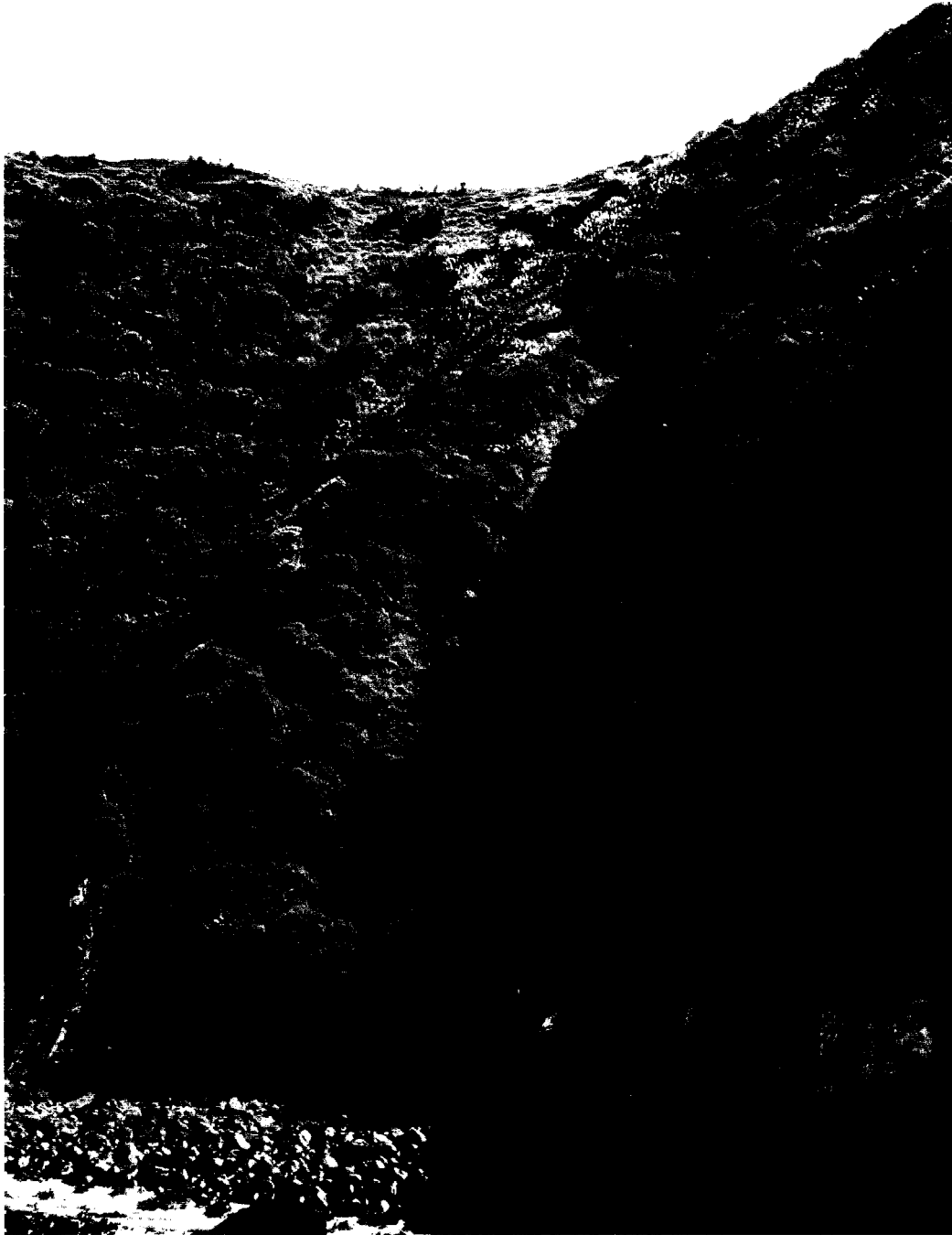


Figure 2.5: Nugget Point boundary section, looking west. Rocks are younging to the left.



Figure 2.6: Stack just offshore from Nugget Point section, looking east. The Psiloceratid bed, fossil locality 640 of Speden and McKellar (1958), is on the left (north) edge of the stacks.

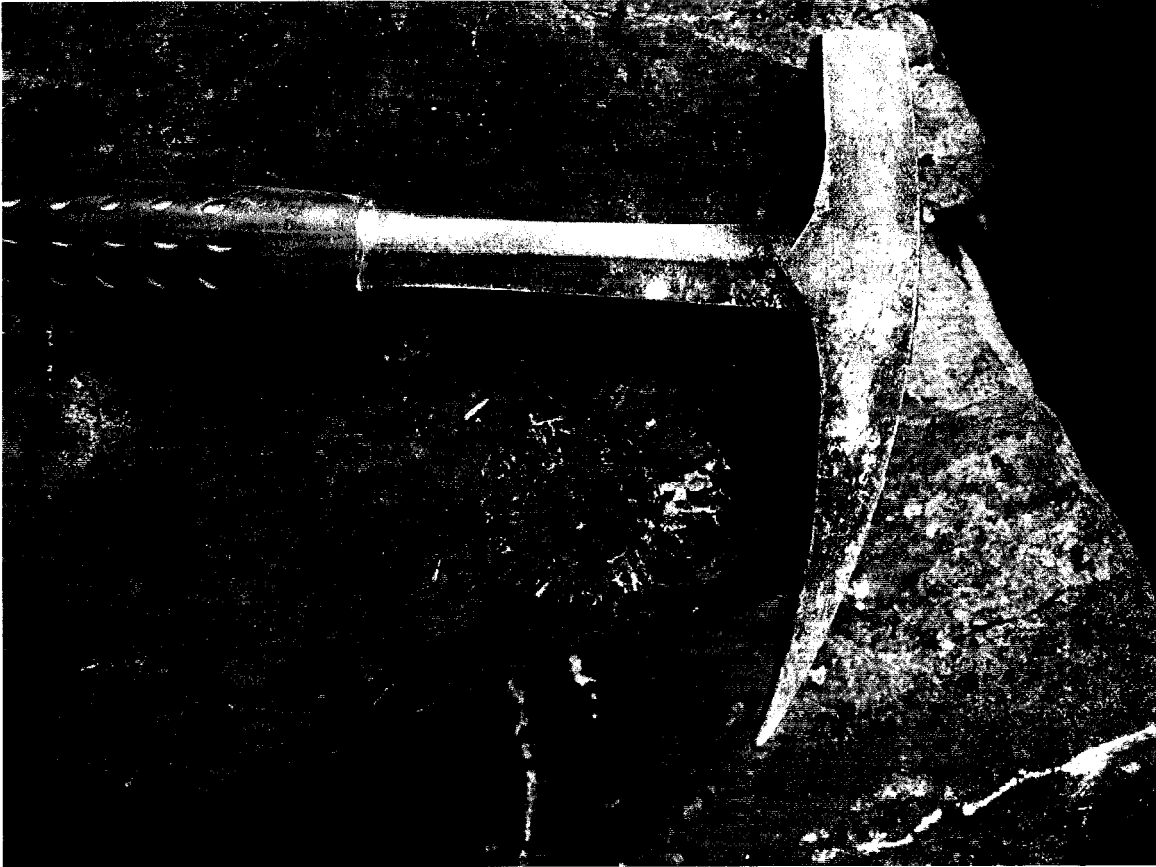


Figure 2.7: *Macrogrammites grammicus* in a float boulder at fossil locality 640 of Speden and McKellar (1958). This corresponds to fossil locality AU16156 and OU 3520 in Stevens (2004).

No other ammonites were discovered, but several specimens of *Otapiria sp.* (McRoberts, pers. comm.) were recovered from Aratauran rocks south of the Psiloceratid bed (Fig. 2.8).

The measured section and stable carbon isotope results from this locality are given in Fig. 2.9. No distinctive patterns are identified in the carbon isotope data from this section. The entire section shows remarkable isotopic homogeneity, in fact (1σ : 0.53‰). The two points showing the heaviest isotope values, at 31 and 53 m,



Figure 2.8: *Otapiria sp.* from top of Nugget Point section

also contain the lowest weight percent organic carbon in the section, and are not considered to be relevant to paleoenvironmental interpretations. The lightest isotope values occur in the lowest part of the section, roughly 100 m before the appearance of the Hettangian ammonites.

2.3.2 *Awakino River*

The Tr–J rocks in the Awakino Gorge were originally mapped by Grant-Mackie (1959). The Otapirian–Aratauran boundary section is exposed by a roadcut along a

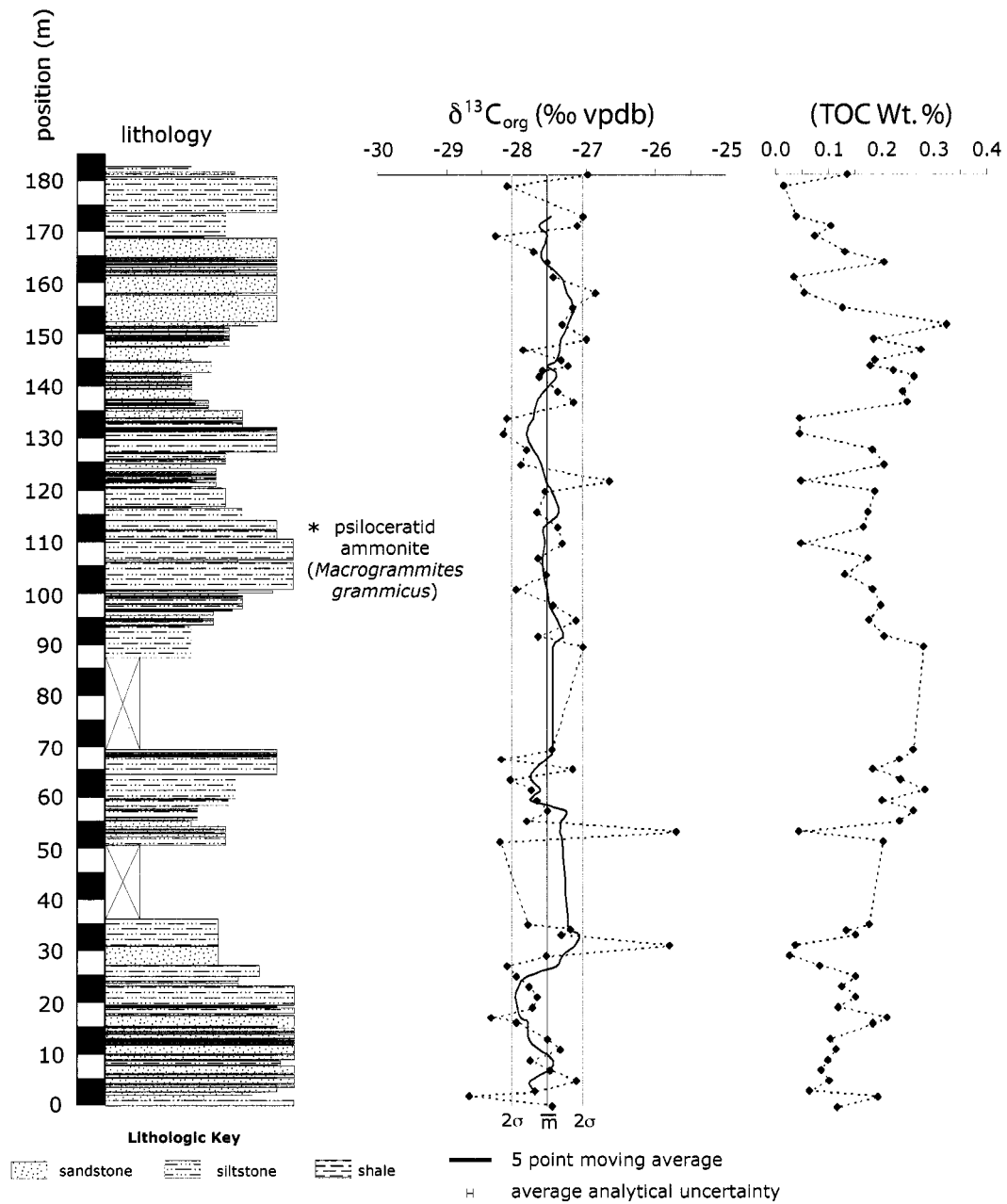


Figure 2.9: $\delta^{13}C_{org}$ record for Tr-J boundary strata in an unnamed bay near Nugget Point, New Zealand

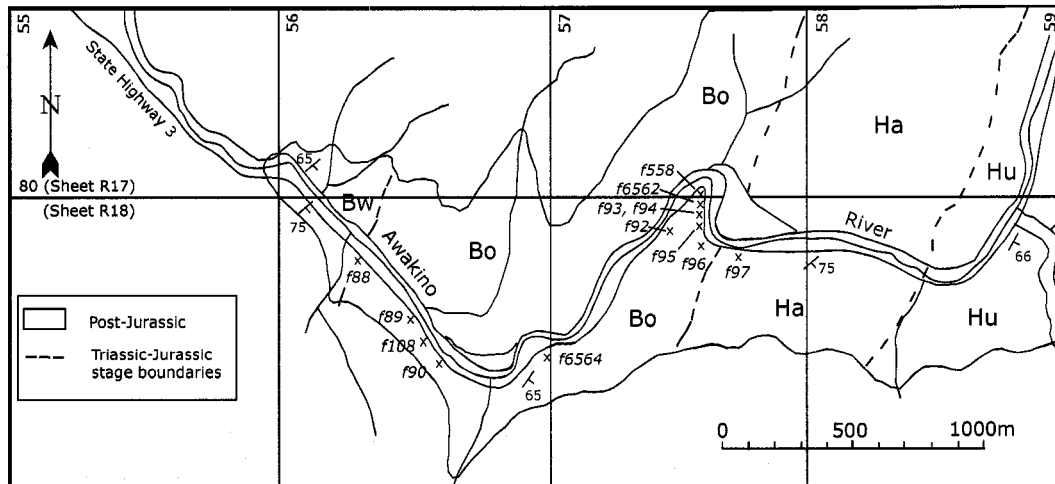


Figure 2.10: Awakino River study area detail (after Zhang and Grant-Mackie (2001))

prominent bend in the Awakino River. A detail map of the study area is shown in Fig. 2.10, and a photograph of the boundary section is shown in Fig. 2.11. The rocks sampled in this study include 240 m of the Ngutunui Formation, divided into the Balfour (Otapirian) and Herangi (Aratauran) Series, all part of the Newcastle Group and the Murihiku Supergroup.

The Otapirian–Aratauran boundary was placed by Zhang and Grant-Mackie (2001) between their fossil localities f96 and f97, based upon a turnover in pollen from Assemblage II (*Foveosporites moretonensis-Densoisporites psilatus-Steevesipollenites claviger* Assemblage) to Assemblage III (*Toripustulatisporites hokonuiensis-Kurtomisporis minor-Polucingulatisporites radiatus* Assemblage). The sample from f97 contains elements indicative of a Jurassic age, including rare *Lycopodiumsporites austroclavitudites* and *Ischyosporites cf. marburgensis*, both typical Jurassic species that have not been reported from the Triassic. f97 also contains typically Otapirian faunas,



Figure 2.11: Tr-J section at Awakino River, looking south

however, including /it *Otapiria dissimilis*, *Clavigera bisculata*, *Kalentera marwicki*, and *Ochotomya*. This led Zhang and Grant-Mackie (2001) to suggest that the Tr-J boundary lies in the Otapirian stage.

Our measured section, stable organic carbon isotope and total organic carbon data are shown in Fig. 2.12. There is no significant correlation between $\delta^{13}\text{C}_{org}$ and TOC ($r^2=0.0872$). There is a transition at 106 m in our section between an interval that is isotopically heavier (μ : -27.75‰) and more stable (1σ : 0.42‰) to an interval that is isotopically lighter (μ : -28.18‰) and more variable (1σ : 0.85‰). The five point

moving average shows an interval of stability between 0 and 100 m, two short-term negative events between 100 and 130 m, a long term positive trend between 130 and 194 m, and a return to more negative values, between 194 and 238 m. This topmost interval is highly variable, however, with three negative-positive shifts of about 2‰ occurring over 40 m.

2.3.3 Marokopa Beach

A well-exposed coastal Otapirian–Aratauran boundary section occurs near the mouth of the Marokopa River (Fig. 2.13). Roughly 1300 m of Otapirian strata are exposed in steep cliffs behind an ironsand beach between beds containing rare Aratauran ammonites and those containing the last *Monotis* on Kiritehere Beach (Fig. 2.14). These rocks were first studied by Henderson and Grange (1922) and mapped by Williamson (1932). MacFarlan (1998) gives a comprehensive review of this section and the surrounding area, and the biostratigraphy in that work was used to guide the isotopic sampling for this study.

Only one identifiable fossil was recovered during our sampling. An ammonite with sutures exposed in cross section was recovered from 295 m (Fig. 2.15) and delivered to Jack Grant-Mackie at the University of Auckland. This specimen was identified by Stevens (2004) as *Eolytoceras tasekoi* and assigned a Late Hettangian age. Trace fossils typical of the upper part of this section can also be seen below the ammonite in Fig. 2.15. These traces occur as fine, tan sand infillings within a darker gray silt matrix.

Our measured section, stable organic carbon isotope and total organic carbon data are shown with biostratigraphic data from MacFarlan (1998) in Fig. 2.16. Like the Awakino River section, the Marokopa section contains an interval (0 to 173 m) that is isotopically heavier (μ : -26.66‰) and more stable (1σ : 0.45‰) followed by

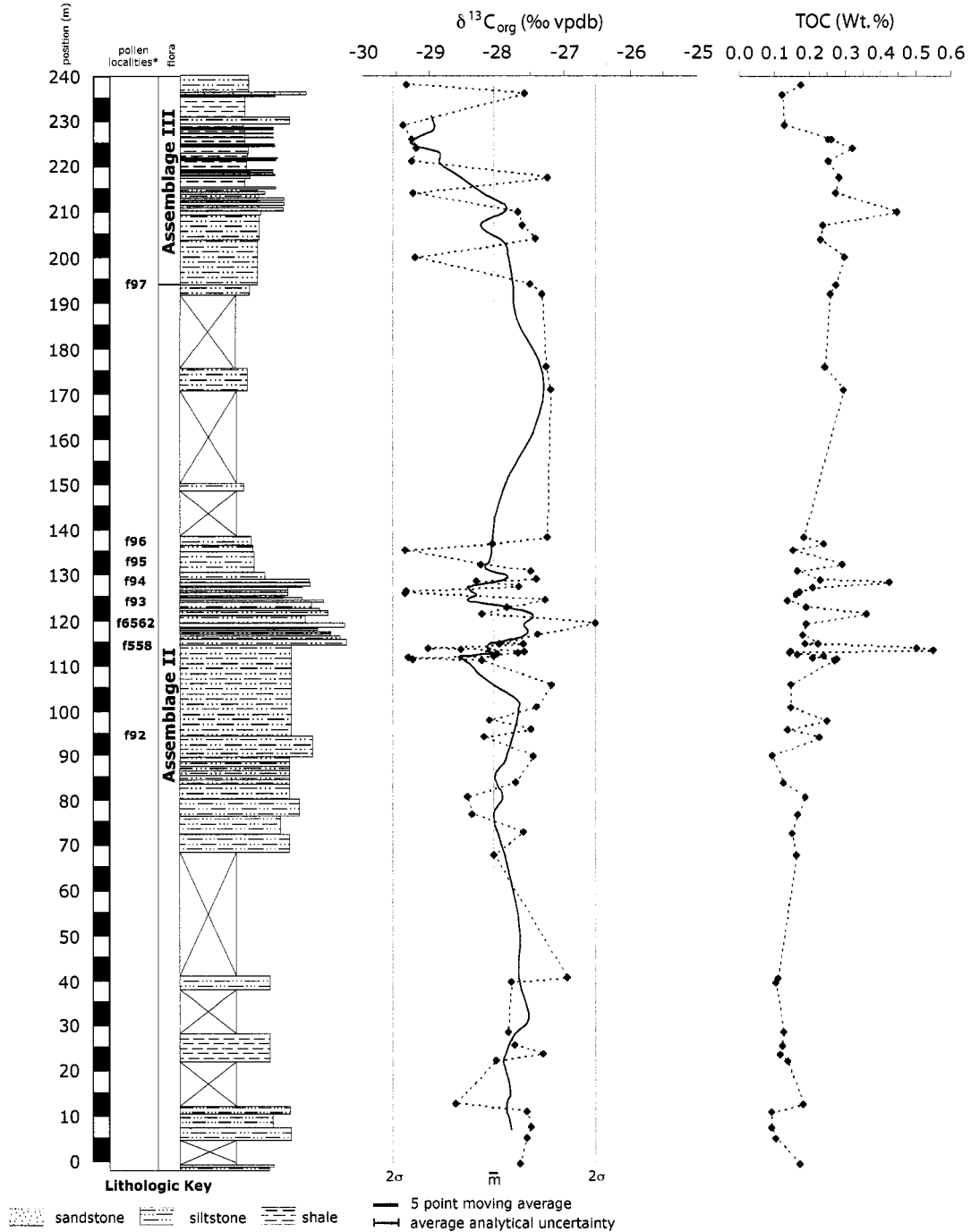


Figure 2.12: $\delta^{13}C_{org}$ record for the Awakino River Otapirian–Aratauran boundary section. Palynology from Zhang and Grant-Mackie (2001).

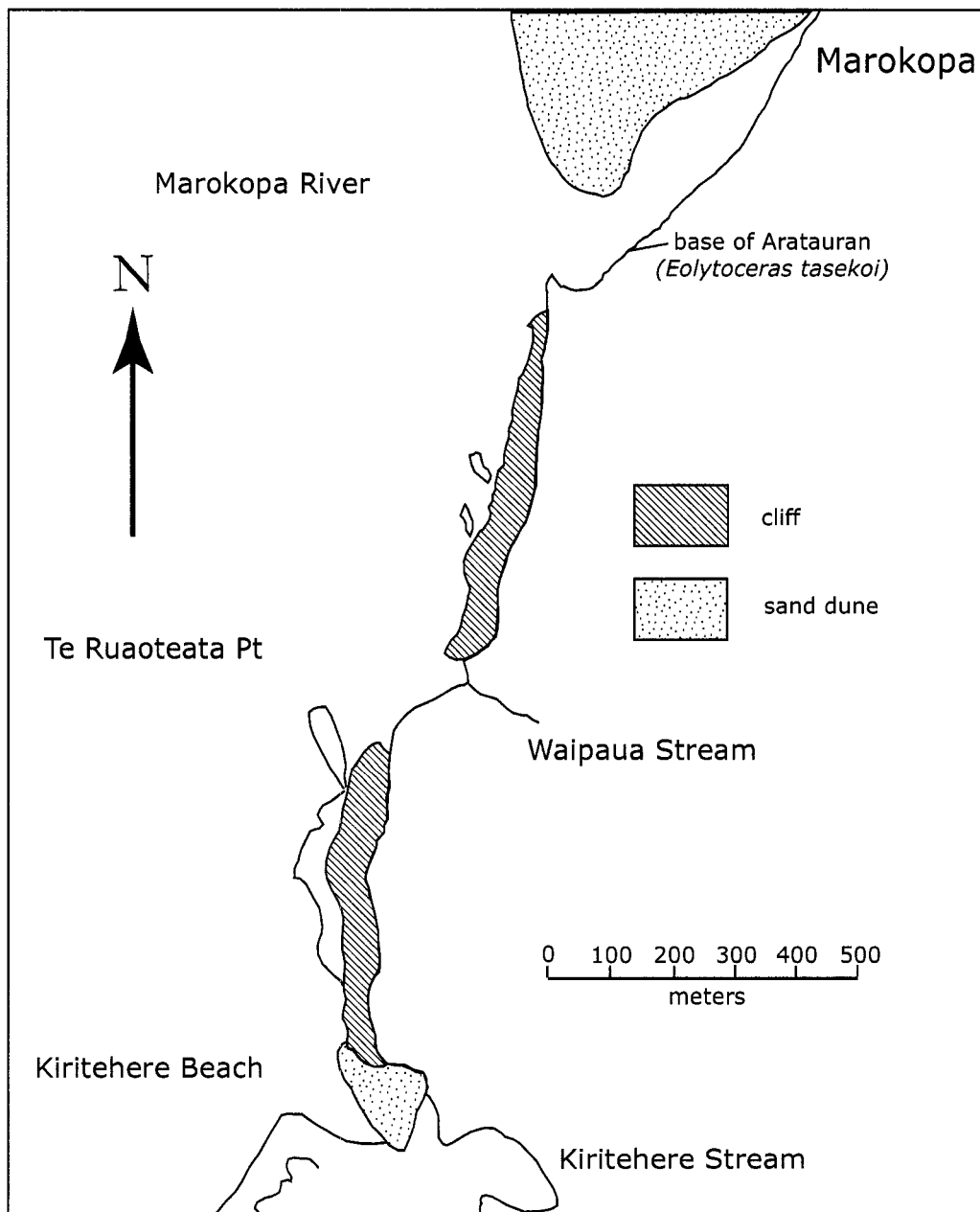


Figure 2.13: Marokopa Beach study area detail (after MacFarlan (1998))



Figure 2.14: Marokopa Beach section, looking south into the Triassic

an interval (173 to 247 m) that is isotopically lighter (μ : -27.51‰) and more variable (1σ : 0.75‰). The topmost interval remains isotopically light (μ : -27.34‰), but is less variable than the preceding interval (1σ : 0.52‰). The five point moving average data suggest a protracted and variable negative trend beginning at 173 m, peaking at 221 m, and returning to mean values 10 m before the appearance of the Hettangian ammonite. Peak negative carbon isotope values occur roughly 15 m above the last occurrence of the brachiopods *Clavigera bisculata* and *Mentzelia kawhiana* and the first occurrence of the bivalve *Pseudolimea fida*.



Figure 2.15: *Eolytoceras tasekoi* recovered from 295 m at Marokopa Beach section

2.4 Discussion and Implications for Global Correlation

Stable organic carbon isotope data for the three sections in this study are shown in Fig. 2.17, aligned according to the first appearance of Jurassic fossils. Moving average data from the Nugget Point and Marokopa sections suggest a negative carbon isotope shift peaking roughly 80 m before the appearance of Middle and Late Hettangian ammonites. Moving average data from the Awakino section suggests a negative carbon isotope shift peaking roughly 80 m before the first appearance of Jurassic flora. These negative shifts are indicated with the gray field on Fig. 20. By comparison,

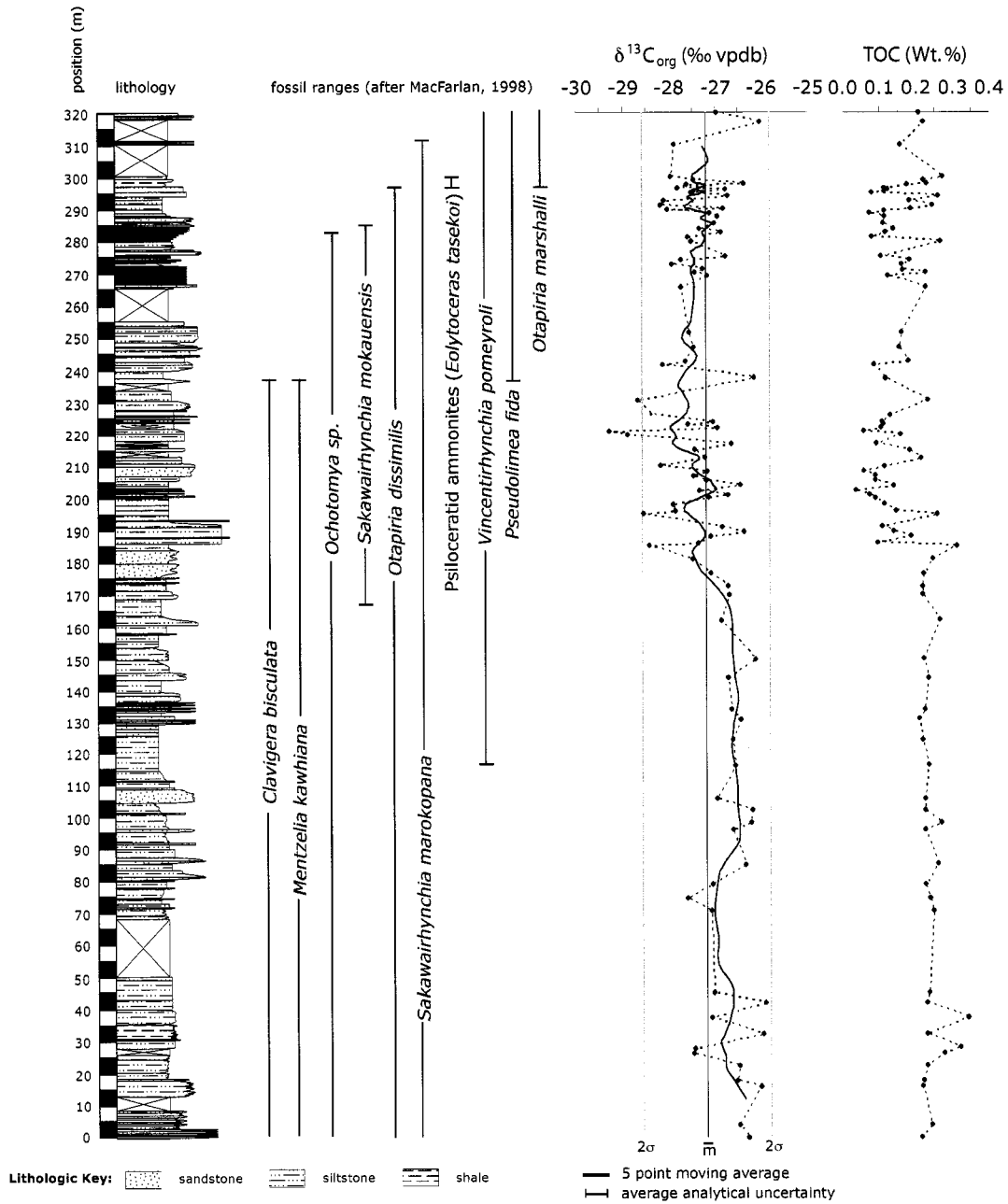


Figure 2.16: $\delta^{13}C_{org}$ record for the Marokopa Beach Tr-J boundary section. Fossil ranges from MacFarlan (1998).

the peak of the negative carbon isotope excursion in the Queen Charlotte Islands occurs roughly 40 m before the Middle Hettangian ammonite recovery (Williford *et al.*, 2007).

If the Otapirian–Aratauran boundary lies between samples f96 and f97 as indicated by Zhang and Grant-Mackie (2001), then the moving average trend in the Awakino section shows a superficial similarity to the globally-recognized pattern of isotopic change across the Tr–J boundary (short term negative shift in the latest Triassic followed by a positive shift in the earliest Jurassic). Based upon their work at the Awakino River section, Zhang and Grant-Mackie (2001) concluded that the Tr–J boundary in New Zealand lies within the Otapirian stage. This conclusion is supported by the definition of the Otapirian–Aratauran boundary at Nugget Point and Marokopa on the basis of the appearance of *Otapiria marshalli* together with Middle and Late Hettangian ammonites, respectively. If the average negative shifts in carbon isotope values revealed by this study represent the negative isotope event more clearly recognized at other localities around the world, and if this negative event is taken as a proxy for the Tr–J boundary, then the Tr–J boundary occurs in close association with the disappearance of the two brachiopods *Clavigera bisculata* and *Mentzelia kawhiana* and appearance of the bivalve *Pseudolimea fida*, well before the Otapirian–Aratauran boundary as currently defined in New Zealand. The absolute data that make up the trends suggested by moving averages show such a high degree of variability, however, that a correlation between the New Zealand sections and others around the world based on these carbon isotope data alone is difficult.

The fact that the New Zealand sections do not show the pattern of carbon isotopic change that has been documented in other sections around the world could be explained in three ways. First is the possibility that the Tr–J carbon isotope excursions do not record a global perturbation to the carbon cycle, and instead reflect local

Litho-, bio-, and stable organic carbon isotope stratigraphy for Oiapirian-Aratauran boundary sections at Marokopa Beach, Awakino Gorge, and Nugget Point, New Zealand. Sections are aligned according to first appearances of Jurassic fauna or flora, indicated by the gray line.

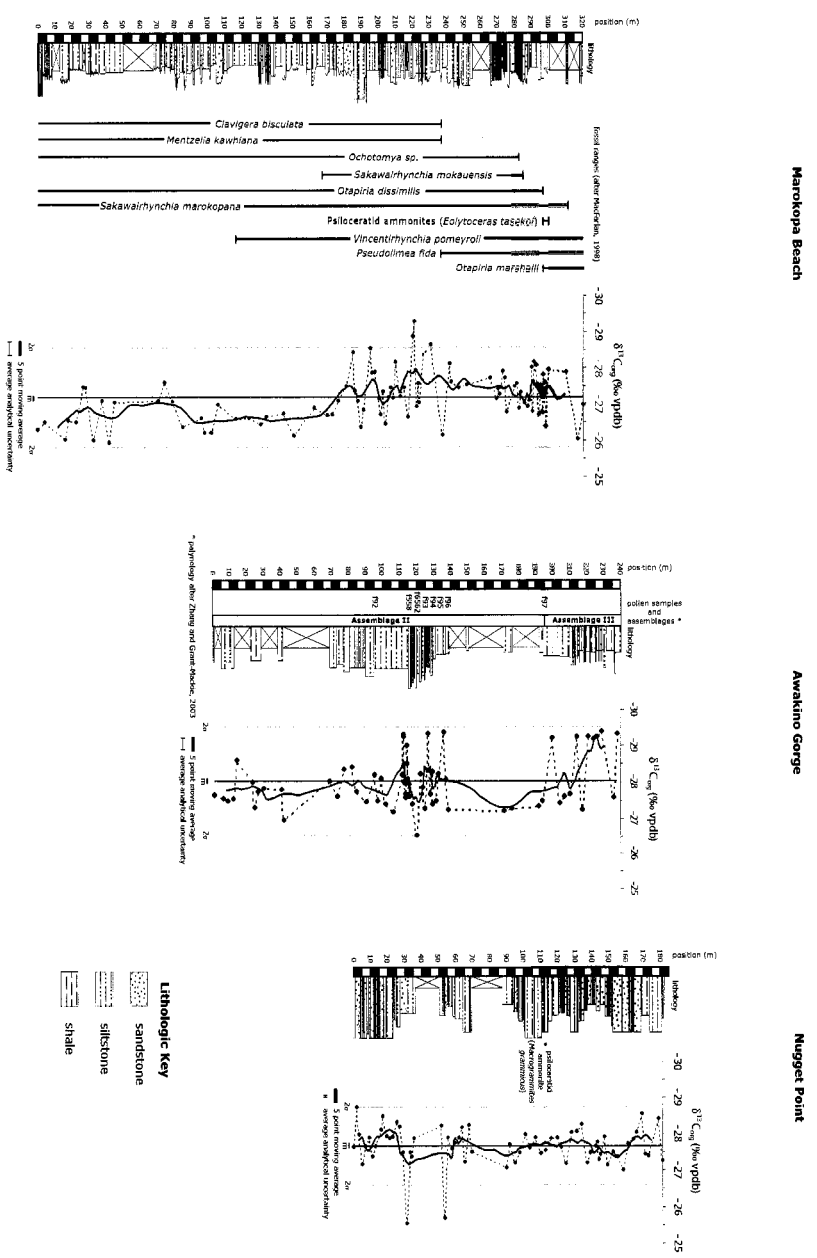


Figure 2.17: $\delta^{13}\text{C}_{org}$ record for Otapirian–Aratauran boundary sections at Marokopa Beach, Awakino Gorge, and Nugget Point, New Zealand. Sections are aligned according to first unambiguous appearances of Jurassic fauna or flora, indicated by the gray line.

events. Any geochemical record will reflect a combination of local and global influences, but the ocean and atmosphere are well mixed on the timescales with which this study is concerned. The reasoning behind this statement is as follows. The mixing time of the modern ocean is about 1.6×10^3 years (Primeau, 2005). At Kennecott Point, there are approximately 100 m of Rhaetian strata, representing between 2 and 4.5×10^6 years (Gallet *et al.*, 2007). If continuous sedimentation is assumed, then each meter of rock represents between 2 and 4.5×10^4 years of deposition, much longer than the mixing time of the modern ocean. For New Zealand, where there are over 1000 m of Rhaetian strata (MacFarlan, 1998), each meter represents roughly 2 to 4.5×10^3 years: less time, but still significantly more than the mixing time of the modern ocean. It has been suggested that ocean circulation was greatly reduced in the Late Permian (e.g. Isozaki, 1997), but the Late Permian model by Hotinski *et al.* (2001) produced deep ocean ventilation at rates comparable to those in the modern environment, even under a dramatically reduced latitudinal temperature gradient. As such, it is reasonable to assume that the entire ocean circulated at least once between each isotope sample that we collected.

When measuring the stable isotopes of bulk organic carbon, variability in the source of organic matter can cause local effects to overshadow global effects. A second explanation for the ambiguity of the New Zealand data is that the high sedimentation rate resulted in low organic carbon content in Tr–J sediments and a high degree of source variability. The high sedimentation rate in the Murihiku Basin diluted the organic carbon content of these sediments with clastic material. As a result, the organic carbon content of Murihiku rocks is less than 0.5%, an order of magnitude lower than that found in Tr–J rocks from the Queen Charlotte Islands, for instance (fig. A.1). The proximity of the Murihiku Basin to the continental margin combined with high uplift, erosion, and sedimentation rates may have led to a highly variable input

of terrestrial organic material. As marine and terrestrial organic matter have different average carbon isotopic compositions, changes in organic matter source through time can lead to isotopic heterogeneity in bulk organic matter (Arthur *et al.*, 1988), especially when total organic content is low. These factors together could have introduced a degree of local noise to the record that swamped any global signal. A third possibility is that the sampling was incomplete, and that isotope excursions exist at stratigraphic levels between the levels that were sampled in this study. These final two possibilities could be addressed by further sampling and compound specific isotope analysis.

2.5 Acknowledgements

Jack Grant-Mackie and Hamish Campbell provided valuable assistance in selecting and locating the Tr-JOtap boundary sections in New Zealand. This work was funded by the NASA Astrobiology Institute, University of Washington node, Peter Ward, P.I.

Chapter 3

AN EXTENDED ORGANIC CARBON-ISOTOPE
RECORD ACROSS THE TRIASSIC/JURASSIC
BOUNDARY IN THE QUEEN CHARLOTTE ISLANDS,
BRITISH COLUMBIA, CANADA

Previously published as:

Williford, K.H., Ward, P.D., Garrison, G.H., Buick, R., 2007. An extended stable organic carbon isotope record across the Triassic–Jurassic boundary in the Queen Charlotte Islands, British Columbia, Canada. *Palaeogeography Palaeoclimatology Palaeoecology* 244(1-4): 290-296.

3.1 Introduction

Over the past five years several stable carbon isotope studies on Triassic–Jurassic (Tr–J) boundary sections have revealed a perturbation to the carbon cycle associated with fossil turnover at the boundary. The first three such studies published, from Canada (Ward *et al.*, 2001), Hungary (Pálffy *et al.*, 2001), and England (Hesselbo *et al.*, 2002), showed a negative excursion of about two per mille (2‰) in the organic carbon stable isotope record ($\delta^{13}\text{C}_{org}$) within several metres of the paleontologically defined Tr–J boundary. Since then, other records have appeared from northern Italy (Galli *et al.*, 2005) and Nevada, USA (Guex *et al.*, 2004; Ward *et al.*, 2007). Of these five localities, only the Muller Canyon section in Nevada has been studied by more than one group. In this instance significant differences were found in the stratigraphic position of the isotope excursions, though the overall isotopic pattern reported is similar (Guex *et al.*,

2004; Ward *et al.*, 2007). The appearance of a negative carbon isotope excursion of similar magnitude within several metres of the paleontologically defined Tr–J boundary at the geographically-widespread localities cited above strongly suggests that this isotopic pattern is primary (i.e. not the result of diagenesis) and records a carbon cycle perturbation of global extent. Especially striking is the similarity between our carbon isotope records from Muller Canyon, Nevada (Ward *et al.*, 2007) and the Queen Charlotte Islands, Canada (this study) in which a negative excursion of 2‰ in organic carbon coincident with boundary extinctions is immediately followed by a larger, protracted positive excursion extending through most of the Hettangian stage.

To our knowledge this is the first study that has examined a continuous record of stable carbon isotopes from the Norian into the Sinemurian. Tipper *et al.* (1991) tentatively placed the Hettangian–Sinemurian boundary at Kennecott point 70 m above the Tr–J boundary and reported *Badouxia* zone ammonites (*Badouxia columbiae*, *Badouxia canadensis*, *Vermiceras rursicostatum*) from 75 to 80 m above the Tr–J boundary. The first appearance of *Vermiceras* coincides with the base of the Sinemurian stage at the GSSP section at East Quantoxhead in West Somerset, England (Bloos and Page, 2002). If the appearance of *Vermiceras* (78 m above the Tr–J) marks the base of the Sinemurian stage at Kennecott Point, then this study includes approximately 60 m of Sinemurian strata.

3.2 Materials and Methods

Isotope samples came from Kennecott Point on the northwest corner of Graham Island in the Queen Charlotte Islands, British Columbia, Canada, and are contiguous with those from our previously published record (Ward *et al.*, 2001, 2004): to the best of our understanding, there are no missing intervals between the two sections. Samples were collected by hand from unweathered material exhumed from the section at metre to

sub metre intervals where possible. This sampling frequency seemed appropriate since the sampled strata contain intermittent turbidites, which would have increased the average sedimentation rate. Within the confines of this sampling scheme, preference was given to darker, more organic-rich rock over lighter, turbiditic, or organic-poor material.

The ratio of stable carbon isotopes ($^{13}\text{C}/^{12}\text{C}$) in sedimentary bulk organic matter (i.e. $\delta^{13}\text{C}_{org}$) was analyzed via elemental analyzercontinuous-flow isotope ratio mass spectrometry (EA-CFIRMS) at the Stable Isotope Research Facility (SIRF). SIRF is operated jointly by the Quaternary Research Center and the Astrobiology Program at the University of Washington.

Surface debris was removed from samples by treating for one hour in a water sonicator. Clean samples were split and ground to a fine powder in a rock-crushing mill. Glassware was baked overnight at 500°C to remove organic carbon. All equipment was washed with methanol between each sample to avoid organic contamination. Approximately one gram of each powdered sample was acidified with an excess of 10% HCl and allowed to react at 40°C for at least 12 hr to remove inorganic carbonate material, especially recalcitrant mineral phases such as siderite (FeCO_3). Samples were then triple rinsed with ultrapure ($>18\text{ M}\Omega$) deionized water and oven dried at 40°C . Isotope analyses were made with a Costech ECS 4010 Elemental Analyzer coupled to a ThermoFinnigan MAT 253 mass spectrometer via a ThermoFinnigan CONFLO III gas interface. Isotope ratios are reported in standard delta (δ) notation relative to Vienna Pee Dee Belemnite (VPDB), where $\delta^{13}\text{C} = [((^{13}\text{C}/^{12}\text{C})_{sample}/(^{13}\text{C}/^{12}\text{C})_{VPDB}) - 1] * 1000$. Average standard deviation of sample replicates was 0.18‰ for $\delta^{13}\text{C}_{org}$ (1σ ; $n = 181$). Average analytical precision based on routine analyses of internal laboratory reference materials was 0.15‰ for $\delta^{13}\text{C}_{org}$ (1σ).

3.3 Results

The extended isotopic record from the Kennebec Point section and its relationship to lithologic and biostratigraphic data are shown in Fig. 3.1. All new isotope samples and measured lithology are plotted above the stratigraphic section shown in Ward *et al.* (2001, 2004), which is based on markers permanently placed in the strata by the Geological Survey of Canada. The 0 mark in the Fig. is the approximate level of mean low tide (below this the section is covered by water), and the Norian bivalve *Monotis* can be found in the lowest 12 m. The Tr–J boundary is located between 108 and 111 m, and is defined by the coincident turnover in radiolaria and negative excursion in organic carbon isotope values (Ward *et al.*, 2001, 2004).

The most striking aspect of our new findings is a positive isotopic excursion beginning immediately above the top of the section previously presented in Ward *et al.* (2001, 2004). The positive excursion is defined by over twenty consecutive samples distributed over about 30 m of section and shows a 5‰ shift heavier than baseline values. At about 40 m above the Tr–J boundary values return to baseline levels of about -31‰ and show a gradual lightening of about 0.5‰ over the upper 90 m of sampled section.

3.4 Discussion

A gradual, negative trend over the course of all or part of the Kennebec Point carbon isotope record might be a result of volcanism associated with the opening of the Atlantic Ocean, especially in the Central Atlantic Magmatic Province (CAMP). CAMP would have released an estimated 8000–9000 Gt of moderately light CO₂ (-5‰) into the atmosphere over about 2 million years (Beerling and Berner, 2002). As a preliminary test, we divided the data into three intervals, the Rhaetian interval (I: 0 m to 109 m), the Boundary interval (II: 109 m to 162 m), and the Hettangian interval (III:

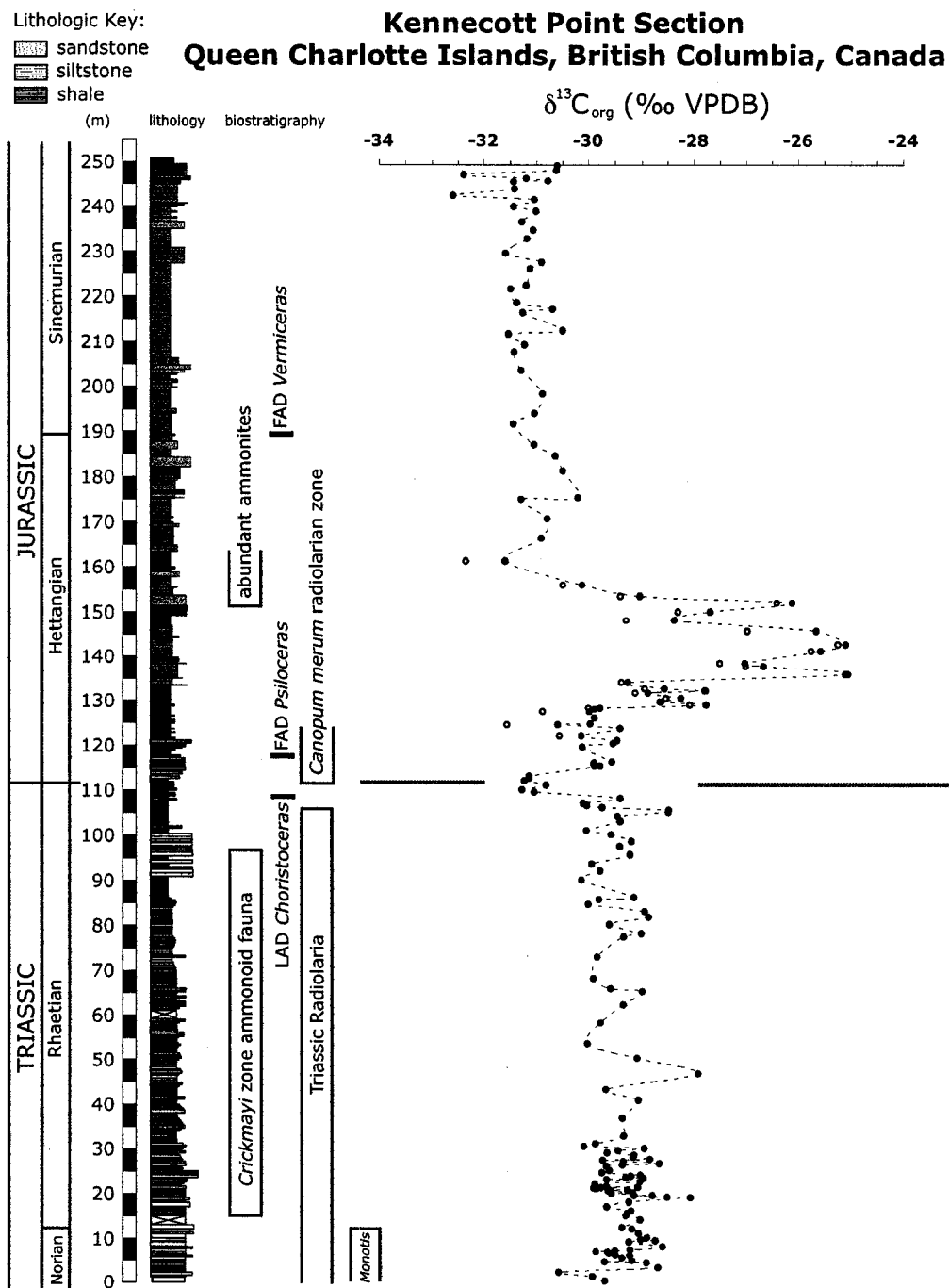


Figure 3.1: $\delta^{13}C_{org}$ record for Norian to Sinemurian strata on Kennecott Point, Queen Charlotte Islands, British Columbia, Canada. Biostratigraphy from Ward *et al.* (2001, 2004) and Tipper *et al.* (1991). Isotope values after double or triple acidification are indicated with open circles.

162 m to 250 m) and performed least squares regressions on intervals I and III (Fig. 3.2). The record can be viewed as two different, but relatively stable states (Rhaetian with a mean of -29.4‰ and standard deviation of $.46\text{‰}$ and Hettangian with mean of -31.2‰ and standard deviation of $.47\text{‰}$) interrupted by an interval of extinction- and recovery-related perturbation with mean of -29.1‰ and standard deviation of 1.77‰ . There is a negative isotopic trend in the Hettangian interval, significant at the 95% confidence level. Any such trend in the Rhaetian is shallower and statistically weaker overall. There is a -1.5‰ offset in the baseline value from the Rhaetian to the Hettangian interval. The low r^2 values for both the Rhaetian and Hettangian intervals indicate that there is a large amount of variability in the record not explained purely by the long-term trend, perhaps due to minor changes in organic matter source.

U-Pb dates of CAMP volcanics in the Newark and Fundy Basins suggest that peak volcanism occurred between 201.7 ± 1.3 Ma (Hodych and Dunning, 1992) and 200.9 ± 1 Ma (Dunning and Hodych, 1990). A tuff located several metres below major radiolarian turnover in the Queen Charlotte Islands gives a U-Pb age of 199.6 ± 0.3 Ma for the marine crisis, just after the peak of CAMP volcanism in North America. $\text{Ar}^{40}/\text{Ar}^{39}$ dates from North Africa suggest younger ages for the peak of CAMP volcanism, ranging from 199.5 ± 0.5 Ma (Knight *et al.*, 2004) to 198.1 (Verati *et al.*, 2005). The Kennecott Point isotope record shows that most of the long-term isotopic lightening, possibly due to CAMP volcanism, is concentrated in the Boundary and Hettangian intervals.

The large positive excursion, now the dominant feature in the Queen Charlotte Islands Tr-J record, is greater in magnitude than any other feature so far reported from stable carbon isotope studies of the Tr-J boundary. Because of the comparatively extreme isotope values, we took great care to determine if this signal is genuine or a result of carbonate contamination. Incomplete removal of carbonate material from

isotope samples can cause spurious, heavy isotope values. To resolve this question, we repeated the acidification process described above between one and three times for the 23 samples encompassing the positive excursion. The average change in isotope values after reacidification was -0.49‰ , and the overall pattern remained the same. Isotope values after double or triple acidification are shown as open circles in Fig. 3.1. Further acidification of all samples in this study (and others like it) might result in small changes to individual isotope values, but changes to the general trends discussed here are unlikely.

Fig. 3.3 shows a partial record from the Kennebec Point section aligned at the Tr–J boundary with the Muller Canyon section (Ward *et al.*, 2007) for comparison. Vertical distance and isotope values are shown to scale. The remarkable similarity in the carbon isotope records presented here and in the Ward *et al.* (2007) study indicate that the carbon isotope record for the Tr–J boundary can be a useful tool for regional and interregional stratigraphic correlation.

3.5 Relationship of the new results to the causes of the Late Triassic extinctions

The underlying causes for the Late Triassic extinctions and for the negative and positive carbon isotope excursions have yet to be adequately explained. The presence of multiple excursions makes the Triassic pattern different than the single negative perturbation recognized at the Cretaceous–Paleogene boundary (e.g. Kaiho *et al.* (1999)). Rather, the Tr–J isotopic record appears more similar to that recovered from the Permian–Triassic boundary, which shows a series of alternating negative and positive excursions (Payne *et al.*, 2004; Ward *et al.*, 2005).

While the large body impact scenario has been invoked for the Late Permian (Becker *et al.*, 2004) and Late Triassic events (Olsen *et al.*, 2002), evidence for both is equivocal. Existing geochemical records spanning the Permian–Triassic boundary do

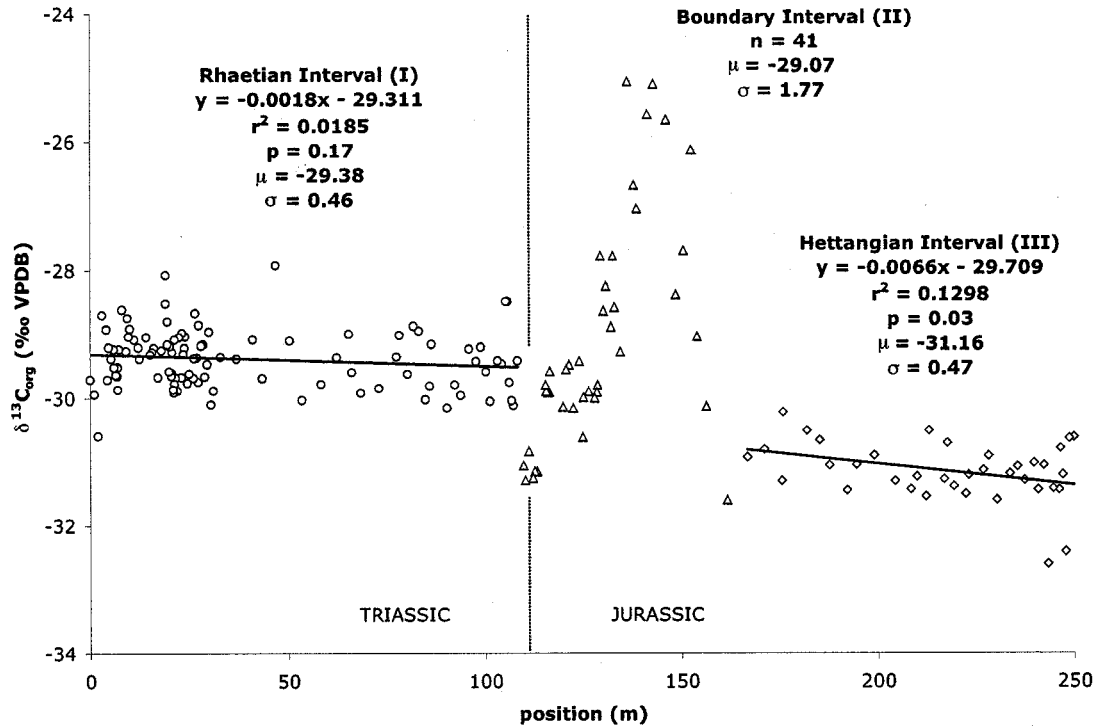


Figure 3.2: Stable organic carbon isotope data from Kennecott Point showing the results of least-squares regressions on the Rhaetian (I) and Hettangian (III) intervals. The Boundary (II) interval was defined as the sequence from the first data point in the negative excursion at the Tr-J boundary (109 m) to the last data point of the positive excursion and return to baseline values in the Jurassic (162 m).

not support the idea of a single, catastrophic event of extraterrestrial origin (Ward *et al.*, 2005; Koeberl *et al.*, 2004), and the several pieces of evidence for impact at the Tr-J (e.g. iridium anomalies, planar deformation features in mineral grains) are not present with enough geographical consistency or local abundance to be conclusive (Tanner *et al.*, 2004). New evidence for photic zone euxinia associated with super-anoxia (Grice *et al.*, 2005) and a dramatic expansion among the sulfate reducing

bacteria (Newton *et al.*, 2004) at the Permian–Triassic boundary indicates that Late Permian extinctions could have been caused by intrinsic mechanisms such as sulfide poisoning (Kump *et al.*, 2005), rather than extrinsic mechanisms such as impact.

We suggest that the Late Triassic extinctions had a similar set of intrinsic mechanisms, and we propose three explanations for the large positive excursion in $\delta^{13}\text{C}_{org}$. The first two explanations involve changes in microbial ecology during the Tr–J transition, whereas the third invokes limitation of biocalcification. An explosion of cyanobacterial populations in the wake of the Tr–J extinctions could have significantly lowered local dissolved inorganic carbon (DIC) (Thompson *et al.*, 2003) and caused a decrease in isotopic fractionation among the primary producers (O’Leary, 1981). There is evidence of such a microbial expansion associated with the Permian–Triassic extinction (Xie *et al.*, 2005), but the widespread microbialite facies associated with that boundary have not been found in Tr–J sections. Alternatively, a change in primary production regime from oxygenic photosynthesizers to anoxygenic photosynthetic sulfur bacteria could also have led to a decrease in carbon isotopic fractionation, as anoxygenic photosynthetic sulfur bacteria tend to show comparatively less fractionation than oxygenic photosynthesizers (Londry and Des Marais, 2003).

A third explanation for the positive excursion in $\delta^{13}\text{C}_{org}$ at Kennecott Point is that the decline among calcifying marine invertebrates during the Tr–J extinction led to a net decrease in the removal of isotopically heavy inorganic carbon from the marine carbon cycle with an associated increase in $\delta^{13}\text{C}_{org}$. Such a scenario would be plausible if a sudden increase in atmospheric CO_2 due to CAMP volcanism led to a biocalcification crisis at the Tr–J boundary (Galli *et al.*, 2005). Supporting this contention, Fig. 3.1 shows that first appearance of abundant ammonites and other shelly fossils coincides with a return to baseline $\delta^{13}\text{C}_{org}$ values. Indeed, a simple mass-balance calculation between carbonate and organic burial (cf. Summons and Hayes

(1992), Fig. 3.1.5) shows that, if prior to the Tr–J mass extinction marine $\delta^{13}\text{C}_{carb}$ was $\sim 0\text{‰}$ and $\delta^{13}\text{C}_{org}$ was $\sim -24\text{‰}$, then 75% of marine DIC was being buried as carbonate and 25% as organic carbon (with mean DIC at -6‰). If carbonate burial were reduced by a third (i.e. to 50% of total carbon burial), then $\delta^{13}\text{C}_{org}$ is forced to -18‰ . This assumes that total carbon burial remains constant, but if it decreases overall, then atmospheric PCO_2 increases, DIC increases and photosynthetic isotopic fractionation increases so that eventually the system settles down to a new equilibrium with isotopically heavier DIC and $\delta^{13}\text{C}_{org}$ near its initial composition.

Fig. 3.3 illustrates the similarity in the overall pattern in $\delta^{13}\text{C}_{org}$ between the Kennebec Point and Muller Canyon Tr–J sections, but it also highlights the difference in magnitude of the positive excursion and the slight difference in baseline values. We hypothesize that the Muller Canyon section represents a shallow water system dominated by changes in biocalcification, whereas the Kennebec Point section represents a deep water system dominated by microbial change. A survey of biomarkers in the organic-rich Tr–J rocks from Kennebec Point and other suitable sections should shed light on this question.

3.6 Acknowledgements

This work was funded by the NASA Astrobiology Institute, University of Washington node, Peter Ward, P.I., and we gratefully acknowledge that financial assistance.

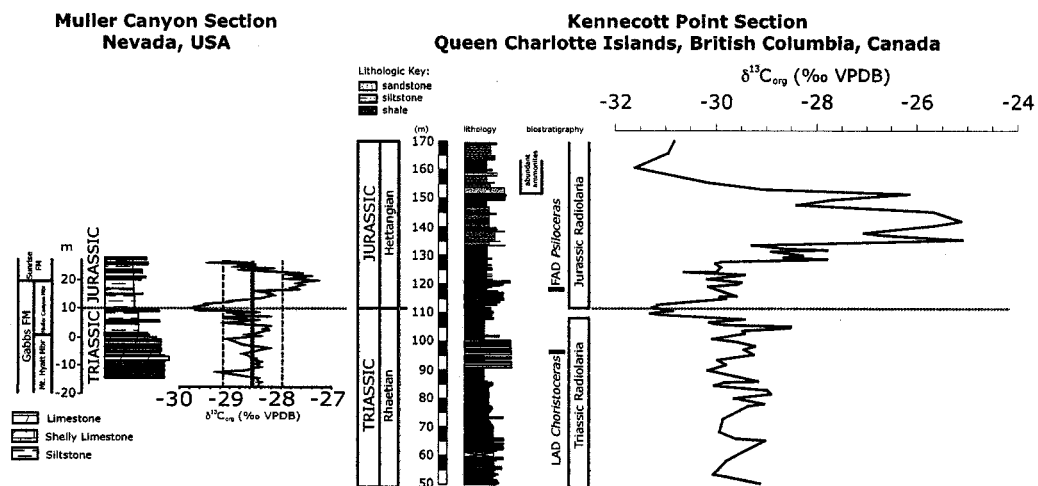


Figure 3.3: Comparison of $\delta^{13}C_{org}$ entire record from Muller Canyon (Ward *et al.*, 2007) and partial record from Kennecott Point. Sections are aligned at the Tr-J boundary. Vertical distance and isotope values are shown to scale.

Chapter 4

**A RECORD OF SULFIDE AND ORGANIC SULFUR
ISOTOPES ACROSS THE TRIASSIC–JURASSIC
BOUNDARY IN THE QUEEN CHARLOTTE ISLANDS,
BRITISH COLUMBIA, CANADA****4.1 Introduction**

The Triassic–Jurassic (Tr–J) boundary was one of the most extreme intervals of biodiversity loss in the Phanerozoic. Whether high extinction rates (Raup and Sepkoski, 1982) or low origination rates (Bambach *et al.*, 2004; Bambach, 2006) were the dominant factor in biodiversity reduction, this interval stands out as a major event in the history of life on Earth. The primary mechanism behind this diversity reduction is unknown. An iridium anomaly in the Newark Supergroup led Olsen *et al.* (2002) to suggest an impact kill mechanism, but supporting evidence for this scenario is lacking (Tanner *et al.*, 2004). The currently favored scenario is intrinsic to the Earth system and is fundamentally driven by an increase in atmospheric CO₂ associated with the emplacement of the Central Atlantic Magmatic Province (Hesselbo *et al.*, 2007; Marzoli *et al.*, 2004).

Like the other “big five mass extinctions,” the Tr–J boundary is accompanied by a significant perturbation in the global carbon cycle. Ward *et al.* (2001, 2004) reported a 2‰ negative excursion in $\delta^{13}\text{C}_{org}$ coincident with a sudden and comprehensive extinction among radiolaria (Carter and Hori, 2005) from the Tr–J boundary section at Kennecott Point in the Queen Charlotte Islands, British Columbia, Canada. Williford *et al.* (2007) extended the stable carbon isotope record from this section into the Sine-

murian, revealing a long term isotopic lightening from the Norian to the Sinemurian and a 5‰ positive excursion in $\delta^{13}\text{C}_{org}$ encompassing much of the Hettangian. The long term trend was attributed to the increase in atmospheric CO_2 that occurred as a result of volcanism associated with the opening of the Atlantic ocean, including the Central Atlantic Magmatic Province. Recent analyses of lipid biomarkers in boundary crossing samples from this locality imply an increase in terrigenous organic matter input (Williford *et al.*, unpublished data). This change would have contributed to the observed change in bulk organic carbon isotope ratios, as terrestrial organic matter is characteristically more enriched in ^{13}C than marine organic matter during times of high atmospheric CO_2 such as the early Jurassic (Arthur *et al.*, 1988).

Biogeochemical cycling of carbon and sulfur are tightly coupled – bacterial sulfate reduction (BSR) in marine sediments accounts for roughly half of the remineralization of organic carbon in Earth's oceans (Jørgensen, 1982). As such, it is not unreasonable to expect perturbations in the sulfur cycle to accompany those in the carbon cycle. We wished to test this prediction by analyzing the record of stable sulfur isotopes from the Tr–J boundary section reported on in Williford *et al.* (2007). There has, as yet, been no published account of stable sulfur isotope ratios across the Tr–J boundary.

Strauss (1997) reviews stable isotope studies of reduced sulfur across the Permian–Triassic, Cretaceous–Tertiary, and Frasnian–Famennian boundaries, and suggests a sequence of isotopic change that might be expected during intervals of mass extinction. When global biomass was reduced due to widespread extinctions, BSR would have decreased due to the decreased availability of organic carbon upon which it depends, leading to a negative trend in sulfur isotope values as less light sulfur was removed from seawater as pyrite. During the radiation following a mass extinction, global biomass would have increased, leading to an increased export of organic carbon to sediments, an increased rate of BSR, and an increase in the isotopic composition of

seawater sulfate as more isotopically light sulfur was exported to sediments (Strauss, 1997). Kajiwara and Kaiho (1992) found no negative isotopic trend in reduced sulfur associated with the Cretaceous–Tertiary boundary, but they reported a rapid increase from -28.4‰ to $+0.3\text{‰}$ in Danian rocks immediately overlying the boundary clay. Geldsetzer *et al.* (1987) found a negative excursion in stable reduced sulfur isotopes in the latest Frasnian, followed by a slow increase from -10‰ to $+5\text{‰}$ leading up to the boundary interval and a rapid increase to $+21\text{‰}$ within the boundary interval itself. Both of these excursions to heavier sulfur isotope values are attributed to anoxia, favorable living conditions for sulfate reducing bacteria, and sulfate-limited BSR with reduced isotopic fractionation.

Stable sulfur isotope ratios have been more widely reported from the Permian/Triassic (P–Tr) boundary (Kajiwara *et al.*, 1994; Worden *et al.*, 1997; Kaiho *et al.*, 2001; Maruoka *et al.*, 2003; Newton *et al.*, 2004; Korte *et al.*, 2004; Grice *et al.*, 2005; Kaiho *et al.*, 2006b,a), across which the largest mass extinction of the Phanerozoic occurred (Erwin, 1994). There is still no convincing evidence for impact at the P–Tr boundary, and like the Tr–J, the mechanism is uncertain (Benton and Twitchett, 2003). Also like the Tr–J, a large flood basalt province was emplaced at the boundary and has been implicated as the driving factor behind the extinctions (Renne *et al.*, 1995).

Two recent studies suggest that sulfur cycle anomalies may have provided an intrinsic kill mechanism at the P–Tr boundary. Modelling by Kump *et al.* (2005) demonstrated that, under conditions likely to have existed during oceanic anoxic events, H_2S concentration in the deep ocean could have increased as a result of increased BSR to such a degree that the chemocline separating oxygenated surface waters from euxinic (anoxic and sulfidic) deep waters would have rapidly risen to the surface. This so called “chemocline upward excursion” would have effectively eliminated what little oxygen there was in the surface ocean as it was consumed in reaction with reduced

sulfur (H_2S), resulting in a condition known as “photic zone euxinia.” Photic zone euxinia is a unique condition that can support anoxygenic photosynthetic green and purple sulfur bacteria of the Chlorobiaceae and Chromatiaceae, respectively, organisms that require light and H_2S to survive. Under normal ocean conditions, H_2S cannot survive in the oxygenated photic zone, as it is rapidly oxidized to SO_4^{2-} . In boundary-crossing samples from the P–Tr Hovea-3 and Meishan-1 cores from Western Australia and South China, respectively, Grice *et al.* (2005) reported abundant isorenieratane, a derivative of the carotenoid pigment isorenieratene and a biomarker for the Chlorobiaceae. Along with increases in aryl isoprenoids, vanadyl porphyrins, the ratio of pyrite to total iron, and stable isotopes of sulfur, this provided unequivocal evidence for photic zone euxinia at the P–Tr boundary.

The sulfur isotope record as it is currently known for the P–Tr is consistent with the occurrence of chemocline upward excursion and photic zone euxinia at the boundary. Building on the results of an earlier study, in which the authors attributed a 5‰ negative shift in carbonate-associated sulfate (a proxy for the isotopic composition of seawater sulfate) to the injection of mantle sulfur as a result of bolide impact (Kaiho *et al.*, 2001), Kaiho *et al.* (2006b) published similar isotopic results from South China and Hungary. In the more recent paper, the authors propose that the isotopically light sulfur could have come in the form of H_2S from a euxinic deep ocean.

Is there evidence for such changes in sulfur cycling at the Tr–J boundary? Were the Tr–J carbon cycle perturbations accompanied by perturbations in the sulfur cycle? We look to the record of stable sulfur isotopes to address these questions.

4.2 Materials and Methods

The ratio of sulfur stable isotopes ($^{34}\text{S}/^{32}\text{S}$) was measured by elemental analyzer continuous-flow isotope-ratio mass spectrometry (EA-CF-IRMS) at the ISOLAB, Uni-

versity of Washington. Sulfur species in the samples underwent flash combustion in a Eurovector elemental analyzer and were thus converted to SO_2 . Within the EA, SO_2 was separated by gas chromatography. A Thermo Finnigan Conflo III was then used to introduce the reference SO_2 and the sample SO_2 gas into a Thermo Finnigan MAT253 isotope-ratio mass spectrometer. Compared to other sulfur isotope mass spectrometry techniques (e.g. dual inlet), EA-CF-IRMS allows a much faster data output.

Finely grounded shale samples and sulfate and sulfide reference material (BaSO_4 internal laboratory standard and NIST-NBS127 and Ag_2S NIST-NZ1) were introduced in the EA packed in tin-foil cups. For each cup an amount of sample and standard corresponding to 50-100 μg of S was weighed and V_2O_5 (from 1mg for light samples up to 10-20 mg for the heaviest samples) was added to each cup to aid combustion.

The elemental analyzer configuration used here was similar to that described by Fry *et al.* (2002) and Baublys *et al.* (2004). Samples were dropped in a quartz reaction tube and small volume of O_2 was injected to induce the flash combustion. The reaction tube was packed with 8-10 cm of sulfur-grade copper wires used to reduced S oxides to SO_2 , framed by layers of quartz chips and quartz wool (Baublys *et al.*, 2004, see) and heated to 1050°C. A helium flow then flushed the sulfur dioxide through a second quartz tube heated to 890°C and packed with SiO_2 to buffer the oxygen isotopes in SO_2 . Any water was removed by a magnesium perchlorate column and SO_2 was purified in a 80 cm sulfur GC Teflon column heated at 80°C.

The analytical precision (1σ) measured on replicates of our internal laboratory standard during each run was $\leq 0.2\text{‰}$. The average analytical precision (1σ) on sample duplicates was higher (0.6 ‰) which we attribute to sample heterogeneity.

To test the relative isotopic contribution of various sulfur species, sample fractions

containing different sulfur species were isolated by chemical processing. The bulk fraction, with no chemical treatment, represents the sum of all possible S species within the samples: sulfide, sulfate, carbonate associated sulfate and organic-S. Carbonate-associated sulfates were removed from the HCl-washed fraction (2N hydrochloric acid, 36-72 hours at 60°C) leaving insoluble sulfates, sulfides and organic-S. A 5.5% NaClO treatment (12-24h, 60°C) was used on HCl-washed fractions to remove organics and retain only the insoluble sulfate and sulfide components. Finally, a nitric acid wash (6N HNO₃, 24-48h, 60°C) was used to oxidize sulfide and isolate a possible barite component. All nitric-acid washed samples showed barite sulfur levels below detection limits or too low (<0.03 wt.%) to significantly influence isotopic measurements. Insoluble sulfate contributions are thus ignored in the following discussion.

4.3 Results

Fig. 4.1 shows the record of $\delta^{13}\text{C}_{org}$ and $\delta^{34}\text{S}_{org+pyrite}$ across the Tr-J boundary. Table 4.1 shows the statistical distribution of stable sulfur isotope data. Statistics for the entire data set are shown along with those for the interval containing the large positive excursion from 134 m to 176 m, and for all data with the highly variable boundary interval from 94 m to 171 m removed. The last category is thought to represent “baseline” values for the section. The distinctions between these categories are based on a qualitative assessment of the variability in the isotope curve, and they facilitate a more nuanced, semi-quantitative statistical assessment of the variability within the sulfur isotope system than is possible by addressing only the total record as a whole.

There is a remarkable similarity in the general pattern of isotopic change between $\delta^{13}\text{C}_{org}$ (Williford *et al.*, 2007) and $\delta^{34}\text{S}_{org+pyrite}$ in this section. In general, the stable sulfur isotopes record two intervals of relative stability in sulfur cycling, each lasting

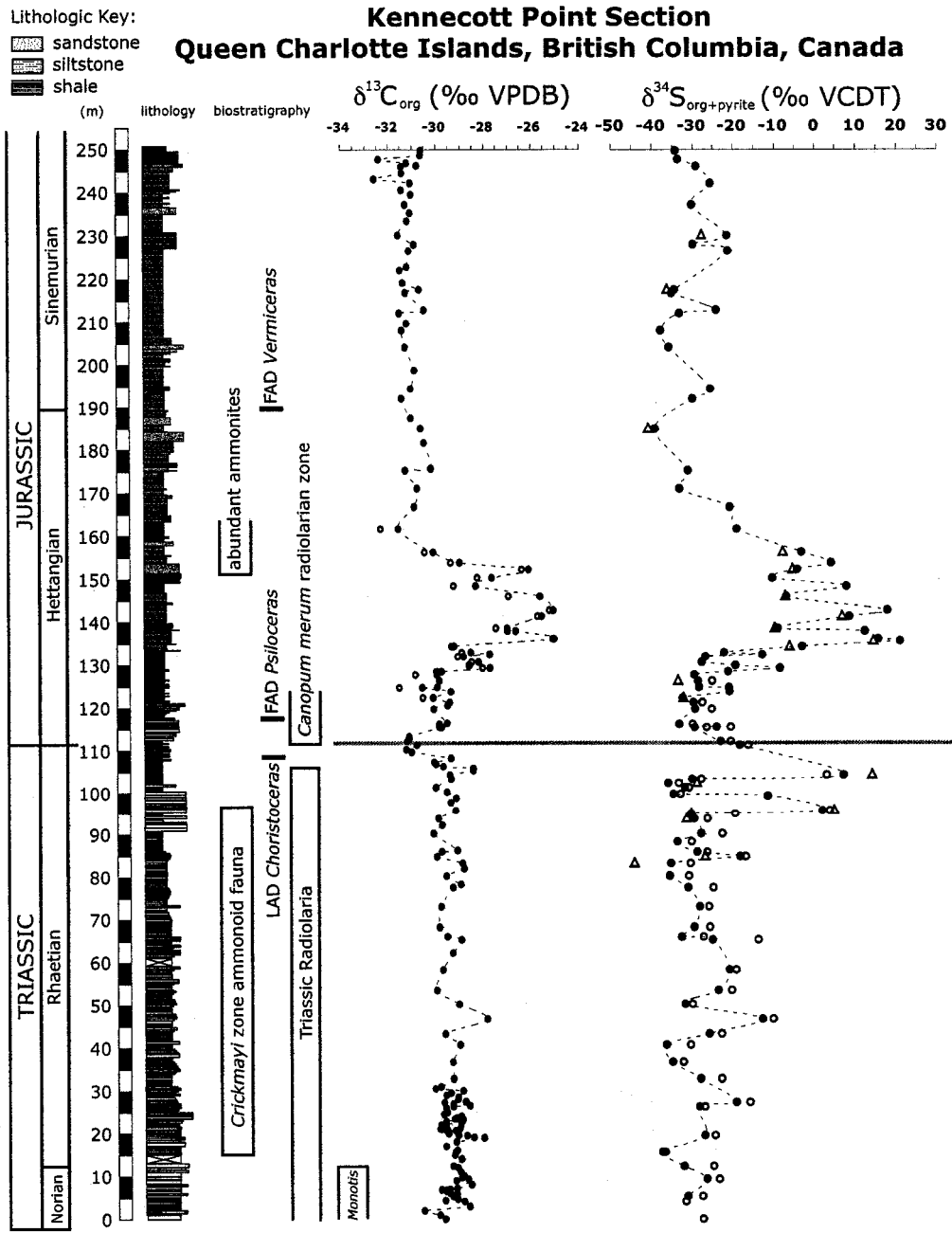


Figure 4.1: $\delta^{13}C_{org}$ and $\delta^{34}S_{org+pyrite}$ record for Norian to Sinemurian strata on Kennecott Point, Queen Charlotte Islands, British Columbia, Canada. Biostratigraphy from Ward *et al.* (2001, 2004) and Tipper *et al.* (1991). On $\delta^{34}S$ plot, solid circles indicate HCl-treated samples, open circles indicate untreated samples, and triangles represent bleach-treated samples.

Table 4.1: Statistical distribution of stable sulfur isotope data. μ and σ are shown for all data (1), for the interval containing the positive excursion in $\delta^{13}\text{C}$ and $\delta^{34}\text{S}$ (2), and for all data with the more variable “boundary interval” removed (3). All values are given for analyses performed after HCl-treatment, or $\delta^{34}\text{S}_{org+pyrite}$ (‰ VCDT).

subset	max	min	μ	σ
1. all data	20.55	-39.38	-22.66	13.97
2. 134m–176m	20.55	-33.45	-3.46	16.31
3. 0m–94m + 171m–250m	-13.31	-39.38	-29.71	5.62

several million years (based on the lengths of the Rhaetian (4 Myr) and Hettangian (3.1 Myr) stages given in Gradstein *et al.* (2004)), and interrupted by a shorter (1-2 Myr) interval of instability. This “boundary interval” begins in the latest Rhaetian with two apparent positive excursions, each somewhat dubious due to few isotopically heavy samples in these intervals. Values return to the baseline with a generally negative aspect across the Tr–J boundary itself. At 134 m in the section, approximately 22 m above the boundary as defined by the radiolarian turnover and negative excursion in $\delta^{13}\text{C}_{org}$, a large positive excursion begins in both the carbon and sulfur systems. The positive excursion in $\delta^{34}\text{S}_{org+pyrite}$ is interrupted by three finer scale negative shifts, the first and third of which are also apparent in the $\delta^{13}\text{C}_{org}$ record. Carbon and sulfur isotope values begin a return towards the baseline at 153 m, in strata that contain abundant Hettangian ammonites. The return to baseline is slower in sulfur isotopes than in carbon. Sulfur reaches an inflection point at 171.1 m, whereas carbon reaches a similar point nearly 10 m earlier, at 161.7 m. Above these inflection points, both isotopic systems remain stable into the Sinemurian and the top of the sampled section.

In an early report on the Hettangian ammonite succession found on Kennecott Point, Tipper and Guex (1994) report an interval of turbiditic “coarse sand” extending from 2 m to 70 m above the first *Psiloceras*. The positive excursions in $\delta^{13}\text{C}_{org}$ and

$\delta^{34}\text{S}_{\text{org+pyrite}}$ occur entirely in this stratigraphic interval. This study uses the more detailed report of lithologic change first reported in Williford *et al.* (2007) with the additional confirmation that a lithologic change occurs in the interval corresponding to the onset of the positive isotope excursions. During Hettangian–Sinemurian sample collection in 2001, it was observed that the green and black shale typical of the Late Triassic succession was only rarely present. There was a change to medium grained silts weathering tan to green, with beds ranging in thickness from 2 to 25 cm and containing abundant woody debris. Sandstone beds increase in frequency, and the rare, intermittent occurrence of laminated black shales is noted throughout this interval.

Fig. 4.2 shows $\delta^{34}\text{S}_{\text{org+pyrite}}$ and weight percent sulfur. There is no apparent relationship between sulfur content and isotopic composition, and there are no obvious trends in sulfur content across the Tr–J boundary. Fig. 4.3 shows the lack of relationship between TOC and weight percent sulfur in these samples.

Carbonate-associated sulfate and barite are both thought to reliably record the isotopic composition of seawater sulfate (Kampschulte and Strauss, 2004) and will, therefore, have an isotopic composition significantly heavier than reduced sulfur precipitated under normal conditions for BSR. Untreated samples are predictably isotopically heavier than those treated with HCl to remove carbonate material, though the difference is typically quite small, suggesting that there is little carbonate-associated sulfate material in these samples. Reduced sulfur is also incorporated into organic matter in the water column or in marine sediments with little or no isotopic fractionation to form organic sulfur compounds (Werne *et al.*, 2003). Samples treated with bleach to remove organic sulfur compounds are generally very isotopically similar to acid treated samples, suggesting that most organic sulfur present was formed from sulfide in marine sediments. Where bleach treated samples show lighter values than

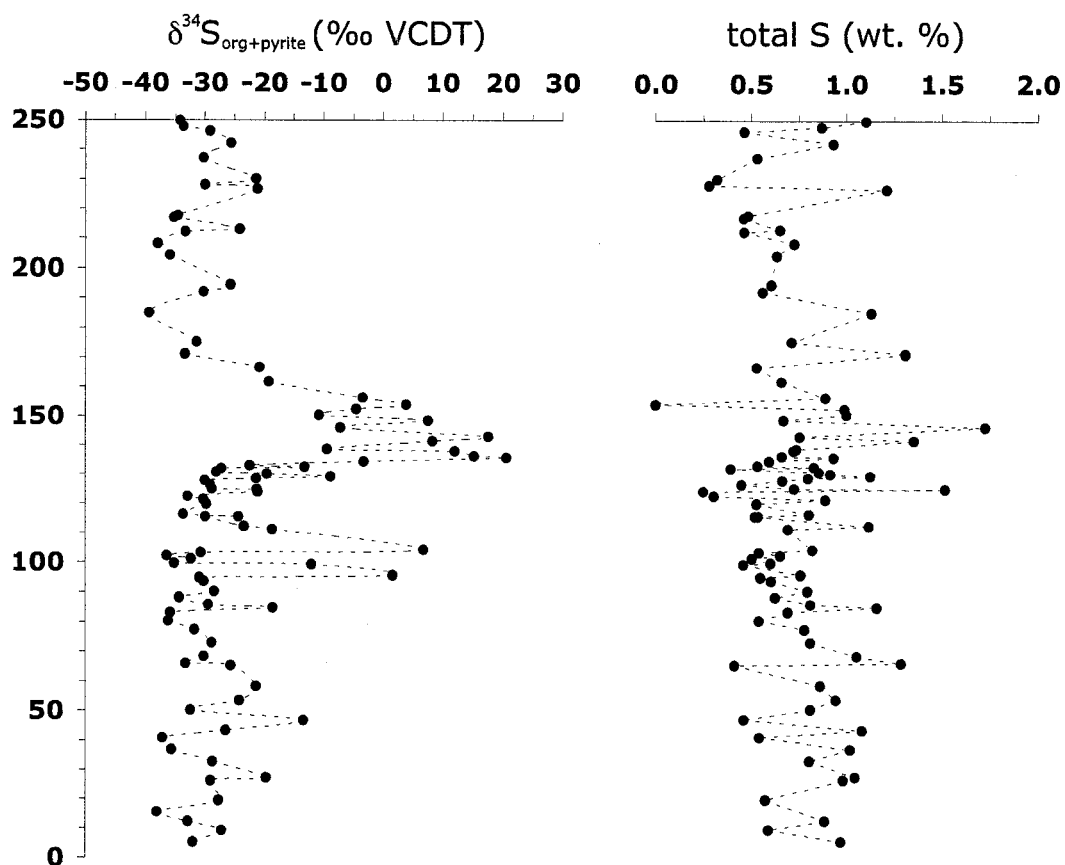


Figure 4.2: $\delta^{34}\text{S}_{\text{org+pyrite}}$ and weight percent sulfur for Norian to Sinemurian strata

acid treated samples, it could be due to the presence of organic sulfur compounds produced in the water column by assimilation of isotopically heavy seawater sulfate.

4.4 Discussion

This sulfur species measured in this study are a mix of organic and pyrite sulfur, both the direct or indirect products of biological activity in marine sediments and to a lesser extent, in the overlying water column. Pyrite is a byproduct of BSR as organisms

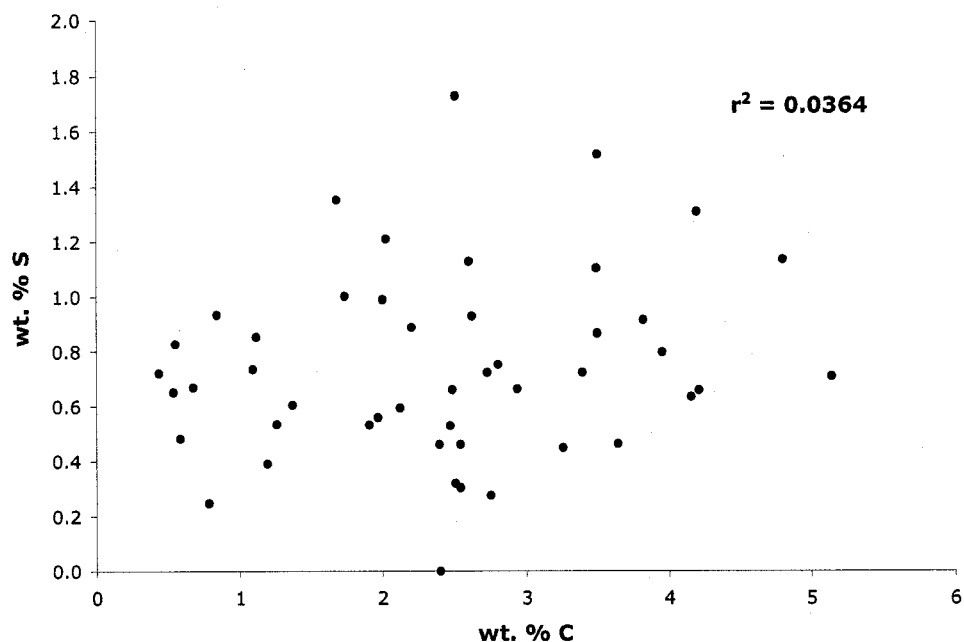


Figure 4.3: TOC vs. weight percent sulfur

reduce dissolved SO_4^{2-} using organic carbon as a substrate. Eqn. 4.1 (Berner, 1984) shows the generalized pathway for BSR, yielding reduced sulfur that reacts with iron to form pyrite.



BSR requires SO_4^{2-} as an electron acceptor and reduced carbon as an electron donor (though H_2 can also be used as an energy source (Meynigal *et al.*, 2003)). When SO_4^{2-} is not limiting, environmental BSR imparts an isotopic fractionation of between 16‰ and 46‰, and fractionation of up to 70‰ can occur in modern

marine sediments where sulfur species pass through several cycles of intermediate reduction (Canfield and Raiswell, 1999). SO_4^{2-} becomes limiting for BSR below 2 mM (Boudreau and Westrich, 1984), and when $[\text{SO}_4^{2-}]_{\text{seawater}}$ falls below 0.2 mM, isotopic fractionation is less than 10‰ (Habicht *et al.*, 2002). Under typical marine conditions, BSR proceeds as an open system, with fresh SO_4^{2-} constantly diffusing to the zone of sulfate reduction from the overlying water column. Under favorable conditions for sulfate reducing bacteria, however, when anoxia and high productivity conspire to deliver labile organic carbon to the zone of sulfate reduction at a rate that exceeds sulfate supply, closed system conditions and Rayleigh fractionation can ensue (Strauss, 1997). Under these conditions, the dissolved sulfate pool becomes progressively enriched in ^{34}S , driving the isotopic composition of the resulting pyrite to heavier values over time. This situation can result in isotopic compositions of sulfides that are heavier than seawater sulfate (Strauss, 1997). Extremely rapid deposition in turbidity flows may also result in transient closed system conditions for BSR (e.g. Meyers *et al.*, 1996).

4.4.1 Isotopic composition of Triassic–Jurassic seawater sulfate

We assume that the dominating factors controlling the isotopic compositions we observe to be the composition of seawater $\delta^{34}\text{S}_{\text{sulfate}}$ and the isotopic fractionation imparted by BSR. To assess the former effect in the absence of sulfate sulfur isotope data for these samples, we must rely on sulfur isotope measurements from marine sulfates elsewhere in the world. Since there is only a minor (0 to +2.4 ‰) fractionation effect associated with the evaporative precipitation of sulfate minerals such as anhydrite (Ault and Kulp, 1959; Raab and Spiro, 1991), the sulfur isotope composition of an evaporite deposit is a reliable proxy for the isotopic composition of seawater sulfate from which it precipitated. In the first compilation of a sulfur isotopic age curve for

the Phanerozoic, Claypool *et al.* (1980) added new data confirming earlier reports (Müller *et al.*, 1966; Pilot *et al.*, 1972) of a Middle Triassic through Late Jurassic evaporite $\delta^{34}\text{S}_{\text{sulfate}}$ of $16 \pm 1.5\text{‰}$. A more recent compilation by Kampschulte and Strauss (2004) including evaporites as well as structurally substituted sulfate in biogenic and whole rock carbonates found the Tr–J transition to be a time of significant change in the isotopic composition of seawater sulfate. Running averages suggest that mean evaporite sulfur isotopic composition increased from 13.9‰ in the Rhaetian to 19.1‰ in the Hettangian. Structurally substituted sulfates remain more constant at relatively low values across the boundary (15.9‰ to 15.8‰), but increase through the early Jurassic to a Toarcian high of 19.2‰ . Anhydrites from the Argo Salt, a large, Late Rhaetian to Early Sinemurian evaporite formation deposited in the Grand Banks Basin offshore of eastern Canada, show $\delta^{34}\text{S}$ values from 12.1‰ to 14.6‰ Holser *et al.* (1988).

Taking a representative Tr–J $\delta^{34}\text{S}_{\text{sulfate}}$ value of 15‰ , the $\delta^{34}\text{S}_{\text{org+pyrite}}$ values observed in this study represent isotopic fractionation of between $+5\text{‰}$ and -55‰ for sulfate reduction. At the early Hettangian peak of the positive excursion in $\delta^{34}\text{S}_{\text{org+pyrite}}$, isotope values exceed any so far reported for Early Jurassic evaporites, suggesting either a previously undocumented increase in global seawater sulfate isotope values and a decrease in the fractionation effect of BSR due to decreasing global seawater sulfate concentration, local effects including a shift to closed system conditions and Rayleigh fractionation in the sediment, or a combination of these conditions.

Berner (2004) uses the basic mass balance shown in Eqn. 4.2 to model changes in seawater SO_4^{2-} concentration during the Phanerozoic. Model results imply that seawater sulfate concentrations decreased across the Tr–J boundary to an earliest Jurassic minimum of approximately 11 mM, the lowest value in the last 350 Myr.

$$\frac{d[SO_4]}{dt} = F_{wmp} + F_{wms} - F_{bp} - F_{bs} \quad (4.2)$$

Where $[SO_4]$ = mass of sulfate-sulfur in the oceans

F_{wmp} = weathering and metamorphic/volcanic release of pyrite sulfur

F_{wms} = weathering and metamorphic/volcanic release of calcium sulfate sulfur

F_{bp} = burial of pyrite sulfur in sediments

F_{wmp} = burial of calcium sulfate sulfur in sediments

$[SO_4^{2-}]_{seawater}$ can decrease, then, with a decrease in the weathering influx of pyrite or sulfate, or with an increase in the burial flux of pyrite or sulfate. Weathering fluxes are controlled largely by atmospheric conditions, and a decline in atmospheric oxygen or increasing aridity could lead to a decreased weathering flux of sulfur species. Paleosols and evaporites in the Pangean interior suggest arid conditions across the Tr–J boundary (Olsen, 1997), but palynological evidence from Greenland (McElwain *et al.*, 1999) and clay mineralogy from Sweden (Ahlberg *et al.*, 2003) imply an Early Jurassic return to humid conditions. Though anoxic conditions occur at and before the Tr–J boundary in the Queen Charlotte Islands, there is lipid biomarker evidence for increased oxygenation in the Hettangian (Williford *et al.*, unpublished data), and independent evidence for a decline in atmospheric oxygen and global anoxia at this time is lacking (McRoberts *et al.*, 1997; Hallam and Wignall, 1999; Pálffy *et al.*, 2001; Hesselbo *et al.*, 2004). The burial flux of pyrite is controlled by the rate of BSR, and the burial flux of sulfate is controlled by the rate of evaporite deposition, considered in further detail below.

4.4.2 *Triassic–Jurassic rifting and evaporite deposition*

The breakup of Pangea began in a series of about 40 rift basins that formed at the intersection of the American and Moroccan plates in the Late Triassic and Early Jurassic (Manspeizer, 1988), and the Atlantic Ocean developed in this region in a diachronous sequence of “rift and drift cycles” (Withjack *et al.*, 1998). Where the floors of the shallow rift basins dipped below sea level, they were accompanied by intermittent southeastward incursions of the Tethys, and large evaporite provinces were deposited (Manspeizer, 1988; Holser *et al.*, 1988). Holser *et al.* (1988) reviewed these evaporite provinces, finding that North Atlantic rift evaporite deposition commenced in Carnian–Norian time under dominantly continental conditions, the first incursions of the Tethys occurred during the Rhaetian–Hettangian transition, marine evaporite deposition peaked in the Hettangian with the deposition of the Argo Salt, and most evaporite deposition was rapidly cut off during a eustatic sea-level rise beginning in the Late Hettangian to Early Sinemurian (Hallam, 1984). Hettangian evaporites are predominantly composed of halite with rare anhydrite horizons, which may reflect an ocean already relatively depleted in sulfate, a condition that appears to have changed later in the Early Jurassic with the localized deposition of the predominantly anhydrite sequences of the Iroquois Formation (Holser *et al.*, 1988).

4.4.3 *Mass balance calculations*

The 200 Ma estimate for $[\text{SO}_4^{2-}]_{\text{seawater}}$ from the best match model run reported in Berner (2004) is approximately 11 mM. Taking this value as the long term baseline concentration, an amount of $[\text{SO}_4^{2-}]_{\text{seawater}}$ equivalent to a 10.8 mM concentration must be removed from the ocean to bring $[\text{SO}_4^{2-}]_{\text{seawater}}$ to 0.2 mM and cause isotopic fractionation during BSR to fall below 10‰. Given a modern mass of sulfate in the oceans of 3.79×10^{18} kg, a concentration of 28 mM, and a slightly larger ocean volume

in the Jurassic (1.39 vs. $1.37 \times 10^9 \text{ km}^3$) (Hay *et al.*, 2006), a 10.8 mM equivalent represents $1.46 \times 10^{18} \text{ kg}$ additional sulfate that must have been removed from the ocean to bring $[\text{SO}_4^{2-}]_{\text{seawater}}$ to 0.2 mM . The onset of the positive excursion occurs over the 2.7 m interval between 132.9 m and 135.7 m . If the entire 250 m of section represents 8 Myr (4 Myr Rhaetian, 3 Myr Hettangian, 1 Myr Sinemurian time) then 2.7 m represents 86.4 kyr . A flux of $1.72 \times 10^{13} \text{ kg/yr}$ would be necessary to remove the required quantity of sulfate in that amount of time. This is two orders of magnitude higher than the depositional flux of evaporitic halite during the Early Jurassic estimated using masses published in (Hay *et al.*, 2006) ($3.98 \times 10^{18} \text{ kg}$ in 24 Ma , or $1.66 \times 10^{11} \text{ kg/yr}$). Given that the ratio of halite to gypsum in evaporites is typically $1:0.25$, this scenario seems unlikely to have been completely responsible for the observed change in $\delta^{34}\text{S}_{\text{org+pyrite}}$. The flux calculated here can be considered a maximum estimate, though, as it is possible that the reduction in $[\text{SO}_4^{2-}]_{\text{seawater}}$ occurred over a longer period of time, and the 2.7 m interval of greatest isotopic change represents only the final interval of depletion beyond the threshold representing the onset of sulfate limiting conditions for BSR.

4.5 Conclusions

Stable sulfur isotopes of organic and pyrite sulfur were measured from the Tr–J section at Kennecott Point, Queen Charlotte Islands, British Columbia, Canada. A positive excursion of nearly 50‰ (VCDT) occurs over the same interval as the 5‰ positive excursion in $\delta^{13}\text{C}_{\text{org}}$ reported by Williford *et al.* (2007). Several finer scale features are evident in both the carbon and sulfur records, including two short term negative shifts that punctuate the positive excursion. Baseline values for the stable intervals (Late Norian to Late Rhaetian and Late Hettangian to Sinemurian) (μ : -39.38‰) imply a well-developed sulfur cycle with recycling of intermediate sulfur species during

bacterial sulfate reduction (BSR) and pyrite formation. Values in the Early Hettangian approach and then exceed those previously reported for Early Jurassic seawater sulfate ($\sim 15\text{‰}$).

Peak evaporite deposition in the Hettangian would have lowered $[\text{SO}_4^{2-}]_{\text{seawater}}$ considerably. This factor, combined with an increase in turbiditic deposition evident in the Hettangian rocks at Kennecott Point, likely led to intermittent, local decoupling of the zone of sulfate reduction in sediments from the water column and an onset of Rayleigh fractionation, driving the isotopic composition of sulfides and organic sulfur towards higher values. These conditions were reversed as the Late Hettangian–Early Sinemurian global transgression (Hallam, 1984) led to the shut down of evaporite deposition (Holser *et al.*, 1988), a return of higher global $[\text{SO}_4^{2-}]_{\text{seawater}}$ concentrations, and less turbiditic deposition locally. Stable sulfur isotope analyses of carbonate-associated sulfates from this locality and others across the Tr–J boundary will offer a valuable complement to the data presented here, providing a more comprehensive picture of the behavior of the global sulfur cycle during this critical interval in the biogeochemical evolution of the planet.

4.6 Acknowledgements

This work was funded by the NASA Astrobiology Institute, University of Washington node, Peter Ward, P.I., and we gratefully acknowledge that financial assistance. Julien Foriel developed the methods for and performed the sulfur isotope analyses and made significant contributions to this manuscript.

Chapter 5

ORGANIC GEOCHEMISTRY OF A TRIASSIC–JURASSIC BOUNDARY SECTION IN THE QUEEN CHARLOTTE ISLANDS, BRITISH COLUMBIA, CANADA

5.1 Introduction

Following the work of Ward *et al.* (2001, 2004) which revealed for the first time a reliable negative excursion in stable organic carbon isotope ratios associated with fossil turnover at the Triassic–Jurassic (Tr–J) boundary, a much larger and protracted positive carbon isotope excursion was identified just after the boundary (Williford *et al.*, 2007). At the time of publication, this was the largest carbon isotope feature yet uncovered at the Tr–J boundary, and it raised interesting questions about the behavior of the carbon cycle during one of the five most significant intervals of biodiversity loss in the Phanerozoic (Raup and Sepkoski, 1982; Tanner *et al.*, 2004; Bambach, 2006). One hypothesis offered by Williford *et al.* (2007) was that the large, positive isotope excursion was the result of changes in microbial ecology associated with Tr–J extinction and recovery. A survey of molecular fossils, or biomarkers, was conducted to test this hypothesis and to better understand the composition of the sedimentary organic matter that had been analyzed for bulk stable organic carbon isotopes in previous studies.

Several previous studies have investigated the organic geochemistry and petrology of the Queen Charlotte Basin to determine the potential for oil and gas exploration in this area (Bustin and Macauley, 1988; Vellutini and Bustin, 1990; Bustin, 1997). Bustin and Mastalerz (1995) studied the Triassic and Jurassic rocks of the Sandilands

and Ghost Creek formations specifically and found them both to be rich in oil-prone organic matter, though only the Sandilands Formation has sufficient aerial extent to lead to significant hydrocarbon generation and accumulation in the basin.

The increasingly widespread application of stable carbon isotope stratigraphy to intervals of mass extinction in the Phanerozoic has revealed that these intervals were accompanied by perturbations in the global carbon cycle (Young *et al.*, 2005; Yans *et al.*, 2007; Payne *et al.*, 2004; Williford *et al.*, 2007; Beerling *et al.*, 2001). These perturbations are typically identified as excursions away from baseline carbon isotope values. Interpretations of these carbon isotope excursions vary, and to what degree carbon cycle perturbations represent cause or effect of mass extinctions remains an open question. Kump and Arthur (1999) offers an excellent model-driven review of this question. If carbon isotopes are to be used as a proxy for changes in the ocean-atmosphere system, certain factors must be constrained. For inorganic carbon, the primary confounding factors are diagenesis and vital effect. For organic carbon, changes in source inputs and maturity of organic matter can lead to changes in bulk carbon isotope values that are unrelated to changes in ocean-atmosphere chemistry. The widely varying biochemical pathways used by different organisms impart different characteristic isotopic fractionation effects, and change through time in the contribution of different organisms to sedimentary organic matter can change the bulk isotopic composition (Hayes *et al.*, 1989; Hayes, 2002).

The most comprehensive way to assess changes in organic matter composition in sedimentary rocks includes the extraction of organic matter, separation into compound classes by liquid chromatography, and analysis of these fractions by gas chromatography-mass spectrometry. In addition to providing some constraints on changes in organic matter source, these techniques have the potential to provide useful information about the behavior of microbial communities during mass extinctions (Grice *et al.*, 2005; Xie

et al., 2005; Wang, 2007).

5.2 Materials and Methods

Seventeen rock samples, ranging in age from Norian to Sinemurian, were chosen for organic geochemical analysis in order to give total age coverage for the section and particularly for intervals of bulk isotopic change at and above the Tr–J boundary. All glassware was combusted overnight at 500°C. Tools were rinsed three times with hexane and dichloromethane (DCM). Samples were broken with a hammer and chisel to remove any weathered exterior surfaces. Each sample was sonicated for 45 minutes in deionized water, then in hexane, and finally in methanol to remove any exterior organic contamination. Clean samples were ground using a vibrating puck mill, which was cleaned between each sample by grinding combusted quartz sand and rinsing with deionized water, hexane, and methanol. Not all samples were analyzed quantitatively (by using recovery and quantification standards), and organic geochemical techniques were undertaken in two different laboratories (Stuart Wakeham's laboratory at the Skidaway Institute of Oceanography, Savannah, Georgia, and Julian Sachs laboratory at the University of Washington School of Oceanography, Seattle, Washington). The comprehensive, quantitative method that resulted is described below, though some of the data reported in this study resulted from earlier variations on this method.

Between 3 and 10 g of each sample was weighed and transferred to a mortar and pestle. Aromatic (C_{25} and benz[e]acephenanthrylene) and aliphatic (n - C_{37} alkane) recovery standards were added to the powdered sample and mixed into the sample with combusted quartz sand. Soluble organic matter was extracted using a 9:1 mixture of dichloromethane (DCM) and methanol at 100°C and 1500 psi for three cycles of 15 min each on an accelerated solvent extractor. Total lipid extracts were dried under a stream of nitrogen gas on a Turbovap. Elemental sulfur was removed by

dissolving the extract in DCM and passing the solution in a small pasteur pipette through activated copper filings. Desulfurized extracts were dried under a stream of nitrogen and brought up in 1 ml of DCM. 25% of this solution was transferred to a liquid chromatography column containing activated silica gel, alumina, and combusted quartz sand and pre-eluted with hexane. An apolar fraction was collected by eluting with 50 ml 9:1 hexane:DCM. An aromatic fraction was collected by eluting with 90 ml 1:1 hexane:DCM. A polar fraction was collected by eluting with 50 ml 1:1 DCM:methanol. The fractions were dried, 50% of each of the aliphatic and aromatic fractions was transferred in DCM to a gas chromatography vial with a combusted glass insert, and *n*-C₃₆alkane quantification standard was added to each vial. 20% of each sample was manually injected onto a HP 6890 gas chromatograph interfaced to a HP 5973 MSD. The column used was an Agilent 123-5562 DB-5MS fused silica capillary column (58.9 m x 320 μ m i.d.) with a 0.25 μ m 5% phenyl-methyl-silicon stationary phase (DB-5). The gas chromatograph oven was programmed from 60°C to 325°C at 15°C/min to 150°C and 6°C/min to 325°C with a hold time of 35 minutes. The carrier gas used was helium at a linear velocity of 1.6 ml/min.

Stable carbon isotope ratios of bitumen and kerogen were measured using a Costech ECS 4010 Elemental Analyzer coupled to a ThermoFinnegan MAT 253 isotope ratio mass spectrometer via a CONFLO III gas interface. Isotope ratios are reported in standard delta (δ) notation relative to Vienna Pee Dee Belemnite (VPDB), where $\delta^{13}\text{C} = [((^{13}\text{C}/^{12}\text{C})_{\text{sample}} / (^{13}\text{C}/^{12}\text{C})_{\text{VPDB}}) - 1] * 1000$. Samples were calibrated against an acetanilide internal laboratory standard ($\delta^{13}\text{C} = -30.38\text{‰}$ VPDB). For kerogen analyses, solvent-extracted rock powder was removed from the solvent extractor cells and treated with an excess of 10% HCl at 40°C for 48h to remove carbonates. Samples were then triple rinsed with ultrapure (>18 M Ω) deionized water and dried at 40°C. Approximately 40 μ g of dried total lipid extract was used for isotope analyses of

bitumen.

5.3 Results

Basic geochemical data are listed in Table 5.1. Total organic carbon (TOC) and bulk $\delta^{13}\text{C}_{org}$ for all samples was reported in previous studies (Ward *et al.*, 2001, 2004, this study, Fig. A.1). TOC ranges from 1.1% to 13.2% organic carbon by weight with an average of 5.2% (Fig A.1). The highest TOC values come from the 7601 samples, collected by David Kring in 2001 at centimeter scale and selected for dark shale laminae thought to have the highest organic content. $\delta^{13}\text{C}_{org}$ ranges from -32.1‰ (at the peak of the Tr-J boundary negative excursion) to -25.1‰ (at the peak of the Hettangian positive excursion), with an average of -29.4‰. Pristane (Pr) is the dominant regular isoprenoid, and in most cases where it is clearly present is more abundant than the $n\text{C}_{17}$ alkane. Phytane (Ph) is generally less abundant than the $n\text{C}_{18}$ alkane, and in most samples the ratio of pristane to phytane is close to 1.0. The notable exception to the latter case is the dramatic increase in Pr/Ph that occurs associated with the Hettangian positive excursion in $\delta^{13}\text{C}_{org}$, where the ratio increases to 8.3 (Fig. 5.13). The ratio of 20*S* to 20*R* enantiomers of the regular C_{29} sterane are used as a measure of maturity (Seifert and Moldowan, 1986). The average value of the 20*S*/(20*R*+20*S*) index for this section is 0.46, supporting low thermal maturity for these samples. Coelution of hopanes and alkanes as well as the large unresolved complex mixture (UCM) in many samples made it difficult to identify discrete peaks for *n*-alkanes in the total ion chromatogram. Discrete peaks are readily identifiable on the major ion chromatograms for these compound classes, however. In order to semiquantitatively assess the relative contribution of hopanes and alkanes throughout the section, the integrated peak area for the C_{30} hopane on the *m/z* 191 fragmentogram was compared to the integrated peak area for the *n*- C_{29}

alkane on the m/z 57 fragmentogram. Typical values for the section are between 5 and 7. This ratio increases to 58.1 in the sample just before the Tr–J boundary, coincident with the onset of the negative excursion in bulk $\delta^{13}\text{C}_{org}$, decreases to 0.1 in the Hettangian at the peak of the positive excursion in bulk $\delta^{13}\text{C}_{org}$, and increases to 15 at the top of the section in the Sinemurian.

5.3.1 Source Integrity

The stable carbon isotopic compositions of bitumen (dried total lipid extract) and kerogen (solvent-extracted and HCl acidified rock powder) were measured and compared to the isotopic composition of total organic carbon ($\delta^{13}\text{C}_{org}$, HCl acidified rock powder) reported in earlier studies (Ward *et al.*, 2001, 2004; Williford *et al.*, 2007) as a preliminary test for bitumen authigenicity, and the results are given in Table 5.2. While the authigenicity of kerogen is rarely in question, bitumen can migrate through porous rocks. If bitumen is allocthonous, the molecular fossils it contains cannot be used as indicators of paleoenvironment at the time of deposition. It is common for bitumen to be isotopically depleted by several permil relative to kerogen (Love *et al.*, 1998), but widely varying isotopic compositions across the organic phases could be due to bitumen migration. Preliminary analyses of several samples in this study show the average difference between kerogen and total organic carbon to be -0.3‰ ($n=7$), the average difference between bitumen and kerogen to be -1.2‰ ($n=3$), and the average difference between bitumen and total organic carbon to be -1.7‰ ($n=3$). This relatively close agreement is a preliminary indication that the bitumen is authigenic, and that isotopic and molecular trends are indicative of syndepositional, rather than late diagenetic effects.

Table 5.1: Summary of organic geochemical data for samples in this study. TOC is weight % organic carbon reported in previous studies. $\delta^{13}\text{C}_{org}$ is bulk stable organic carbon isotope data reported in previous studies. Errors shown are 1σ . Pr: Pristane, Ph: Phytane, $n\text{-C}_{17}$ and $n\text{-C}_{18}$ are normal alkanes with 17 and 18 carbon atoms, respectively. $20S/(20R+20S)$ is the ratio of the 20S epimer to the sum of the 20R and 20S epimers of the C_{29} regular sterane. $\text{H30}/n\text{C}_{29}$ is the ratio of peak integrations from the C_{30} hopane peak on the m/z 191 fragmentogram to the C_{29} n -alkane on the m/z 57 fragmentogram.

Section	ID	position (m)	TOC (wt.%)	$\delta^{13}\text{C}_{org}$ (‰ vpdb)	Pr/ $n\text{-C}_{17}$	Ph/ $n\text{-C}_{18}$	Pr/Ph	20S/ (20R+20S)	H30/ $n\text{-C}_{29}$
QCIJ	238	240.6	4.6%	-31.4 ± 0.0	1.3	1.0	1.1	0.46	15.0
QCIJ	187	204.2	4.1%	-31.3 ± 0.1			1.4	0.38	7.2
QCIJ	99.5	146.0	2.5%	-25.7 ± 0.0	1.4	0.3	8.3		0.1
QCIJ	91.4	142.8	2.8%	-25.1 ± 0.0	1.4	0.3	8.3		0.2
QCIJ	78.7	138.6	1.1%	-27.0 ± 0.0	1.1	0.8	0.9		0.4
QCIJ	55	132.9	1.4%	-28.6 ± 0.1					5.5
QCI99	3.1	119.8	5.0%	-30.1 ± 0.3	0.4	0.7	0.8	0.38	6.9
QCI99	16	116.3	3.6%	-29.9 ± 0.1	0.7	0.7	1.0	0.49	6.0
QCI99	12	115.5	3.4%	-29.8 ± 0.1	1.0	0.7	1.0	0.39	9.3
QCI99	21.5	112.3	3.0%	-31.3 ± 0.0	0.5	0.6	0.9	0.53	10.0
7601	26.6	109.0	13.2%	-32.1 ± 0.1					
QCI99	27.3	108.3	3.0%	-31.3 ± 0.1	0.5	0.4	0.7	0.49	58.1
7601	10.7	106.6	12.2%	-30.1 ± 0.0	1.3	0.7	1.3	0.43	26.7
7601	17.4	106.3	9.5%	-29.9 ± 0.1	3.1	2.0	0.9	0.57	54.6
7601	24.3	106.0	9.7%	-29.6 ± 0.1	3.5	2.0	0.9	0.48	5.5
QCI99	35.8	104.3	2.5%	-29.5 ± 0.1	0.4	0.3	1.0	0.47	6.6
FI4	21.5	-22.0	6.4%	-29.7 ± 0.2	0.8	1.4	1.0	0.48	0.9
Average			5.2%	-29.4 ± 0.1	1.3	0.9	1.7	0.46	13.3

Table 5.2: Stable organic carbon isotope values of bulk organic matter (org), kerogen (ker), and bitumen (bit). Isotopic differences between bitumen and kerogen, bitumen and bulk organic matter, and kerogen and bulk organic matter are also indicated. Errors shown are 1σ .

ID	$\delta^{13}\text{C}_{org}$	$\delta^{13}\text{C}_{ker}$	$\delta^{13}\text{C}_{bit}$	bit-ker	bit-org	ker-org
QCIJ 238	-31.4 ± 0.0	-31.3 ± 0.1				-0.1
QCIJ 91.4	-25.1 ± 0.0	-25.4 ± 0.1				-0.3
QCIJ 55	-28.6 ± 0.1	-28.4 ± 0.2				0.2
7601 17.4	-29.9 ± 0.1	-30.6 ± 0.0	-31.5 ± 0.0	-0.9	-1.6	-0.7
7601 21.10	-29.4 ± 0.1	-30.1 ± 0.0	-31.5 ± 0.1	-1.4	-2.1	-0.7
7601 24.3	-29.6 ± 0.1	-30.0 ± 0.2	-31.3 ± 0.1	-1.3	-1.7	-0.4
QCI99 74	-30.0 ± 0.1	-30.2 ± 0.0				-0.2
Average				-1.2	-1.7	-0.3

5.3.2 Aliphatic Fractions

Fig. 5.1 shows the total ion chromatograms of aliphatic hydrocarbon fractions arranged stratigraphically with lithologic and bulk organic carbon isotope data ($\delta^{13}\text{C}_{org}$). The large UCM apparent in most chromatograms indicates a high degree of biodegradation (e.g. Grice *et al.*, 2000, and references therein). Most samples are dominated by hopanes, with a lower abundance of *n*-alkanes. In the early Hettangian samples showing the heaviest bulk carbon isotope values, however, UCM is decreased or nonexistent, and *n*-alkanes with an odd-over-even predominance are dominant.

5.3.3 *n*-alkanes and acyclic isoprenoids

n-Alkanes are present in all samples (Fig. 5.4), though they are most abundant in the Hettangian samples associated with the positive excursion in $\delta^{13}\text{C}_{org}$, and nearly unresolvable in samples QCIJ 55 and 7601 26.6. Fig. 5.2 shows the m/z 57 fragmentogram from Hettangian sample QCIJ 99.5 in which acyclic isoprenoids Pr and Ph as well as the *n*-alkane series with a clear odd-over-even predominance (CPI:

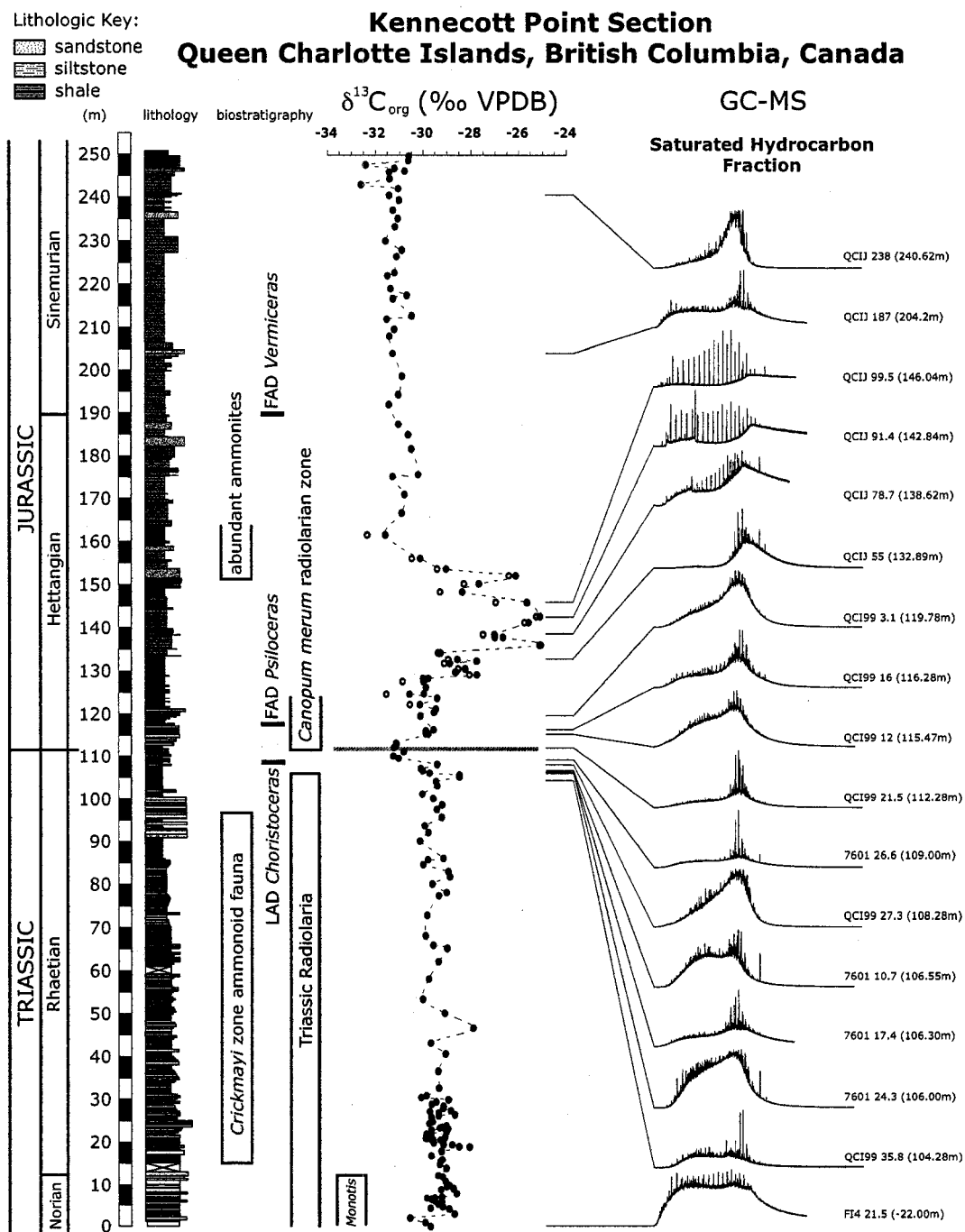


Figure 5.1: Aliphatic fraction total ion chromatograms for all samples shown with litho-, bio- and carbon isotope stratigraphy reported in Williford *et al.* (2007). Chromatograms are aligned using the C_{36}n -alkane.

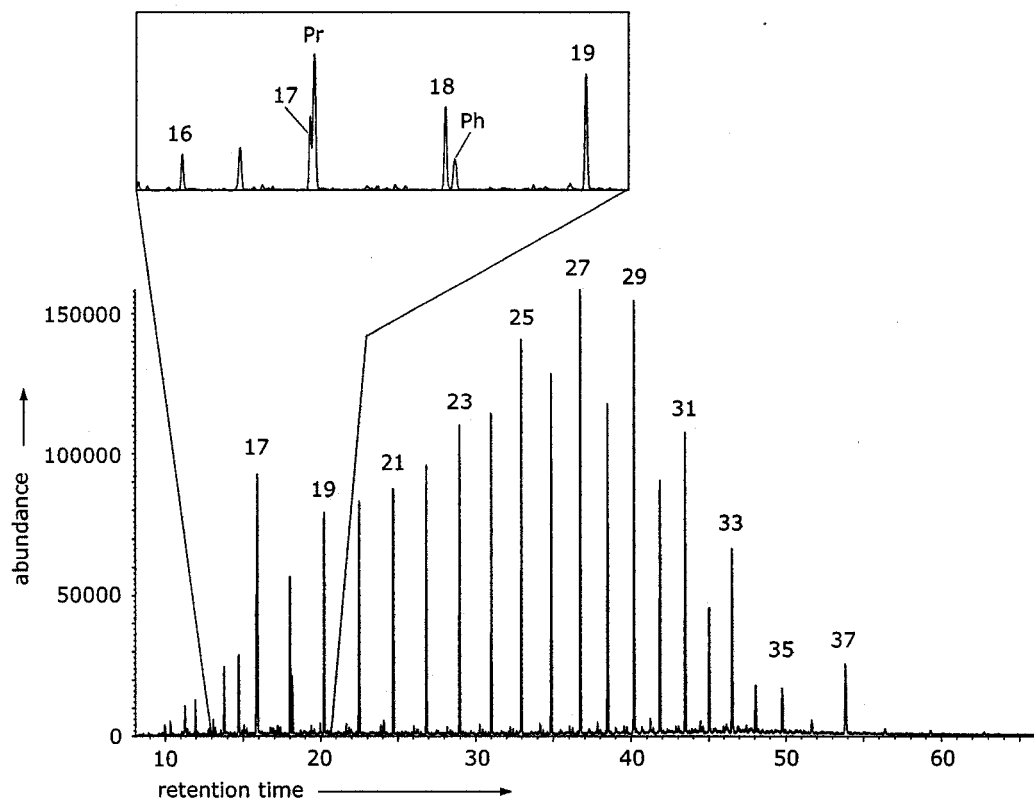


Figure 5.2: m/z 57 chromatogram from sample QCIJ 99.5, near the peak of the large positive excursion in $\delta^{13}\text{C}_{org}$ in the Hettangian. n -alkanes are indicated by their carbon number, acyclic isoprenoids pristane (Pr) and phytane (Ph) are shown in the expanded region between n -C₁₆ and n -C₁₉ alkanes.

1.27, see Source Indicators section below for details) are readily identifiable. n -C₁₇ and n -C₁₉ are from algae or cyanobacterial sources (e.g. Gelpi *et al.*, 1970).

In more highly biodegraded samples such as QCI99 27.3, n -alkanes are present in lower concentrations, and the UCM is large (Fig. 5.3). It is unusual for n -alkanes to be present at all in samples with such a large UCM, as these compounds typically dis-

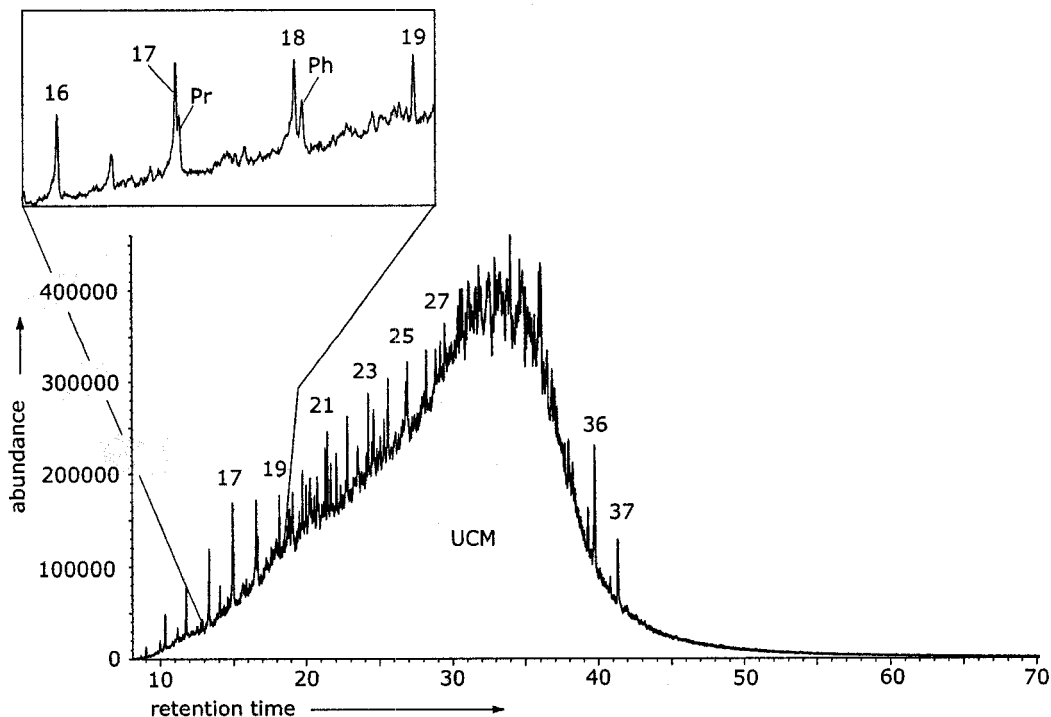


Figure 5.3: m/z 57 fragmentograms from sample QCI99 27.3, showing high degree of biodegradation and unresolved complex mixture (UCM). n -alkanes are indicated by their carbon number, acyclic isoprenoids pristane (Pr) and phytane (Ph) are shown in the expanded region between nC_{16} and nC_{19} alkanes.

appear at a low level of biodegradation. This could indicate a mixture of biodegraded and fresher material (K. Grice, pers. comm.).

5.3.4 Hopanoids

$17\alpha(H),21\beta(H)$ -hopanes between C_{29} and C_{35} are the dominant compounds in most of the samples in this study. 25-norhopanes (N29) are present in significant quantities

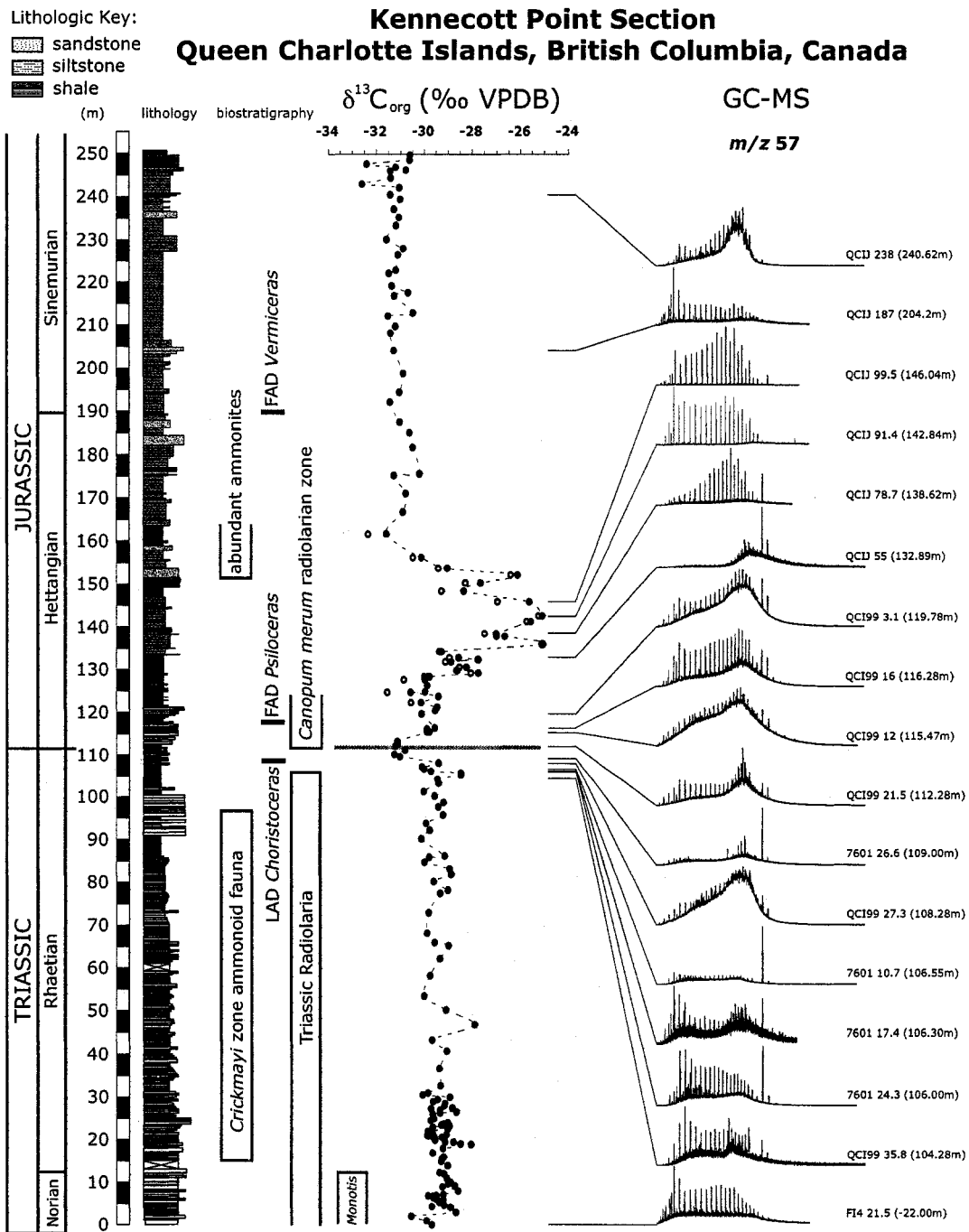


Figure 5.4: m/z 57 chromatogram from all samples shown with litho-, bio- and carbon isotope stratigraphy reported in Williford *et al.* (2007). Fragmentograms are aligned using the C_{36} n -alkane.

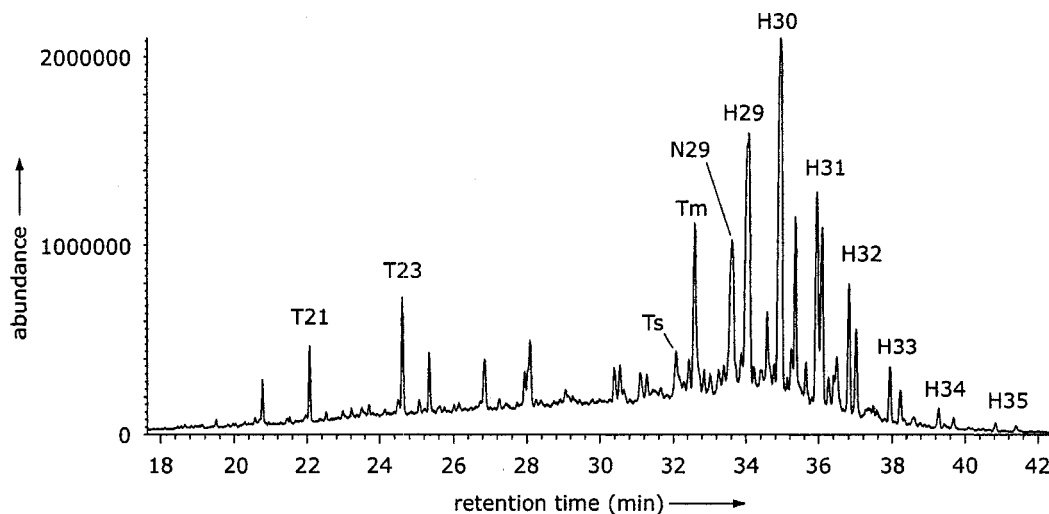


Figure 5.5: m/z 191 fragmentogram from latest Rhaetian sample QCI99 27.3, showing tricyclic terpanes and hopanoids. T21 and T23 are C_{21} and C_{23} tricyclic terpanes, Ts and Tm are 22,29,30-trinor-17 α -hopane and 22,29,30-trinor-18 α -hopane, respectively. N29 is the C_{29} 25-norhopane. H29 is 30-nor-17 α ,21 β -hopane. H30 is 17 α ,21 β -hopane, and H31-H35 pairs are the 17 α homohopane stereoisomers. First eluting isomer is 22 S followed by 22 R .

as well, indicating a high degree of biodegradation (Peters *et al.*, 1996; Bennett *et al.*, 2006). C_{31} - C_{35} hopane stereoisomers are readily identifiable, as are the 17 α - and 17 β -22,29,30-trisnorhopanes (Tm and Ts). The two dominant peaks eluting before Ts/Tm are identified as C_{21} and C_{23} tricyclic terpanes based upon the work of Bustin and Mastalerz (1995). Fig. 5.5 shows a representative hopanoid fingerprint in the m/z 191 chromatogram from the sample with the highest concentration of hopanes, QCI99 27.3. All m/z 191 chromatograms in the study are shown stratigraphically in Fig. 5.6.

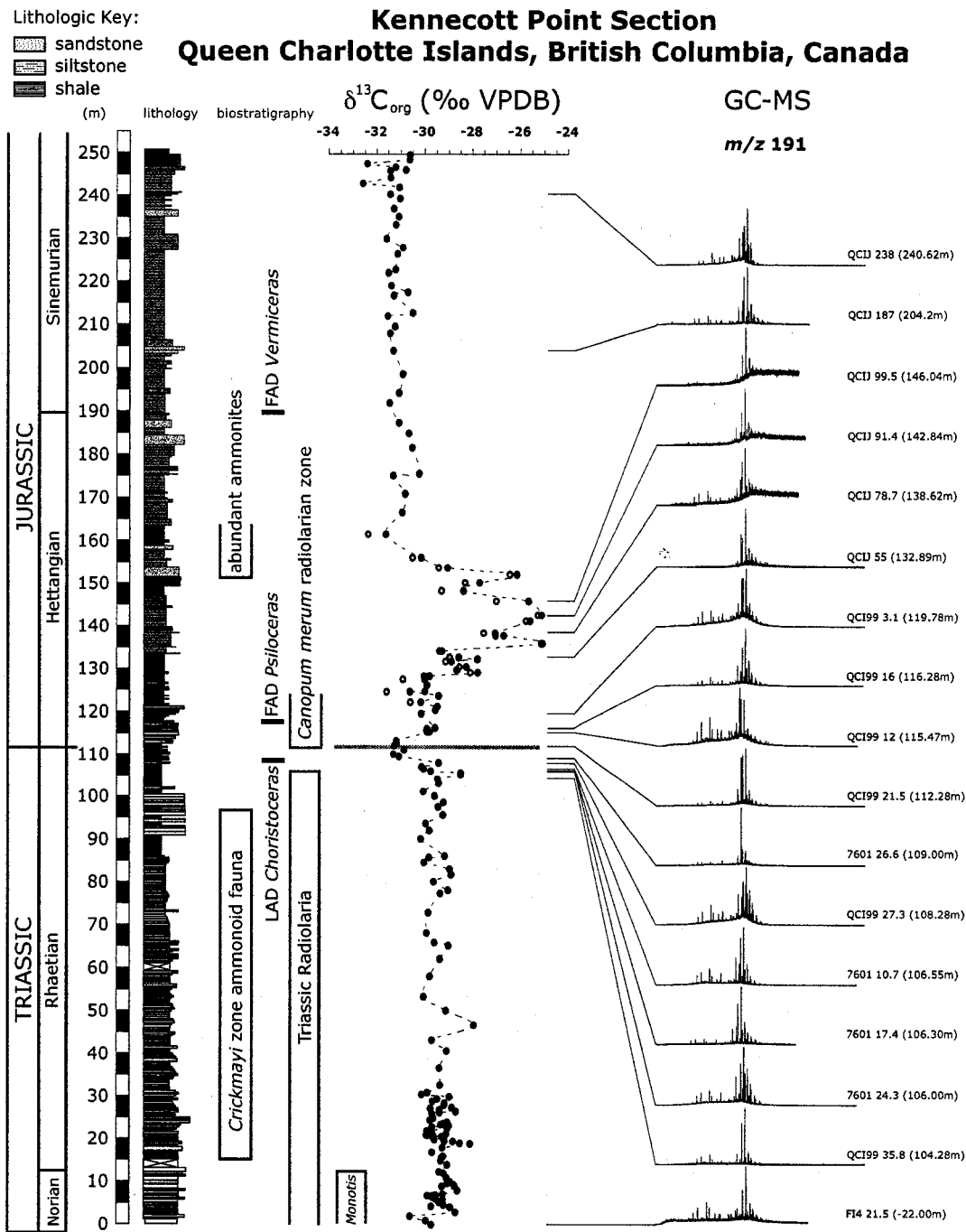


Figure 5.6: *m/z* 191 chromatograms from all samples shown with litho-, bio- and carbon isotope stratigraphy reported in Williford et al. (2007).

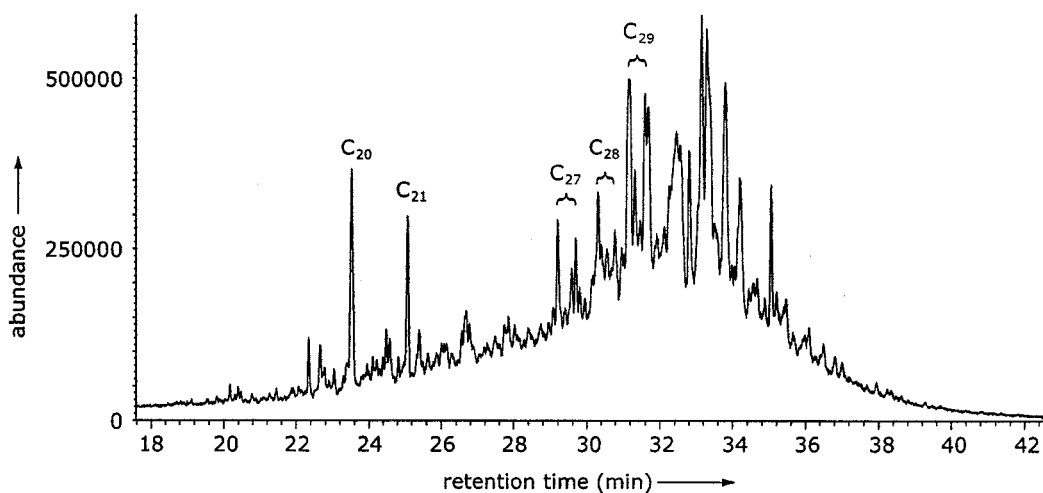


Figure 5.7: m/z 217 fragmentogram from latest Rhaetian sample QCI99 27.3, showing steranes. C_{27} , C_{28} , and C_{29} regular steranes are shown as groups of four peaks each with the following elution order: $(20S) \alpha\alpha\alpha$, $(20S) \alpha\beta\beta$, $(20R) \alpha\beta\beta$, $(20R) \alpha\alpha\alpha$.

5.3.5 Steranes

Steranes are present in most samples in this study but only in trace quantities insufficient for peak integration and quantitation in Hettangian samples that are part of the positive excursion in $\delta^{13}C_{org}$. On the m/z 217 chromatogram, the C_{27} , C_{28} , and C_{29} regular steranes are readily identifiable, each present as four peaks corresponding (in order of elution) to $(20S) \alpha\alpha\alpha$, $(20S) \alpha\beta\beta$, $(20R) \alpha\beta\beta$, and $(20R) \alpha\alpha\alpha$ forms. The dominant peaks earlier in the series are identified as the C_{20} and C_{21} diasteranes. Fig. 5.7 shows the sterane fingerprint in m/z 217 of sample QCI99 27.3, and Fig. 5.8 shows the m/z chromatograms of all samples arranged stratigraphically.

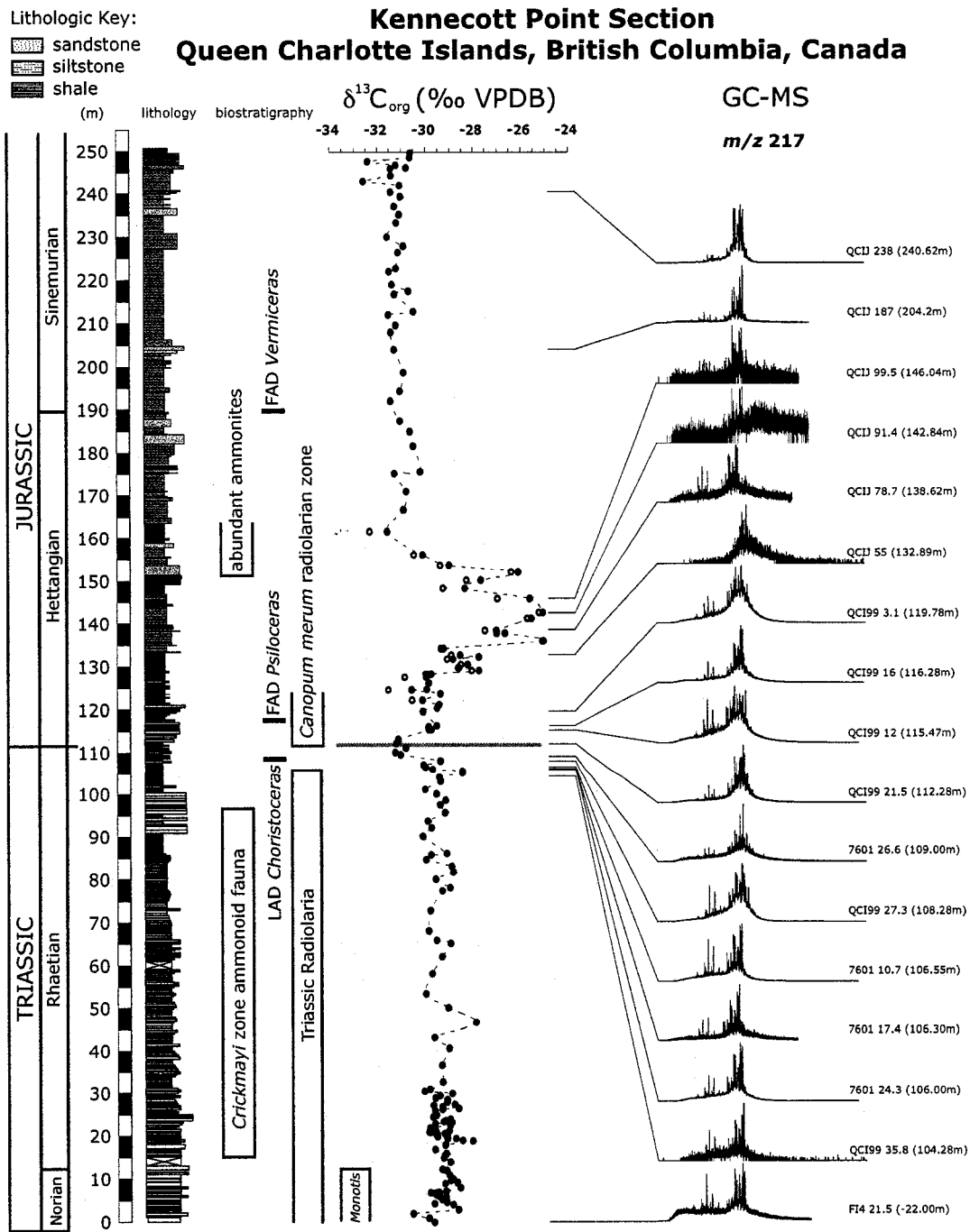


Figure 5.8: m/z 217 chromatograms from all samples shown with litho-, bio- and carbon isotope stratigraphy reported in Williford et al. (2007).

5.3.6 Aromatic Fractions

Fig. 5.9 shows aromatic fraction chromatograms for all samples in the study. All samples contain a large UCM, though samples QCIJ 91.4 and QCI 99.5 are clearly the least biodegraded. All samples were checked for the presence of isorenieratane, chlorobactane and okenanae on m/z 133, but these compounds were not detected.

5.3.7 Phenanthrene and alkyl phenanthrenes

Fig. 5.10 shows the distribution of phenanthrenes and alkyl phenanthrenes in sample QCIJ 99.5. The presence of these compounds indicates a low degree of biodegradation (Peters:2005) or low thermal maturity as indicated by other measures.

5.4 Discussion

5.4.1 Maturity

The ratio of (20*R*) and (20*S*) isomers of the C₂₉ regular sterane (20*S*/(20*R*+20*S*)) is used here as an indicator of thermal maturity. Biogenic input of C₂₉ sterane is exclusively in the (20*R*) $\alpha\alpha\alpha$ form. With increasing thermal maturity, the 20*S* epimer is formed until equilibrium is reached at approximately 55% 20*S* and 45% 20*R*. After equilibrium is reached ($R_o \sim 0.8$), the potential of this proxy is exhausted (Waples and Machihara, 1990). Values are shown in Table 5.1. The average value for this section is 0.46, which is 83.6% of the equilibrium value for this system.

5.4.2 Source Indicators

While it is impossible to formally classify the kerogen type of samples in this study due to the lack of Rock Eval pyrolysis data, Fig. 5.11 shows the relationship between Pr/*n*-C₁₇ and Ph/*n*-C₁₈, which can provide information about source, maturity,

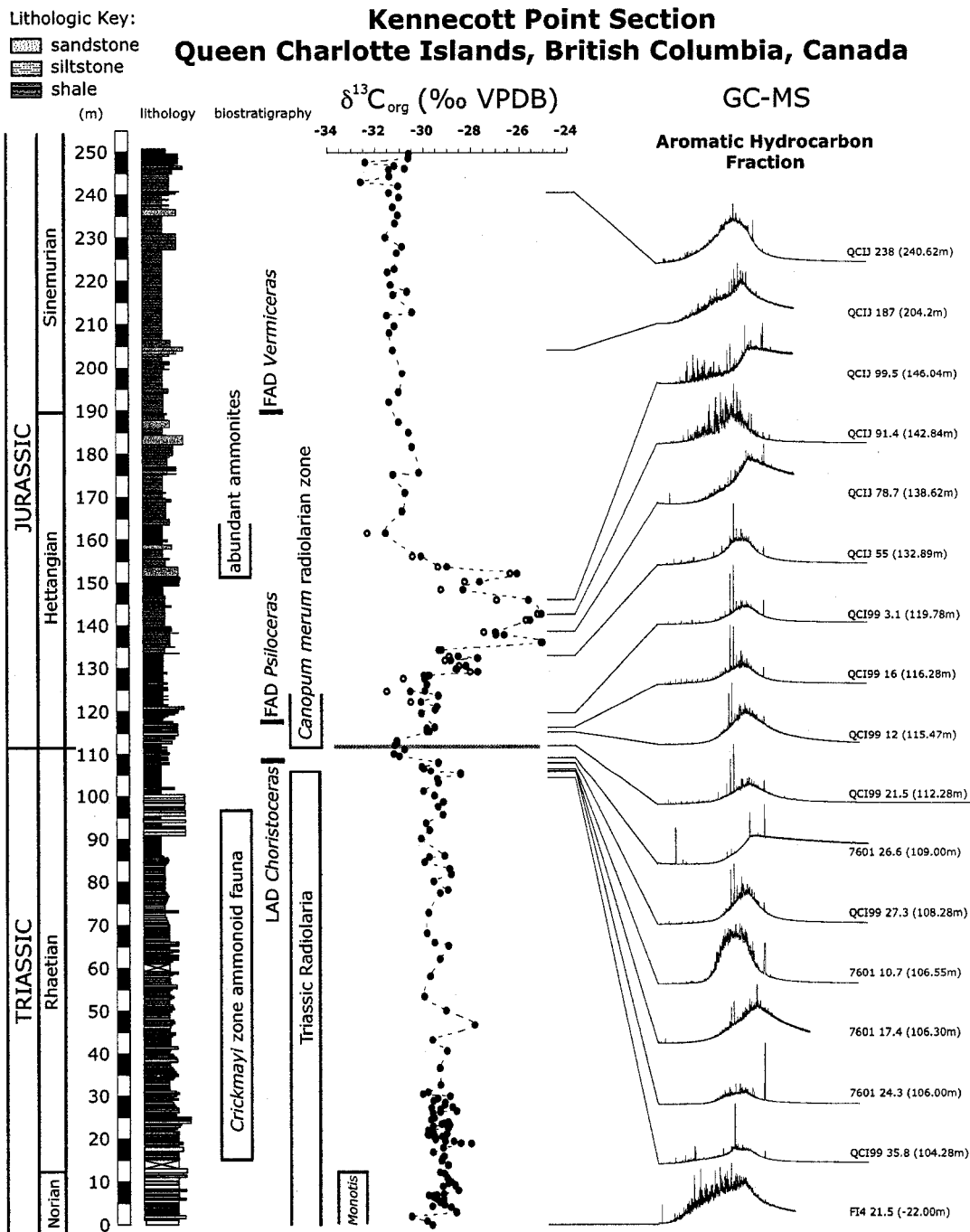


Figure 5.9: Aromatic fraction total ion chromatograms from all samples shown with litho-, bio- and carbon isotope stratigraphy reported in Williford et al. (2007).

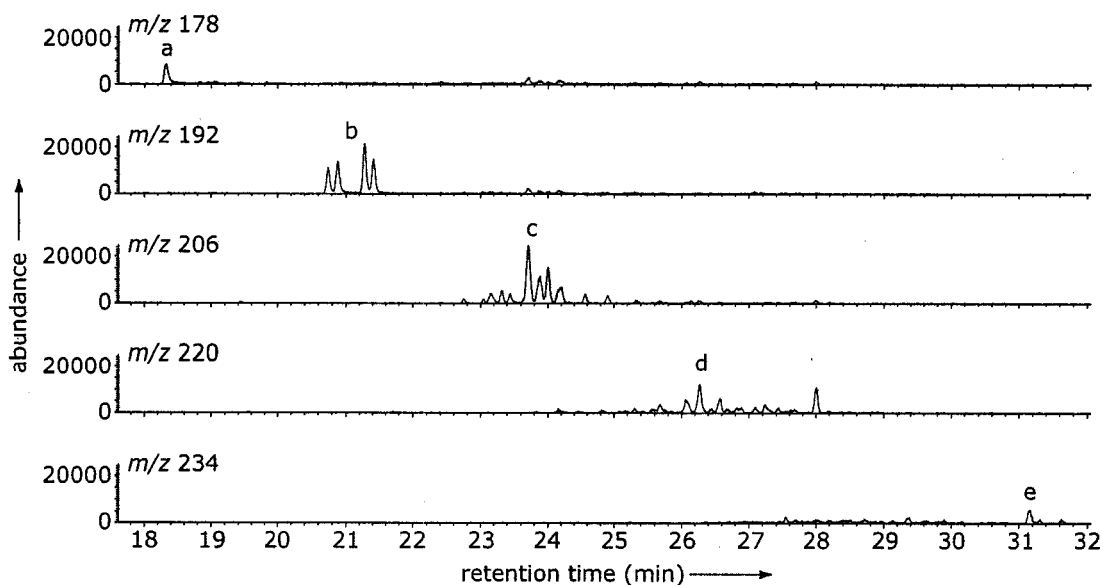


Figure 5.10: m/z 178, 192, 206, 220, and 234 showing phenanthrenes (a), methyl- (b), dimethyl (c), trimethyl (d), and tetramethylphenanthrenes (e) from the aromatic fraction of Hettangian sample QCIJ 99.5.

biodegradation, and redox conditions during deposition (Hunt, 1995). Most samples plot in the reducing to intermediate marine algal Type II to Type II-III mixed kerogen regions. However, samples QCIJ 99.5 and 91.4, from the peak of the positive excursion in bulk $\delta^{13}C_{org}$, plot well into the oxidizing, Terrestrial Type III kerogen region, suggesting an increased contribution of terrestrial material during the time of deposition. This interpretation is supported by the odd over even predominance (OEP) of long chain n -alkanes in these Hettangian samples. The C_{23} - C_{33} Carbon Preference Index (CPI) (Eqn. 5.1) (Peters *et al.*, 2005) is 1.27 for both QCIJ 99.5 and 91.4, and 1.03 for QCI99 27.3.

$$\frac{(nC_{25} - nC_{33})_{odd} + (nC_{23} - nC_{31})_{odd}}{2 \times (nC_{24} - nC_{32})_{even}} \quad (5.1)$$

This suggests an increased contribution of higher plant source material in samples from the peak of the Hettangian positive excursion in bulk $\delta^{13}C_{org}$ compared to samples at or just before the negative excursion in bulk $\delta^{13}C_{org}$ coincident with the Tr-J boundary. This interval is characterized by Tipper and Guex (1994) as a homogenous "coarse turbiditic sandstone." In a more detailed analysis of lithostratigraphy, we find that laminated shales and siltstones are present in this interval, though rare, there is an increase in the frequency and thickness of turbidites over this interval, and there is a general increase in grain size, bed thickness, and apparent oxygenation. Increasing turbiditic deposition over this stratigraphic interval may have delivered organic material with a high terrigenous component, previously deposited in a shallower, more oxygenated setting closer to the continental margin.

A ternary diagram showing the relative distribution of regular C_{27} , C_{28} , and C_{29} steranes (Fig. 5.12) indicates a significant degree of terrigenous input in the section, as most samples fall well into the C_{29} region (Peters et al., 1993). The youngest sample in the section, QCIJ 238, Sinemurian in age, shows the highest predominance of C_{29} sterane, which may indicate a high degree of terrigenous input. This sample was collected by P. Ward in 2001, approximately 1m above a bed labeled as a 1 foot thick sandstone with hummocky cross-stratification. Hummocky cross-stratification forms above, but near storm wave base (Dumas and Arnott, 2006), and storm deposition could have brought an influx of terrigenous material. Deposition above storm wave base would indicate a significant relative fall in sea level compared with the deep-water environment lower in the section. The Early Jurassic was a time of low, but generally rising global sea level (Miller *et al.*, 2005). Evidence for a Sinemurian regression in England has been cited (Hallam, 1999) and refuted (Hesselbo and Coe,

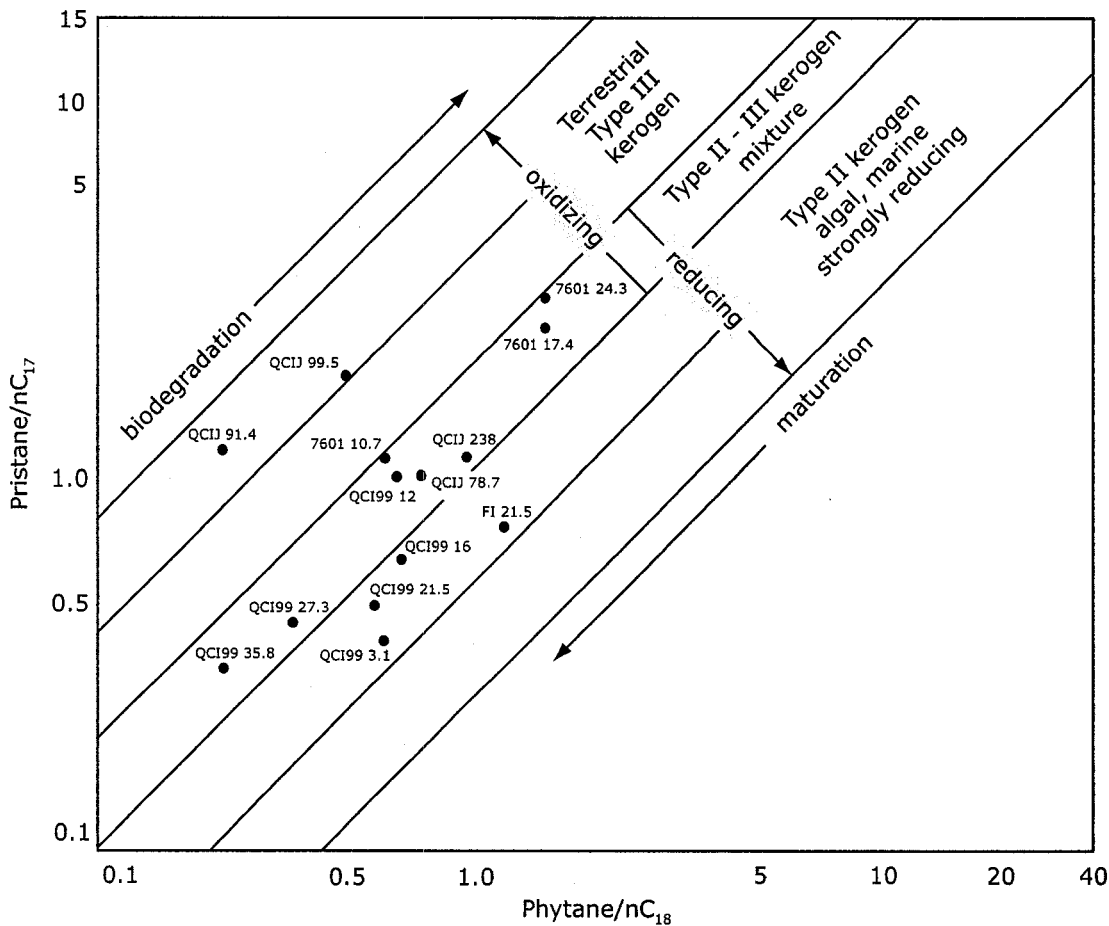


Figure 5.11: Pr/ n -C₁₇ vs. Ph/ n -C₁₈

2000). Interestingly, the samples with the next highest C₂₉ sterane contribution are those closest to the Tr-J boundary. This could be due simply to a facies change, as has been observed at the Tr-J section at New York Canyon in Nevada, USA (Hallam and Wignall, 2000). Alternatively, the pulse of terrestrial material could be associated with a rooted land plant die-off and altered erosional regime during the

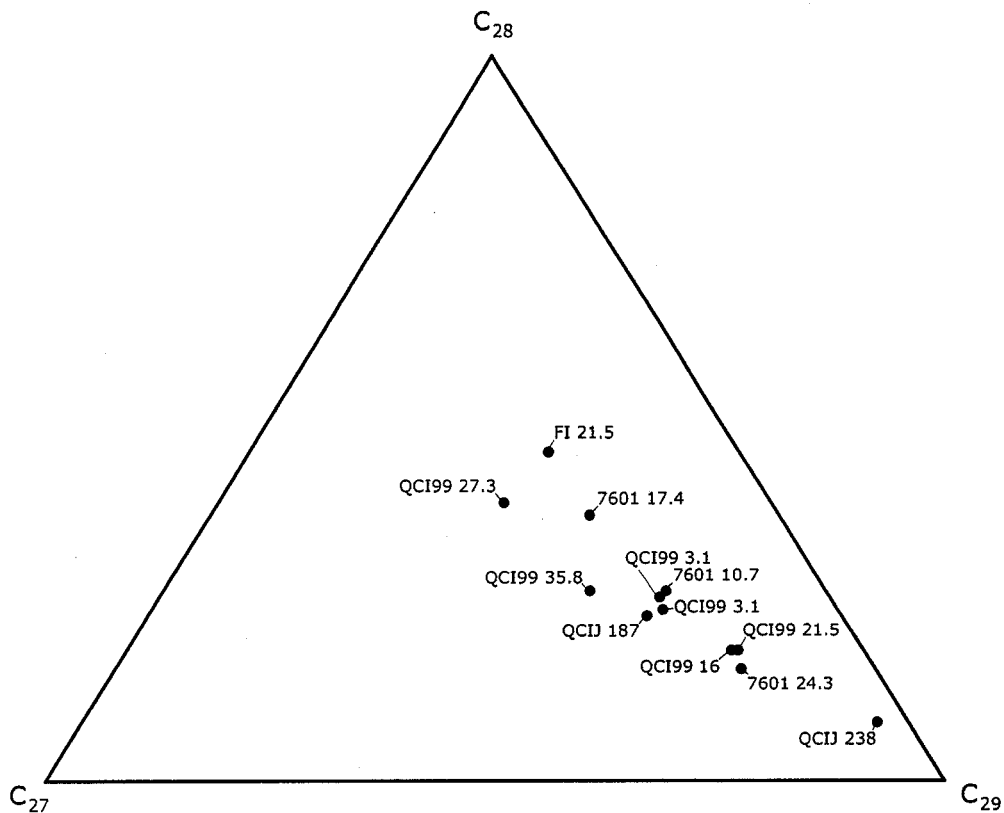


Figure 5.12: Ternary diagram showing the relative distributions of regular C_{27} , C_{28} , and C_{29} steranes

extinction event similar to what appears to have occurred at the Permian–Triassic boundary (Ward *et al.*, 2000). Samples above and below the boundary plot in a more intermediate position on the ternary diagram.

Pr/Ph ratios have been used as a proxy for redox conditions in the sediment at the time of deposition, though this application has largely fallen out of favor due to other variables known to affect this ratio (e.g., salinity, early diagenesis) (Peters *et al.*,

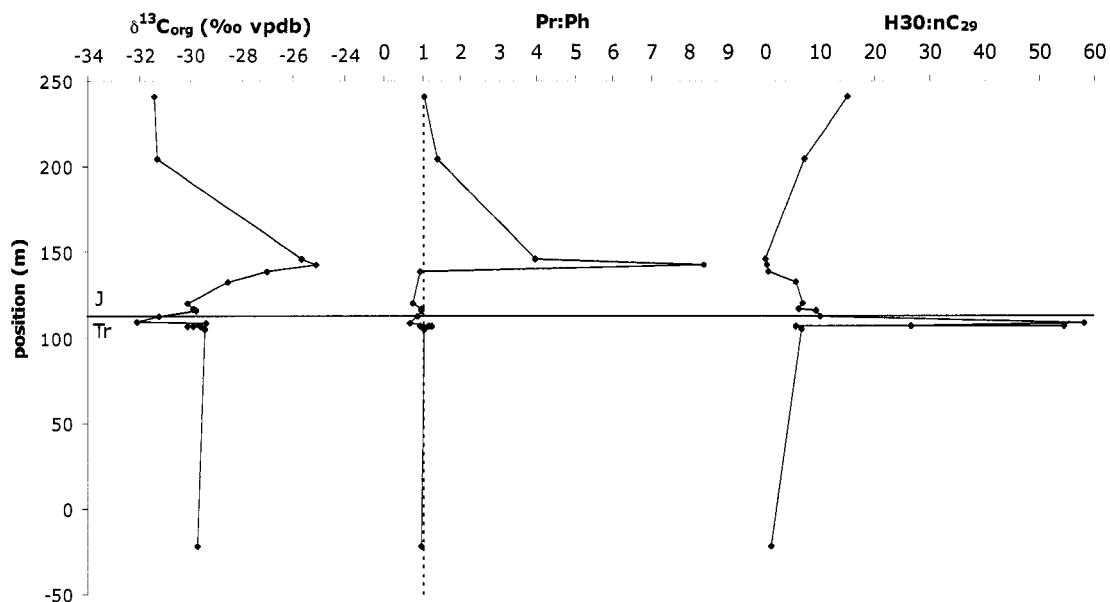


Figure 5.13: Bulk $\delta^{13}\text{C}_{org}$, Pr/Ph, and H30:nC₂₉ across the Tr–J boundary. H30:nC₂₉ is the ratio of the integrated peak areas from the C₃₀ hopane peak on the m/z 191 fragmentogram and the nC₂₉ peak on the m/z 57 fragmentogram. Tr–J boundary is indicated by the horizontal line at 110 m.

2005). Those concerns aside, the low Pr/Ph values in most of the samples, especially those at the Tr–J boundary, could indicate more anoxic conditions. The pronounced increase in Pr/Ph associated with the Hettangian positive excursion in bulk $\delta^{13}\text{C}_{org}$ could be due to an increase in terrestrial material, as tocopherols (E vitamins) from land plants are thought to be likely Pr precursors (Goossens *et al.*, 1984).

The increase in Pr/Ph is accompanied by a shift in the relative contribution of hopanes and *n*-alkanes. C₃₀ hopane is the most abundant hopanoid and nC₂₉ is an abundant alkane in almost all samples in this study. The ratio of the integrated peak areas for the dominant ions associated with each of these compounds (m/z 191 for C₃₀ hopane and m/z 57 for nC₂₉ alkane) is used here as a proxy for the relative abundance

of the compounds. The positive excursion in bulk $\delta^{13}\text{C}_{org}$ and increase in Pr/Ph is associated with a decrease in H30:nC₂₉ to values an order of magnitude less than those from surrounding samples, and nearly two orders of magnitude less than average values for the section. These observations imply that the organic matter in this interval was deposited under oxidizing conditions, had a high terrigenous component, and was subject to less bacterial degradation than organic material higher and lower in the section.

Also striking is the dramatic increase in hopane concentrations relative to *n*-alkanes that occurs just before the Tr–J boundary and peaks just before the onset of the negative excursion in bulk $\delta^{13}\text{C}_{org}$. This could be explained by a collapse in primary productivity associated with a rapid die-off among the eukaryotic phytoplankton and a bloom in heterotrophic water column bacteria. Indeed, there is a rapid extinction of >90% of Rhaetian radiolaria at precisely this stratigraphic interval (Carter and Hori, 2005; Ward *et al.*, 2001, 2004), perhaps due to removal of their primary food source. Transient blooms of prasinophyte algae and acritarchs that typically occur in disturbed ecosystems where grazers have been eliminated were identified coincident with the Tr–J boundary negative carbon isotope excursion in the St. Audrie’s Bay (van de Schootbrugge *et al.*, 2007) and Tiefengraben (Kuerschner *et al.*, 2007) sections. The rapid remineralization in the water column by aerobic bacterial heterotrophy of isotopically light, photosynthetically derived carbon would have contributed to the observed negative carbon isotope excursion.

While Fig. 5.13 shows semiquantitative data for hopane and alkane abundance so that trends can be evaluated using all samples in the study (even those samples which were analyzed without recovery and quantitation standards), Figs. 5.14 and 5.15 show fully quantitative data for the eight samples which were analyzed using the most comprehensive methods. Similar patterns emerge in these absolute molecular

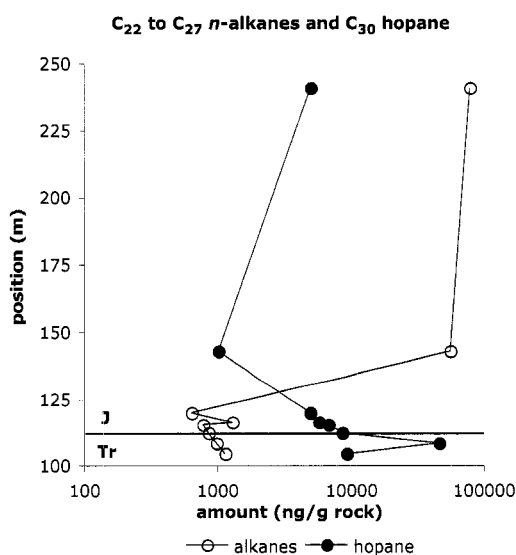


Figure 5.14: Total amount of nC_{22} to nC_{27} alkanes and C_{30} hopanes in Rhaetian to Sinemurian samples

abundances a spike in C_{30} hopane abundance immediately precedes the Tr–J boundary, a spike in long chain n -alkane abundance immediately follows the boundary, and the relative contribution of hopanes to alkanes shifts in the Hettangian. In the Sinemurian sample QCIJ 238, hopane concentration increases to a value more similar to (yet still less than) those lower in the section, while long chain n -alkanes remain at high levels. n -alkanes $\geq C_{22}$, especially with an odd over even predominance, indicate a terrigenous higher plant source (Peters *et al.*, 2005). This pattern implies two important things about this section: 1) high biodegradation and bacterial contributions to organic matter are the norm, and low hopane values in the Hettangian are an anomaly, and 2) the increase in terrigenous input begins in the Hettangian and remains high into the Sinemurian.

Fig. 5.15 shows a detail of the 20 m around the Tr–J boundary, where a decreasing

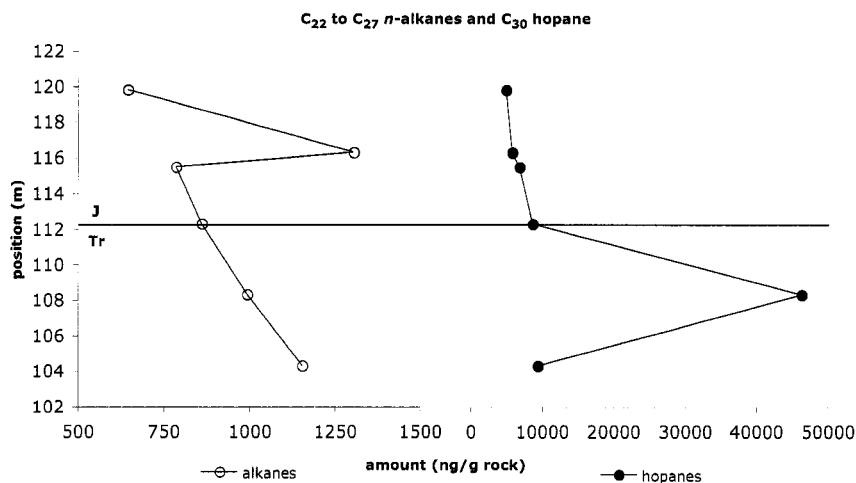


Figure 5.15: Total amount of nC_{22} to nC_{27} alkanes and C_{30} hopanes in Rhaetian to Sinemurian samples

trend in abundance of long chain ($> C_{22}$) n -alkanes is clearly apparent. If the sample with the highest abundance value (QCI99 16) is removed, the trend has $r^2=0.98$. This trend is interrupted by a deviation to a value that is approximately 170% of the expected value for the apparent trend. If these long chain n -alkanes are derived from terrestrial plant waxes, as is commonly the case, this pattern could represent a slow decline in terrestrial plant abundance interrupted by a short term pulse of terrestrial plant material to marine sediments in the wake of a die off and resultant shift in the erosional regime on the continent such as that seen at the P-T boundary (Ward *et al.*, 2000). Kuerschner *et al.* (2007) found that distinctive Late Triassic pollen types including *Ovalipollis* and *Rhaetipollis* disappear coincident with the marine extinctions and the negative carbon isotope excursion, suggesting that terrestrial plant extinctions were synchronous with the marine event. The large spike in C_{30} hopane immediately preceding the boundary is also very clear in absolute abundance data shown here, and

the spike occurs against a background trend of gently decreasing hopane abundance.

5.5 Conclusions

A record of lipid biomarkers is presented from the Triassic–Jurassic (Tr–J) boundary section on Kennecott Point, Queen Charlotte Islands, British Columbia, Canada. Lipids from seventeen rock samples ranging in age from Norian to Sinemurian were extracted and characterized using gas chromatography mass spectrometry (GC-MS). Organic material was found, in general, to be of low to moderate thermal maturity and highly to severely biodegraded. Pristane/phytane (Pr/Ph) ratios are generally <1, indicating low oxygen conditions during deposition. Abundant C₂₉ steranes are indicative of a significant terrigenous component to the organic material in this section, especially in the early Hettangian and at the top of the section in the Sinemurian. This could be related to facies change (relative sea level fall) or a land plant die-off associated with Tr–J extinction event. Samples from strata containing the positive excursion in $\delta^{13}\text{C}_{org}$ reported by Williford *et al.* (2007) have a significantly different character than samples higher and lower in the section. These samples have high Pr/Ph ratios, are much less biodegraded, and contain few hopanes and steranes but abundant *n*-alkanes with a clear odd over even predominance. This was likely due at least in part to an increase in turbiditic deposition over this stratigraphic interval, which would have brought organic material with a higher terrigenous component, deposited under oxidizing conditions closer to the continental margin. There is a spike in hopane abundance just before the Tr–J boundary, coincident with the negative excursion in $\delta^{13}\text{C}_{org}$ first reported by Ward *et al.* (2001) and a major radiolarian extinction (Carter and Hori, 2005). This could represent a decline in net primary production as bacterial heterotrophy outstripped primary productivity in the wake of the Tr–J event, contributing to the negative excursion in $\delta^{13}\text{C}_{org}$. The apparent

decline in bacterial influence and export of light carbon to surface waters in the Hettangian, combined with an influx in terrigenous organic material, could have had the opposite effect, driving stable carbon isotopes towards heavier values.

5.6 Acknowledgements

This work was funded by the NASA Astrobiology Institute, University of Washington node, Peter Ward, P.I., and we gratefully acknowledge that financial assistance.

Chapter 6

CONCLUSIONS

This chapter will discuss the implications of the data presented in this study for the Triassic–Jurassic (Tr–J) boundary record, for the understanding of mass extinctions in general, and for planetary habitability and Astrobiology. This study extends the record of biogeochemical change across the Tr–J boundary in time – reporting records of stable carbon and sulfur isotopes as well as lipid biomarkers from the Norian into the Sinemurian for the Queen Charlotte Islands in British Columbia, Canada – and in space – reporting records of stable carbon isotopes from three Tr–J boundary sections in New Zealand, the first such work in the Southern Hemisphere. As important as the data are the subtler questions that arise in the gathering, as these are the doorways that open onto new avenues of inquiry. Some of these questions will be addressed here.

6.1 *Implications for the Triassic–Jurassic boundary record*

6.1.1 Causes and consequences of Tr–J boundary events

The currently favored primary cause for the Tr–J mass extinction is the eruption of the Central Atlantic Magmatic Province (CAMP) (Hesselbo *et al.*, 2007). CAMP would have released up to 2.1×10^4 Gt CO₂ and 5.7×10^4 Gt SO₂, leading to rapid global warming, ocean acidification, and potentially CaCO₃ undersaturation (Berner and Beerling, 2007). There is ample independent evidence for a calcification crisis at the Tr–J boundary (Galli *et al.*, 2005; van de Schootbrugge *et al.*, 2007). There

is a strong negative relationship between sea surface temperature and net primary productivity in the modern ocean (Behrenfeld *et al.*, 2006), and it is reasonable to expect that rapid warming would have caused a decline in productivity at the Tr–J boundary as well. A decline among the phytoplankton would have contributed to the radiolarian extinctions as the primary food source became scarce. Radiolarian extinctions are likely indicative of wider extinctions among non-fossilizing zooplankton, and a collapse of the food web combined with the calcification crisis would have made conditions difficult for marine macrofauna. This scenario is supported by the blooms of prasinophyte algae and acritarchs coincident with the negative carbon isotope excursion at the Tr–J boundary, as these organisms are known to be associated with disturbed ecosystems, present when other phytoplankton are absent, and tend to be associated with the elimination of grazers such as foraminifera and radiolaria (van de Schootbrugge *et al.*, 2007; Kuerschner *et al.*, 2007).

6.1.2 CAMP

As it becomes increasingly clear that CAMP volcanism was the most likely primary cause of the Tr–J mass extinction, determining the relative timing of the emplacement of CAMP and other Tr–J boundary events is critical. Marzoli *et al.* (1999) found that basalt deposits in Morocco are coincident with the boundary, a conclusion supported by Marzoli *et al.* (2004) and Verati *et al.* (2007). The latter study shows $^{40}\text{Ar}/^{39}\text{Ar}$ ages for Moroccan basalts ranging from 197.8 ± 0.7 Ma to 201.7 ± 2.4 Ma with a peak at 199.1 ± 1 Ma. By contrast, Whiteside *et al.* (2007) argue based on palynology, magnetostratigraphy, and cyclostratigraphy that the oldest CAMP deposits in the Newark Basin postdate the local extinction by ~ 600 kyr. Nomade *et al.* (2007) reviewed all published ages for CAMP deposits to date and found that they range from 202 to 190 Ma, with extrusive activity commencing at ~ 200 Ma and peaking

at 199 Ma in Africa. Williford *et al.* (2007) found a statistically significant secular trend of isotopic lightening in $\delta^{13}\text{C}_{org}$ after the major isotopic perturbations at the Tr–J boundary, extending into the Sinemurian (Fig. 3.2, this study). Longer term emplacement of CAMP deposits in the early Jurassic, as suggested by the Nomade *et al.* (2007) compilation, accompanied by a slow increase in atmospheric CO_2 and associated increase in photosynthetic fractionation is consistent with these carbon isotope data.

6.1.3 Triassic–Jurassic carbon and sulfur cycling

This study adds support to the emerging consensus that the global carbon cycle was perturbed during and immediately after the Tr–J boundary. A long term negative trend in organic carbon isotopes is evidence of a gradual increase in atmospheric CO_2 occurring over the entire Hettangian and into the Sinemurian stage. The previously reported 2‰ negative excursion in $\delta^{13}\text{C}_{org}$ is followed by a short return to baseline values and then a more protracted 5‰ positive excursion encompassing much of the Hettangian stage. Extensive radiolarian extinctions as well as a spike in the ratio of hopanes to alkanes in the same stratigraphic interval as the negative carbon isotope excursion support the idea that this isotope event was caused at least in part by a collapse in primary productivity.

An increase in atmospheric CO_2 and global warming would have enhanced continental weathering and ultimately increased the export of phosphorus to the oceans. This would have increased productivity, contributing to the positive excursion in carbon isotopes observed in several Tr–J boundary sections (Galli *et al.*, 2005; Williford *et al.*, 2007; Ward *et al.*, 2007). Global sea-level regression at the Tr–J boundary followed by a Hettangian–Sinemurian transgression and an increased input of terrigenous material in the Early Hettangian contributed to the positive excursion in

organic carbon isotopes. A decline in the export of isotopically heavy inorganic carbon to marine sediments during the Tr–J boundary calcification crisis could also have contributed to the positive excursion in $\delta^{13}\text{C}_{org}$ (Williford *et al.*, 2007).

The increase in turbiditic deposition observed in Hettangian rocks of the Queen Charlotte Islands may have been the primary factor causing the positive excursions in both carbon and sulfur isotopes. Turbidity currents would have delivered more ^{13}C -enriched terrigenous organic matter, previously deposited closer to the continents. In the absence of evidence for global anoxia in the Hettangian, it is difficult to explain the sulfur isotope observations reported here without considering local depositional effects. A shift to non-steady-state sediment deposition may have led to a decoupling of the water column and the zone of sulfate reduction, causing bacterial sulfate reduction to occur under sulfate limited conditions, Rayleigh fractionation, and transient increases in the isotopic composition of reactants and products above the composition of seawater sulfate (e.g. Meyers *et al.*, 1996; Strauss, 1997). This happened in an ocean already depleted in sulfate, as evidenced by large Hettangian evaporite deposits such as the Argo Salt, consisting primarily of halite with only rare anhydrite horizons (Holser *et al.*, 1988). These evaporite deposits are part of the North Atlantic rift zone, and the Rhaetian–Hettangian rifting was probably related to the global regression that occurred at this time (e.g. Hallam and Wignall, 2000).

6.2 General implications for mass extinctions

The lack of convincing evidence for impact at the Tr–J boundary (Tanner *et al.*, 2004) forces the consideration of intrinsic kill mechanisms including perturbations to biogeochemical cycles. Such is also the case for the largest of all mass extinctions, at the Permian–Triassic (P–Tr) boundary (Ward *et al.*, 2005), (though there is some highly controversial evidence for impact at the P–Tr (Becker *et al.*, 2004; Renne

et al., 2004)), and indeed the similarities between the Tr–J and P–Tr events have continued to mount in recent years. Payne *et al.* (2004) found that the large negative carbon isotope excursion at the P–Tr boundary was followed by a series of three more carbon cycle perturbations characterized by short term negative excursions followed by larger, more protracted positive excursions, and that the carbon cycle did not stabilize until well into the Anisian, the first stage of the Middle Triassic. The Tr–J carbon isotope records from the Queen Charlotte Islands (Williford *et al.*, 2007) and Nevada (Guex *et al.*, 2004; Ward *et al.*, 2007) show a pattern that looks very similar to one of the negative-positive couplets identified in the Early Triassic. Biotic recovery after the P–Tr extinction was delayed until the carbon cycle began to stabilize in the Middle Triassic (Payne and Kump, 2007). Similarly, ammonite recovery after the Tr–J boundary was delayed until carbon and sulfur cycling began to stabilize in the Middle to Late Hettangian (Williford *et al.*, 2007, this study).

Both the P–Tr and Tr–J extinctions are associated with large igneous provinces, the Siberian traps (Renne and Basu, 1991; Renne *et al.*, 1995; Kamo *et al.*, 2003) and CAMP (Marzoli *et al.*, 1999; Nomade *et al.*, 2007), respectively. Large igneous provinces are associated with both the formation and breakup of the Pangean supercontinent, and they may be an inherent part of supercontinent formation and breakup in general (Vaughan and Storey, 2007). Declining continental shelf habitat on the exterior and climatic extremes on the interior make the formation of a supercontinent potentially detrimental to the biosphere. If flood volcanism is indeed the fundamental mechanism by which a supercontinent disintegrates, it may be that major mass extinctions are also an inherent part of supercontinent formation and breakup.

6.3 Implications for planetary habitability and Astrobiology

Animals did not evolve on Earth until approximately 570 million years ago (Xiao *et al.*, 1998), at least 2.5 billion years after the emergence of microbial life on the planet. The major biogeochemical cycles of the planet were thus established and mediated by the microbial biosphere for billions of years before the emergence of animals. Because of the narrow range of environmental tolerance of the eukarya, and especially the animals, relative to the bacteria and archaea (e.g. Gunde-Cimerman *et al.*, 2005; Alpert, 2006), the definition of habitability for animal life is quite different than that for microbial life. At least five times during the Phanerozoic Eon, during intervals that have come to be called the great mass extinctions, planetary habitability for animals was dramatically reduced. Habitability for microbial life was apparently either unaffected or increased during these intervals (e.g. Baud *et al.*, 1997; Butterfield, 2007).

It may be, in fact, that imbalances in the biogeochemical cycles mediated largely by the microbial biosphere, and expansions of certain parts of the microbial biosphere, were at least secondarily responsible for causing the mass extinctions or delaying the recovery from the mass extinctions. In the case of the largest mass extinction at the P–Tr boundary, for instance, global warming, ocean stagnation and superanoxia led to an expansion in the sulfate reducing bacteria and an increase in the production of H₂S in marine sediments such that the chemocline separating oxygenated surface waters from anoxic, sulfidic deep waters penetrated the photic zone (Grice *et al.*, 2005). This could have resulted in the release of a quantity of H₂S into the atmosphere sufficient to cause sulfide toxicity in terrestrial plants and animals as well as ozone depletion and increased UV flux (Kump *et al.*, 2005). Seawater sulfate concentration was 20 mM at the the P–Tr boundary, twice the concentration at the Tr–J boundary (Berner, 2004). Perhaps the lower sulfate concentration during the Tr–J extinction prevented

global photic zone euxinia from developing as sulfate reduction in marine sediments was more readily limited.

The only major mass extinction that can be reliably associated with an extraterrestrial mechanism is the Cretaceous–Paleogene (K–P) event (Alvarez *et al.*, 1980). After nearly three decades of careful searching for similar evidence of extraterrestrial impact at mass extinction boundary sections around the world, only limited, highly controversial evidence has been found (Becker *et al.*, 2004; Renne *et al.*, 2004). We are left to explore other extinction mechanisms, then, those intrinsic to the Earth system. Stable isotope measurements, such as those in this study, make it clear that each of the five major mass extinctions of the Phanerozoic were accompanied by large scale perturbations to global biogeochemical cycles.

At least three of the big five extinctions (P–Tr, Tr–J, K–Pg) were accompanied by flood basalt volcanism, increasing atmospheric CO₂ and global warming. In the case of the P–Tr and Tr–J mass extinctions, these seem to be the primary mechanisms which may have led to other kill mechanisms (e.g. anoxia, hypercapnia, clathrate destabilization, photic zone euxinia and sulfide toxicity). As indicated above, flood volcanism may be an inherent part of the formation and breakup of a supercontinent. Furthermore, the supercontinent phase may be an inherent part of plate tectonics (Vaughan and Storey, 2007). Plate tectonics may be a necessary requirement for long term planetary habitability in the general sense (Ward and Brownlee, 2000), but it may also be responsible for short term decreases in habitability for complex life.

There is ample room for exploration of the connection between flood volcanism, impact, and extinction, particularly concerning the key question of why some large impacts and large igneous provinces are *not* associated with mass extinctions. It may well be the case that neither impact nor volcanism alone is sufficient to cause a mass extinction, and that a combination of these, their associated downstream effects, or

some as yet undetermined mechanism is required. Certainly there is no universal rule governing the response of the biosphere to a given phenomenon, and the highly complex combination of planetary ecology, tectonics, geochemistry, spatiotemporal localization, orbital parameters, and countless other factors introduce a high degree of stochasticity into the dynamics of global biodiversity through time.

The great Phanerozoic mass extinctions at once highlight the fragility and the resilience of animal life on Earth. The Phanerozoic age of animals is characterized by episodic catastrophes during which the world became a barren wasteland, populated for millions of years only by the opportunistic few, the “disaster species.” Inevitably, however, biodiversity returned after even the most extreme of these extinctions, sometimes including a wide array of novel forms filling ecological niches that had never existed before. An early reduction in the number of animal body plans occurred some time after the deposition of the Burgess Shale, though this “decimation” event (Gould, 1989) or sequence of events cannot yet be constrained in time and space due to the extreme rarity of fossil sites with soft body preservation. Phylum-level diversity (or disparity) has remained constant since the Cambrian. The most extreme planetary conditions during the Phanerozoic were thus insufficient to completely eliminate complex life or permanently decrease global biodiversity. In the case of the Tr–J extinction, the highly successful Triassic ammonites suffered near complete extinction (Hallam, 1981), but during radiations in the Jurassic and Cretaceous periods, these animals achieved previously unsurpassed diversity (Ward, 1980). Late Triassic extinctions among the tetrapods opened the way for the great radiation of dinosaurs that would take place in the Jurassic (Olsen *et al.*, 2002; Irmis *et al.*, 2007), leading to a transformation of terrestrial ecosystems by the end of the Cretaceous. In this sense, and on time scales of hundreds of millions of years, mass extinctions acted as drivers of biological and ecological diversity.

BIBLIOGRAPHY

- Ahlberg, A., Olsson, I., and Simkevicius, P., 2003. Triassic-Jurassic weathering and clay mineral dispersal in basement areas and sedimentary basins of southern Sweden. *Sedimentary Geology* 161(1): 15–29.
- Akikuni, K., Hori, R., Grant-Mackie, J., and Ikehara, M., 2006. Stable carbon isotope stratigraphy of the Triassic/Jurassic boundary sequence in Murihiku Terrane at Kawhia and Awakino, New Zealand. In: *InterRad 11 and Triassic Stratigraphy Symposium*. Wellington.
- Aldridge, R. and Smith, M., 1993. Conodonts. In: Benton, M., ed., *The Fossil Record*, volume 2, pages 563–572. Chapman and Hall, London.
- Algeo, J., Berner, R., Maynard, J., and Scheckler, S., 1995. Late Devonian oceanic anoxic events and biotic crises; “rooted” in the evolution of vascular land plants? *GSA Today* 5: 64–66.
- Alpert, P., 2006. Constraints of tolerance: why are desiccation-tolerant organisms so small or rare? *Journal of Experimental Biology* 209: 1575–1584.
- Alvarez, L. W., Alvarez, W., Asaro, F., and Michel, H. V., 1980. Extraterrestrial Cause for the Cretaceous-Tertiary Extinction - Experimental Results and Theoretical Interpretation. *Science* 208(4448): 1095–1108.
- Arenillas, I., Arz, J. A., Grajales-Nishimura, J. M., Murillo-Muñetón, G., Alvarez, W., Camargo-Zanoguera, A., Molina, E., and Rosales-Domínguez, C., 2006. Chicxulub impact event is Cretaceous/Paleogene boundary in age: New micropaleontological evidence. *Earth and Planetary Science Letters* 249(3-4): 241–257.
- Arthur, M., Dean, W., and Pratt, L. M., 1988. Geochemical and climatic effects of increased marine organic carbon burial at the Cenomanian/Turonian boundary. *Nature* 335: 714–717.
- Ault, W. and Kulp, J., 1959. Isotopic geochemistry of sulphur. *Geochimica et Cosmochimica Acta* 16: 201–235.
- Bambach, R., 2006. Phanerozoic biodiversity mass extinctions. *Annual Review of Earth and Planetary Sciences* 34: 127–155.

- Bambach, R. K., Knoll, A. H., and Wang, S. C., 2004. Origination, extinction, and mass depletions of marine diversity. *Paleobiology* 30(4): 522–542.
- Barattolo, F. and Romano, R., 2005. Shallow carbonate platform bioevents during the Upper Triassic-Lower Jurassic: an evolutive interpretation. *Bollettino Della Societa Geologica Italiana* 124(1): 123–142.
- Baublys, K. A., Golding, S. D., Young, E., and Kamber, B. S., 2004. Simultaneous determination of delta33SV-CDT and delta34SV-CDT using masses 48, 49 and 50 on a continuous flow isotope ratio mass spectrometer. *Rapid Communications in Mass Spectrometry* 18: 2765–2769.
- Baud, A., Cirilli, S., and Marcoux, J., 1997. Biotic response to mass extinction: The lowermost Triassic microbialites. *Facies* 36: 238–242.
- Becker, L., Poreda, R. J., Basu, A. R., Pope, K. O., Harrison, T. M., Nicholson, C., and Iasky, R., 2004. Bedout: A Possible End-Permian Impact Crater Offshore of Northwestern Australia. *Science* 304(5676): 1469–1476.
- Beerling, D., Lomax, B., Upchurch, G., Nichols, D., Pillmore, C., Handley, L., and Scrimgeour, C., 2001. Evidence for the recovery of terrestrial ecosystems ahead of marine primary production following a biotic crisis at the Cretaceous-Tertiary boundary. *Journal of the Geological Society* 158: 737–740.
- Beerling, D. J. and Berner, R. A., 2002. Biogeochemical constraints on the Triassic—Jurassic boundary carbon cycle event. *Global Biogeochemical Cycles* 16: 101–113.
- Beerling, D. J., Lomax, B. H., Royer, D. L., Upchurch, G. R., Jr., and Kump, L. R., 2002. An atmospheric pCO₂ reconstruction across the Cretaceous-Tertiary boundary from leaf megafossils. *Proceedings of the National Academy of Sciences of the United States of America* 99(12): 7836–7840.
- Behrenfeld, M. J., O'Malley, R. T., Siegel, D. A., McClain, C. R., Sarmiento, J. L., Feldman, G. C., Milligan, A. J., Falkowski, P. G., Letelier, R. M., and Boss, E. S., 2006. Climate-driven trends in contemporary ocean productivity. *Nature* 444(752–755).
- Bennett, B., Fustic, M., Farrimond, P., Huang, H., and Larter, S., 2006. 25-Norhopanes: Formation during biodegradation of petroleum in the subsurface. *Organic Geochemistry* 37: 787–797.
- Benton, M., 1995. Diversification and extinction in the history of life. *Science* 268(5207): 52–58.

- Benton, M. J., 1993. Reptilia. In: Benton, M., ed., *The Fossil Record*, volume 2, pages 681–715. Chapman and Hall, London.
- Benton, M. J. and Twitchett, R. J., 2003. How to kill (almost) all life: the end-Permian extinction event. *Trends in Ecology and Evolution* 18(7): 358–365.
- Berner, R. A., 1984. Sedimentary pyrite formation: an update. *Geochimica et Cosmochimica Acta* 48: 605–615.
- Berner, R. A., 2002. Examination of hypotheses for the Permo-Triassic boundary extinction by carbon cycle modeling. *Proceedings of the National Academy of Sciences of the United States of America* 99(7): 4172–4177.
- Berner, R. A., 2004. A model for calcium, magnesium and sulfate in seawater over Phanerozoic time. *American Journal of Science* 304: 438–453.
- Berner, R. A., 2006. GEOCARBSULF: A combined model for Phanerozoic atmospheric O₂ and CO₂. *Geochimica et Cosmochimica Acta* 70(23): 5653–5664.
- Berner, R. A. and Beerling, D. J., 2007. Volcanic degassing necessary to produce a CaCO₃ undersaturated ocean at the Triassic–Jurassic boundary. *Palaeogeography Palaeoclimatology Palaeoecology* 244(1-4): 368–373.
- Bloos, G. and Page, K., 2002. Global Stratotype Section and Point for the base of the Sinemurian stage (Lower Jurassic). *Episodes* 25: 22–28.
- Bottjer, D., Droser, M., Sheehan, P., and McGhee, G., 2001. The ecological architecture of major events in the Phanerozoic history of marine invertebrate life. In: Allmon, W. and Bottjer, D., eds., *Evolutionary Paleocology*, pages 35–61. Columbia University Press.
- Boudreau, B. and Westrich, J., 1984. The dependence of bacterial sulfate reduction on sulfate concentrations in marine sediments. *Geochimica et Cosmochimica Acta* 48: 2504–2516.
- Bowring, S. A., Erwin, D. H., Jin, Y. G., Martin, M. W., Davidek, K., and Wang, W., 1998. U/Pb Zircon Geochronology and Tempo of the End-Permian Mass Extinction. *Science* 280(5366): 1039–1045.
- Brasier, M., McLoughlin, N., Green, O., and Wacey, D., 2006. A fresh look at the fossil evidence for early Archaean cellular life. *Philosophical Transactions of the Royal Society B - Biological Sciences* 361(1470): 887–902.

- Brenchley, P. J., Marshall, J. D., Carden, G. A. F., Robertson, D. B. R., Long, D. G. F., Meidla, T., Hints, L., and Anderson, T. F., 1994. Bathymetric and isotopic evidence for a short-lived Late Ordovician glaciation in a greenhouse period. *Geology* 22(4): 295–298.
- Briggs, R., Middleton, M., and Nelson, C., 2004. Provenance history of a Late Triassic–Jurassic Gondwana margin forearc Provenance history of a Late Triassic–Jurassic Gondwana margin forearc basin, Murihiku Terrane, North Island, New Zealand: petrographic and geochemical constraints. *New Zealand Journal of Geology and Geophysics* 47: 589–602.
- Brocks, J., Logan, G., Buick, R., and Summons, R., 1999. Archean molecular fossils and the early rise of eukaryotes. *Science* 285(5430): 1033–1036.
- Buggisch, W., 1991. The Global Frasnian-Famennian Kellwasser Event. *Geologische Rundschau* 80(1): 49–72.
- Bustin, R., 1997. Petroleum source rocks, organic maturation and thermal history of the Queen Charlotte Basin, British Columbia. *Bulletin of Canadian Petroleum Geology* 45(3): 255–278.
- Bustin, R. and Macauley, G., 1988. Organic petrology and rock-eval pyrolysis of the Jurassic Sandilands and Ghost Creek Formations, Queen Charlotte Islands. *Bulletin of Canadian Petroleum Geology* 36(2): 168–176.
- Bustin, R. and Mastalerz, M., 1995. Organic petrology and geochemistry of organic-rich rocks of the Late Triassic and Early Jurassic Sandilands and Ghost Creek Formations, Queen Charlotte Islands, British Columbia. *Marine and Petroleum Geology* 12: 70–81.
- Butterfield, N., 2007. Macroevolution and macroecology through deep time. *Palaeontology* 50: 41–55.
- Campbell, H., Mortimer, N., and Turnbull, I., 2003. Murihiku Supergroup, New Zealand: redefined. *Journal of the Royal Society of New Zealand* 33(1): 85–95.
- Campbell, J. and Coombs, D., 1966. Murihiku Supergroup (Triassic–Jurassic) of Southland and South Otago. *New Zealand Journal of Geology and Geophysics* 9: 393–398.
- Canfield, D. and Raiswell, R., 1999. The Evolution of the Sulfur Cycle. *American Journal of Science* 299: 697–723.

- Carter, E. and Hori, R., 2005. Global correlation of the radiolarian faunal change across the Triassic–Jurassic boundary. *Canadian Journal of Earth Sciences* 42(5): 777–790.
- Clarkson, E., 1996. *Invertebrate Palaeontology and Evolution*. Chapman and Hall, Cambridge, 3rd edition.
- Claypool, G., Holser, W., Kaplan, I., Sakai, H., and Zak, I., 1980. The age curves of sulfur and oxygen isotopes in marine sulfate and their mutual interpretation. *Chemical Geology* 28(190-260).
- Cooper, R., 2004. The New Zealand Geological Timescale. *Institute of Geological and Nuclear Sciences Monograph* 22.
- Courtillot, V. E., Besse, J., Vandamme, D., Montogny, R., Jaeger, J. J., and Capetta, H., 1986. Deccan flood basalts at the Cretaceous-Tertiary boundary? *Earth and Planetary Science Letters* 80: 361–374.
- Crampton, J., Beu, A., Campbell, H., Cooper, R., Morgans, H., Raine, J., Scott, G., Stevens, G., Strong, C., and Wilson, G., 1995. An interim New Zealand geological time scale. *Institute of Geological and Nuclear Sciences Report* 95/9: 1–6.
- Crowley, T. and Baum, S., 1991. Toward reconciliation of Late Ordovician (approximately-440 Ma) glaciation with very high CO₂ levels. *Journal of Geophysical Research-Atmospheres* 96(D12): 22597.
- Crutzen, P., 2003. How long have we been in the Anthropocene era? *Climatic Change* 61(3): 251–257.
- Crutzen, P., 2005. *The "Anthropocene"*. Springer, New York.
- Cuny, G., 1996. French vertebrate faunas and the Triassic-Jurassic boundary. *Palaeogeography Palaeoclimatology Palaeoecology* 119(3-4): 343–358.
- D'Hondt, S., Donaghay, P., Zachos, J. C., Luttenberg, D., and Lindinger, M., 1998. Organic Carbon Fluxes and Ecological Recovery from the Cretaceous-Tertiary Mass Extinction. *Science* 282(5387): 276–279.
- Dickens, G., Oneil, J., D.K., R., and Owen, R., 1995. Dissociation of oceanic methane hydrate as a cause of the carbon-isotope excursion at the end of the Paleocene. *Paleoceanography* 10(6): 965–971.

- Dumas, S. and Arnott, R., 2006. Origin of hummocky and swaley cross-stratification – The controlling influence of unidirectional current strength and aggradation rate. *Geology* 34(12): 1073–1076.
- Dunning, G. and Hodych, J., 1990. U/Pb zircon and baddeleyite ages for the Palisades and Gettysburg sills of the northeastern United States: implications for the age of the Triassic/Jurassic boundary. *Geology* 18: 795–798.
- Erwin, D. H., 1993. *The Great Paleozoic Crisis: Life and Death in the Permian*. Columbia University Press, New York.
- Erwin, D. H., 1994. The Permo-Triassic Extinction. *Nature* 367(6460): 231–236.
- E.S., C. and Hori, R. a., 1993. Radiolarian faunal turnover at the T/J boundary: Western Canada and Japan. In: *IGCP 458 Triassic/Jurassic boundary events: Mass extinction, global environmental change, and driving forces*.
- Ezaki, Y., Liu, J. B., and Adachi, N., 2003. Earliest Triassic microbialite micro- to megastructures in the Huaying area of Sichuan Province, South China: Implications for the nature of oceanic conditions after the end-Permian extinction. *Palaios* 18(4-5): 388–402.
- Farley, K. and Mukhopadhyay, S., 2001. An Extraterrestrial Impact at the Permian-Triassic Boundary? *Science* 293(5539): 2343.
- Fedo, C., Whitehouse, M., and Kamber, B., 2006. Geological constraints on detecting the earliest life on Earth: a perspective from the Early Archaean (older than 3.7 Gyr) of southwest Greenland. *Philosophical Transactions of the Royal Society B - Biological Sciences* 361(1470): 851–687.
- Fry, B., Silva, S. R., Kendall, C., and Anderson, R. K., 2002. Oxygen isotope corrections for online delta34S analysis. *Rapid Communications in Mass Spectrometry* 16: 854–858.
- Gallet, Y., Krystyn, L., Besse, J., and Marcoux, J., 2003. Improving the Upper Triassic numerical time scale from cross-correlation between Tethyan marine sections and the continental Newark basin sequence. *Earth and Planetary Science Letters* 212: 255–261.
- Gallet, Y., Krystyn, L., Marcoux, J., and Besse, J., 2007. New constraints on the End-Triassic (Upper Norian–Rhaetian) magnetostratigraphy. *Earth and Planetary Science Letters* 255(3-4): 458–470.

- Galli, M. T., Jadoul, F., Bernasconi, S. M., and Weissert, H., 2005. Anomalies in global carbon cycling and extinction at the Triassic/Jurassic boundary: evidence from a marine C-isotope record. *Palaeogeography Palaeoclimatology Palaeoecology* 216: 203–314.
- Geldsetzer, H. H. J., Goodfellow, W. D., McLaren, D. J., and Orchard, M. J., 1987. Sulfur-isotope anomaly associated with the Frasnian-Famennian extinction, Medicine Lake, Alberta, Canada. *Geology* 15(5): 393–396.
- Gelpi, E., Schneiderman, H., Man, J., and Oró, J., 1970. Hydrocarbons of geochemical significance in microscopic algae. *Phytochemistry* 9: 603–612.
- George, A. and Chow, N., 2002. The depositional record of the Frasnian–Famennian interval in a fore-reef succession, Canning Basin, Western Australia. *Palaeogeography Palaeoclimatology Palaeoecology* 181: 347–374.
- Golonka, J., 2007. Late Triassic and Early Jurassic palaeogeography of the world. *Palaeogeography Palaeoclimatology Palaeoecology* 244(1-2): 297–307.
- Goossens, H., De Leeuw, J., Schenck, P., and Brassell, S., 1984. Tocopherols as likely precursors of pristane in ancient sediments and crude oils. *Nature* 312: 440–442.
- Gould, S., 1989. *Wonderful Life*. W.W. Norton and Co., New York.
- Gradstein, F., Ogg, J., Smith, A., Agterberg, F., Bleeker, W., Cooper, R., Davydov, V., Gibbard, P., Hinnov, L., House, M., Lourens, L., Luterbacher, H., McArthur, J., Melchin, M., Robb, L., Shergold, J., Villeneuve, M., Wardlaw, B., Ali, J., Brinkhuis, H., Hilgen, F., Hooker, J., Howarth, R., Knoll, A., Laskar, J., Monechi, S., Plumb, K., Powell, J., Raffi, I., Röhl, U., Sadler, P., Sanfilippo, A., Schmitz, B., Shackleton, N., Shields, G., Strauss, H., Van Dam, J., van Kolfschoten, T., Veizer, J., and Wilson, D., 2004. *A Geologic Time Scale 2004*. Cambridge University Press.
- Grant-Mackie, J., 1959. Hokonui stratigraphy of the Awakino-Mahoenui area southwest Auckland. *New Zealand Journal of Geology and Geophysics* 2: 755–787.
- Grice, K., Alexander, R., and Kagi, R., 2000. Diamondoid hydrocarbon ratios as indicators of biodegradation in Australian crude oils. *Organic Geochemistry* 31(1): 67–73.
- Grice, K., Cao, C. Q., Love, G. D., Bottcher, M. E., Twitchett, R. J., Grosjean, E., Summons, R. E., Turgeon, S. C., Dunning, W., and Jin, Y. G., 2005. Photic zone euxinia during the Permian-Triassic superanoxic event. *Science* 307: 706–709.

- Guex, J., Bartolini, A., Atudorei, V., and Taylor, D., 2004. High-resolution ammonite and carbon isotope stratigraphy across the Triassic—Jurassic boundary at New York Canyon (Nevada). *Earth and Planetary Science Letters* 225: 29–41.
- Gunde-Cimerman, N., Oren, A., and Plemenitas, A., eds., 2005. *Adaptation to Life at High Salt Concentrations in Archaea, Bacteria, and Eukarya*. Cellular Origin, Life in Extreme Habitats and Astrobiology. Springer.
- Habicht, K. S., Gade, M., Thamdrup, B., Berg, P., and Canfield, D. E., 2002. Calibration of Sulfate Levels in the Archean Ocean. *Science* 298(5602): 2372–2374.
- Haggart, J., Carter, E., Beattie, M., Bown, P., Inkin, R., Kring, D., Johns, M., McNicoll, V., Orchard, M., Perry, R., Schröder-Adams, C., Smith, P., Suneby, L., Tipper, H., and Ward, P., 2001. Stratigraphy of Triassic/Jurassic boundary strata, Queen Charlotte Islands, British Columbia: potential global system stratotype boundary. In: *IGCP 458 Field Meeting, October 13–17, Taunton, UK*.
- Hallam, A., 1981. The End-Triassic Bivalve Extinction Event. *Palaeogeography Palaeoclimatology Palaeoecology* 35(1): 1–44.
- Hallam, A., 1984. Pre-Quaternary sea-level changes. *Annual Review of Earth and Planetary Sciences* 12: 205–243.
- Hallam, A., 1999. Evidence of sea level fall in sequence stratigraphy: Examples from the Jurassic. *Geology* 27(4): 343–346.
- Hallam, A., 2002. How catastrophic was the end-Triassic mass extinction? *Lethaia* 35(2): 147–157.
- Hallam, A. and Wignall, P., 1999. Mass extinctions and sea-level changes. *Earth Science Reviews* 48: 217–250.
- Hallam, A. and Wignall, P. B., 2000. Facies changes across the Triassic-Jurassic boundary in Nevada, USA. *Journal of the Geological Society* 157: 49–54.
- Harper, D., Brunton, C., Cocks, L., Copper, P., Doyle, E., Jeffrey, A., Owen, E., Parkes, M., Popov, L., and Prosser, C., 1993. Brachiopoda. In: Benton, M., ed., *The Fossil Record*, volume 2, pages 427–462. Chapman and Hall, London.
- Hart, M. B. and Williams, C., 1993. Protozoa. In: Benton, M., ed., *The Fossil Record*, volume 2, pages 43–70. Chapman and Hall, London.

- Hay, W., Migdisov, A., Balukhovskiy, A., Wold, C., Floegel, S., and Soding, E., 2006. Evaporites and the salinity of the ocean during the Phanerozoic: Implications for climate, ocean circulation and life. *Palaeogeography Palaeoclimatology Palaeoecology* 240: 3–46.
- Hayes, J., 2002. Isotopic order, biogeochemical processes, and earth history. Goldschmidt Lecture, Davos, Switzerland, August, 2002. *Geochimica et Cosmochimica Acta* 68(8): 1691–1700.
- Hayes, J., Freeman, K., Popp, B., and Hoham, C., 1989. Compound-specific isotopic analyses: A novel tool for reconstruction of ancient biogeochemical processes. *Organic Geochemistry* 16(4-6): 1115–1128.
- Henderson, J. and Grange, L., 1922. Notes to accompany a geological sketch-map of the Marokopa District. *New Zealand journal of science and technology* 5: 177–183.
- Hesselbo, S. and Coe, A., 2000. Evidence of sea level fall in sequence stratigraphy: examples from the Jurassic: Comment. *Geology* 28(1): 95–96.
- Hesselbo, S., McRoberts, C., and Pálffy, J., 2007. Triassic–Jurassic boundary events: Problems, progress, possibilities. *Palaeogeography Palaeoclimatology Palaeoecology* 244(1-4): 1–10.
- Hesselbo, S., Robinson, S., and Surlyk, F., 2004. Sea-level change and facies development across potential Triassic–Jurassic boundary horizons, SW Britain. *Journal of the Geological Society* 161: 365–379.
- Hesselbo, S. P., Robinson, S. A., Surlyk, F., and Piasecki, S., 2002. Terrestrial and marine extinction at the Triassic–Jurassic boundary synchronized with major carbon-cycle perturbation: A link to initiation of massive volcanism? *Geology* 30: 251–254.
- Hildebrand, A. R., Penfield, G. T., Kring, D. A., Pilkington, M., Camargo, A., Jacobsen, S. B., and Boynton, W. V., 1991. Chicxulub Crater - a Possible Cretaceous Tertiary Boundary Impact Crater on the Yucatan Peninsula, Mexico. *Geology* 16(4-6): 867–871.
- Hinrichs, K. U., Hmelo, L. R., and Sylva, S. P., 2003. Molecular fossil record of elevated methane levels in late Pleistocene coastal waters. *Science* 299(5610): 1241–1217.
- Hodych, J. and Dunning, G., 1992. Did the Manicouagan impact trigger end-of-Triassic mass extinction? *Geology* 20: 51–54.

- Holser, W., Clement, G., Lubomir, F., and Wade, J., 1988. Evaporite deposits of the North Atlantic rift. In: Manspeizer, W., ed., *Triassic-Jurassic Rifting Part B*, chapter 22, pages 525–556. Elsevier.
- Holser, W. and Magaritz, M., 1987. Events near the Permian-Triassic boundary. *Modern Geology* 11(2): 155–180.
- Hotinski, R., Bice, K., Kump, L., Najjar, R., and Arthur, M., 2001. Ocean stagnation and end-Permian anoxia. *Geology* 29(1): 7–10.
- Houghton, J. T., Ding, Y., Griggs, D., Noguer, M., van der Linden, P. J., and Xiaosu, D., eds., 2001. *Climate Change 2001: The Scientific Basis*. Cambridge University Press.
- Hounslow, M. W., Posen, P. E., and Warrington, G., 2004. Magnetostratigraphy and biostratigraphy of the Upper Triassic and lowermost Jurassic succession, St. Audrie's Bay, UK. *Palaeogeography Palaeoclimatology Palaeoecology* 213(3-4): 331–358.
- Hsü, K. and McKenzie, J., 1985. 'Strangelove' ocean in the earliest Tertiary. *American Geophysical Union – Geophysics Monograph* 32: 487–892.
- Huey, R. B. and Ward, P. D., 2005. Hypoxia, global warming, and terrestrial Late Permian extinctions. *Science* 308(5720): 398–401.
- Hunt, J., 1995. *Petroleum geochemistry and geology*. W.H. Freeman and Co., New York, 2nd edition.
- Irmis, R. B., Nesbitt, S. J., Padian, K., Smith, N. D., Turner, A. H., Woody, D., and Downs, A., 2007. A Late Triassic Dinosauriform Assemblage from New Mexico and the Rise of Dinosaurs. *Science* 317(5836): 358–361.
- Isozaki, Y., 1997. Permo-Triassic boundary superanoxia and stratified superocean: Records from lost deep-sea. *Science* 276(5310): 235–238.
- Jablonski, D., 1991. Extinctions: A Paleontological Perspective. *Science* 253(5021): 754–757.
- Joachimski, M. and Buggisch, W., 1993. Anoxic events in the Late Frasnian - Causes of the Frasnian-Famennian faunal crisis? *Geology* 21(8): 675–678.
- Jørgensen, B., 1982. Mineralization of organic matter in the sea bed - the role of sulfate reduction. *Nature* 296: 643–645.

- Kaiho, K., Chen, Z.-Q., Kawahata, H., Kajiwara, Y., and Sato, H., 2006a. Close-up of the end-Permian mass extinction horizon recorded in the Meishan section, South China: Sedimentary, elemental, and biotic characterization and a negative shift of sulfate sulfur isotope ratio. *Palaeogeography Palaeoclimatology Palaeoecology* 239(3-4): 396–405.
- Kaiho, K., Kajiwara, Y., Chen, Z.-Q., and Gorjan, P., 2006b. A sulfur isotope event at the end of the Permian. *Chemical Geology* 235(1-2): 33–47.
- Kaiho, K., Kajiwara, Y., Nakano, T., Miura, Y., Kawahata, H., Tazaki, K., Ueshima, M., Chen, Z., and Shi, G., 2001. End-Permian catastrophe by a bolide impact: evidence of a gigantic release of sulfur from the mantle. *Geology* 29: 815–818.
- Kaiho, K., Kajiwara, Y., Tazaki, K., Ueshima, M., Takeda, N., Kawahata, H., Arinobu, T., Ishiwatari, R., Hirai, A., and Lamolda, M. A., 1999. Oceanic primary productivity and dissolved oxygen levels at the Cretaceous/Tertiary boundary: Their decrease, subsequent warming, and recovery. *Paleoceanography* 14: 511–524.
- Kajiwara, Y. and Kaiho, K., 1992. Oceanic anoxia at the Cretaceous/Tertiary boundary supported by the sulfur isotopic record. *Palaeogeography Palaeoclimatology Palaeoecology* 99: 151–162.
- Kajiwara, Y., Yamakita, S., Ishida, K., Ishiga, H., and Imai, A., 1994. Development of a largely anoxic stratified ocean and its temporary massive mixing at the Permian/Triassic boundary supported by the sulfur isotopic record. *Palaeogeography Palaeoclimatology Palaeoecology* 111: 367–379.
- Kamo, S., Czamanske, G., Amelin, Y., Fedorenko, V., Davis, D., and Trofimov, V., 2003. Rapid eruption of Siberian flood-volcanic rocks and evidence for coincidence with the Permian–Triassic boundary and mass extinction at 251 Ma. *Earth and Planetary Science Letters* 214: 75–91.
- Kampschulte, A. and Strauss, H., 2004. The sulfur isotopic evolution of Phanerozoic seawater based on the analysis of structurally substituted sulfate in carbonates. *Chemical Geology* 204: 255–286.
- Katsumata, H. and Shimoyama, A., 2001. Thiophenes in the Cretaceous/Tertiary boundary sediments at Kawaruppu, Hokkaido, Japan. *Geochemical Journal* 35(1): 67–76.
- Keith, M., 1982. Violent volcanism, stagnant oceans and some inferences regarding petroleum, strata-bound ores and mass extinctions. *Geochimica et Cosmochimica Acta* 46(12): 2621–2637.

- Keller, G., 2003. Biotic effects of impacts and volcanism. *Earth and Planetary Science Letters* 215(1-2): 249–264.
- Keller, G., 2005. Impacts, volcanism and mass extinction: random coincidence or cause and effect? *Australian Journal of Earth Sciences* 52(4-5): 725–757.
- Kent, D., Olsen, P., and Witte, W., 1995. Late Triassic–earliest Jurassic geomagnetic polarity sequence and paleolatitudes from drill cores in the Newark rift basin, eastern North America. *Journal of Geophysical Research* 100: 14965–14998.
- Kershaw, S., Zhang, T. S., and Lan, G. Z., 1999. A microbialite carbonate crust at the Permian-Triassic boundary in South China, and its palaeoenvironmental significance. *Palaeogeography Palaeoclimatology Palaeoecology* 146(1-4): 1–18.
- Kidder, D. and Worsley, T., 2004. Causes and consequences of extreme Permo-Triassic warming to globally equable climate and relation to the Permo-Triassic extinction and recovery. *Palaeogeography Palaeoclimatology Palaeoecology* 203(3-4): 207–237.
- Kidder, D. L. and Erwin, D. H., 2001. Secular distribution of biogenic silica through the phanerozoic: Comparison of silica-replaced fossils and bedded cherts at the series level. *Journal of Geology* 109(4): 509–522.
- Kiessling, W., Aberhan, M., Brenneis, B., and Wagner, P., 2007. Extinction trajectories of benthic organisms across the Triassic-Jurassic boundary. *Palaeogeography Palaeoclimatology Palaeoecology* 244(1-4): 201–222.
- Knight, K., Nomade, S., Renne, P., Marzoli, A., Bertrand, H., and Youbi, N., 2004. The Central Atlantic Magmatic Province at the Triassic–Jurassic boundary: paleomagnetic and $^{40}\text{Ar}/^{39}\text{Ar}$ evidence from Morocco for brief, episodic volcanism. *Earth and Planetary Science Letters* 228: 143–160.
- Koeberl, C., Farley, K., Peucker-Ehrenbrink, B., and Sephton, M., 2004. Geochemistry of the end-Permian extinction event in Austria and Italy: No evidence for an extraterrestrial component. *Geology* 32: 1053–1056.
- Korte, C., Kozur, H., Joachimski, M., Strauss, H., Veizer, J., and Schwark, L., 2004. Carbon, sulfur, oxygen and strontium isotope records, organic geochemistry and biostratigraphy across the Permian/Triassic boundary in Abadeh, Iran. *International Journal of Earth Science* 93: 565–581.
- Kuerschner, W. M., Bonis, N. R., and Krystyn, L., 2007. Carbon-isotope stratigraphy and palynostratigraphy of the Triassic–Jurassic transition in the Tiefengraben

- section — Northern Calcareous Alps (Austria). *Palaeogeography Palaeoclimatology Palaeoecology* 244(1-4): 257–280.
- Kump, L. R. and Arthur, M. A., 1999. Interpreting carbon-isotope excursions: carbonates and organic matter. *Chemical Geology* 161: 181–198.
- Kump, L. R., Pavlov, A., and Arthur, M. A., 2005. Massive release of hydrogen sulfide to the surface ocean and atmosphere during intervals of oceanic anoxia. *Geology* 33(5): 397–400.
- Leakey, R. and Lewin, R., 1996. *The Sixth Extinction : Patterns of Life and the Future of Humankind*. Anchor.
- Londry, K. and Des Marais, D., 2003. Stable Carbon Isotope Fractionation by Sulfate Reducing Bacteria. *Applied Environmental Microbiology* 69: 2942–2949.
- Longridge, L. M., Carter, E. S., Smith, P. L., and Tipper, H. W., 2007. Early Hettangian ammonites and radiolarians from the Queen Charlotte Islands, British Columbia and their bearing on the definition of the Triassic–Jurassic boundary. *Palaeogeography Palaeoclimatology Palaeoecology* 244(1-4): 142–169.
- Love, G., Snape, C., and Fallick, A., 1998. Differences in the mode of incorporation and biogenicity of the principal aliphatic constituents of a Type I oil shale. *Organic Geochemistry* 28(12): 797–811.
- Lovelock, J., Maggs, R., and Rasmussen, R., 1972. Atmospheric Dimethyl Sulphide and the Natural Sulphur Cycle. *Nature* 237: 452–453.
- Lucas, S. G. and Tanner, L. H., 2007. Tetrapod biostratigraphy and biochronology of the Triassic–Jurassic transition on the southern Colorado Plateau, USA. *Palaeogeography Palaeoclimatology Palaeoecology* 244(1-4): 242–256.
- Lyell, C., 1830. *Principles of Geology*. John Murray, London.
- MacFarlan, D., 1998. Mesozoic stratigraphy of the Marokopa area, southwest Auckland, New Zealand. *New Zealand Journal of Geology and Geophysics* 41: 297–310.
- Magaritz, M., Bard, R., Baud, A., and Holser, W. T., 1994. The carbon-isotope shift at the Permian/Triassic boundary in the southern Alps is gradual. *Nature* 331: 337–339.
- Manspeizer, W., 1988. Triassic - Jurassic rifting and opening of the Atlantic: An overview. In: Manspeizer, W., ed., *Triassic-Jurassic Rifting Part A*, chapter 3, pages 41–79. Elsevier.

- Margolis, S., Mount, J., Showers, W., and Ward, P., 1985. Late Cretaceous/Tertiary boundary paleoceanographic events, oxygen and carbon isotope stratigraphy, and biotic extinctions. *Eos, Transactions, American Geophysical Union* 66(46): 933.
- Martin, P. and Wright, H., Jr., eds., 1967. *Pleistocene Extinctions: The Search for a Cause*. Yale University Press.
- Maruoka, C., Koeberl, P. H., and Reimold, W., 2003. Sulfur geochemistry across a terrestrial Permian–Triassic boundary section in the Karoo Basin South Africa. *Earth and Planetary Science Letters* 206: 101–117.
- Marzoli, A., Bertrand, H., Knight, K., Cirilli, S., Buratti, N., Verati, C., Nomade, S., Renne, P., Youbi, N., Martini, R., Allenbach, K., Neuwerth, R., Rapaille, C., Zaninetti, L., and Bellieni, G., 2004. Synchrony of the Central Atlantic magmatic province and the Triassic-Jurassic boundary climatic and biotic crisis. *Geology* 32(11): 973–976.
- Marzoli, A., Renne, P. R., Piccirillo, E. M., Ernesto, M., Bellieni, G., and Min, A. D., 1999. Extensive 200-million-year-old continental flood basalts of the Central Atlantic Magmatic Province. *Science* 284(5414): 616–618.
- Maubeuge, P.-L., 1964. Comptes rendus du colloque. In: Maubeuge, P.-L., ed., *Colloque du Jurassique a Luxembourg (1962)*. l'Institut Grand-Ducal, Section des Sciences Naturelles, Physiques et Mathématiques.
- McCune, A. and Schaeffer, B., 1986. Triassic and Jurassic fishes: patterns of diversity. In: Padian, K., ed., *The Beginning of the Age of Dinosaurs*, pages 171–181. Cambridge University Press, Cambridge.
- McElwain, J. C., Beerling, D. J., and Woodward, F. I., 1999. Fossil plants and global warming at the Triassic-Jurassic boundary. *Science* 285(5432): 1386–1390.
- McGhee, G., Jr., 1996. *The Late Devonian Mass Extinction*. Columbia University Press, New York.
- McGhee, G., Jr., Orth, C., Quintana, L., Gilmore, J., and Olsen, E., 1986. Late Devonian "Kellwasser Event" mass-extinction horizon in Germany; no geochemical evidence for a large-body impact. *Geology* 14(9): 776–779.
- McKay, A., 1877. Reports relative to collections of fossils in the South-East district of the province of Otago. *New Zealand Geological Survey Report Geological Exploration 1873-1874* 8B: 59–73.

- McRoberts, C., 1994. The Triassic–Jurassic exostratigraphic transition in the Lombardian Alps, Italy. *Palaeogeography Palaeoclimatology Palaeoecology* 110(145–166).
- McRoberts, C., Furrer, H., and Jones, D., 1997. Palaeoenvironmental interpretation of a Triassic–Jurassic boundary section from western Austria based on palaeoecological and geochemical data. *Palaeogeography Palaeoclimatology Palaeoecology* 136: 79–85.
- Megonigal, J., Hines, M., and Visscher, P., 2003. Anaerobic Metabolism: Linkages to Trace Gases and Aerobic Processes. In: Schlesinger, W., ed., *Biogeochemistry*, volume 8 of *Treatise on Geochemistry* (eds. H.D. Holland and K.K. Turekian). Elsevier-Pergamon, Oxford.
- Meyers, P. A., Silliman, J. E., and Shawb, T. J., 1996. Effects of turbidity flows on organic matter accumulation, sulfate reduction, and methane generation in deep-sea sediments on the Iberia Abyssal Plain. *Organic Geochemistry* 25(1–2): 69–78.
- Milkov, A., 2004. Global estimates of hydrate-bound gas in marine sediments: how much is really out there? *Earth Science Reviews* 66(3–4): 183–197.
- Milkov, A. and Sassen, R., 2003. Two-dimensional modeling of gas hydrate decomposition in the northwestern Gulf of Mexico: significance to global change assessment. *Global and Planetary Change* 36(1–2): 31–46.
- Miller, K. G., Kominz, M. A., Browning, J. V., Wright, J. D., Mountain, G. S., Katz, M. E., Sugarman, P. J., Cramer, B. S., Christie-Blick, N., and Pekar, S. F., 2005. The Phanerozoic Record of Global Sea-Level Change. *Science* 310(5752): 1293–1298.
- Mita, H. and Shimoyama, A., 1999. Characterization of n-alkanes, pristane and phytane in the Cretaceous/Tertiary boundary sediments at Kawaruppu, Hokkaido, Japan. *Geochemical Journal* 33(5): 285–294.
- Mojzsis, S., Arrhenius, G., McKeegan, K., Harrison, T., Nutman, A., and Friend, C., 1996. Evidence for life on Earth before 3,800 million years ago. *Nature* 384(6604).
- Morante, R. and Hallam, A., 1996. Organic carbon isotopic record across the Triassic–Jurassic boundary in Austria and its bearing on the cause of the mass extinction. *Geology* 24(5): 391–394.
- Morbey, J., 1975. The palynostratigraphy of the Rhaetian stage, Upper Triassic in the Kendelbachgraben, Austria. *Palaeontographica B* 152: 1–75.

- Müller, G., Nielsen, H., and Ricke, W., 1966. Schwefel-Isotopen-Verhältnisse in Formations-wässern und Evaporiten Nord- und Süddeutschlands. *Chemical Geology* 1: 211–220.
- Muller, S. and Ferguson, H., 1936. Triassic and lower Jurassic formations of west central Nevada. *Geological Society of America Bulletin* 47: 241–252.
- Mundil, R., Ludwig, K., Metcalfe, I., and Renne, P., 2004. Age and Timing of the Permian Mass Extinctions: U/Pb Dating of Closed-System Zircons. *Science* 305(5691): 1760–1763.
- Mundil, R. and Palfy, J., 2005. Triassic-Jurassic time scale and mass extinction: Current status and new constraints. In: *Geochimica et Cosmochimica Acta Suppl. S.*
- Newell, N., 1967. Paraconformities. In: Teichert, C. and Yochelson, E., eds., *Essays in Paleontology and Stratigraphy, R.C. Moore Commemorative Volume*, pages 349–367. University of Kansas Press, Lawrence, Kansas.
- Newell, N. D., 1962. Paleontological gaps and geochronology. *Journal of Paleontology* 36(3): 592–610.
- Newton, R., Pevitt, E., Wignall, P., and Bottrell, S., 2004. Large shifts in the isotopic composition of seawater sulphate across the Permo-Triassic boundary in northern Italy. *Earth and Planetary Science Letters* 218: 331–345.
- Nicol, D., 1961. Biotic associations and extinction. *Systematic Zoology* 10(1): 35–41.
- Nomade, S., Knight, K., Beutel, E., Renne, P., Verati, C., Féraud, G., Marzoli, A., Youbi, N., and Bertrand, H., 2007. Chronology of the Central Atlantic Magmatic Province: Implications for the Central Atlantic rifting processes and the Triassic–Jurassic biotic crisis. *Palaeogeography Palaeoclimatology Palaeoecology* 244(1-4): 326–344.
- O’Leary, M., 1981. Carbon Isotope Fractionation in Plants. *Phytochemistry* 20: 553–567.
- Olsen, P., Kent, D., Cornet, B., Witte, W., and Schlische, R., 1996. High-resolution stratigraphy of the Newark rift basin (Early Mesozoic, Eastern North America). *Geological Society of America Bulletin* 108: 40–77.
- Olsen, P. E., 1997. Stratigraphic record of the Early Mesozoic breakup of Pangea in the Laurasia-Gondwana rift system. *Annual Review of Earth and Planetary Sciences* 25: 337–401.

- Olsen, P. E. and Kent, D. V., 1996. Milankovitch climate forcing in the tropics of Pangaea during the Late Triassic. *Palaeogeography Palaeoclimatology Palaeoecology* 122(1-4): 1–26.
- Olsen, P. E., Kent, D. V., Sues, H. D., Koeberl, C., Huber, H., Montanari, A., Rainforth, E. C., Powell, S. J., Szajna, M. J., and Hartline, B. W., 2002. Ascent of dinosaurs linked to an iridium anomaly at the Triassic—Jurassic boundary. *Science* 296: 1305–1307.
- Olsen, P. E., Shubin, N., and Anders, M., 1987. New Early Jurassic tetrapod assemblages constrain Triassic–Jurassic tetrapod extinction event. *Science* 237: 1025–1029.
- Orth, C., Gilmore, J., Quintana, L., and Sheehan, P., 1986. Terminal Ordovician extinction; geochemical analysis of the Ordovician/Silurian boundary, Anticosti Island, Quebec. *Geology* 14(5): 433–436.
- Pace, N., 1997. A Molecular View of Microbial Diversity and the Biosphere. *Science* 276(5313): 734–740.
- Pálffy, J., Demeny, A., Haas, J., Carter, E. S., Görög, A., Halász, D., Oravecz-Scheffer, A., Hetényi, M., Márton, E., Orchard, M. J., Ozsvárt, P., Vető, I., and Zajzon, N., 2007. Triassic–Jurassic boundary events inferred from integrated stratigraphy of the Csovar section, Hungary. *Palaeogeography Palaeoclimatology Palaeoecology* 244(1-4): 11–33.
- Pálffy, J., Demeny, A., Haas, J., Hetenyi, M., Orchard, M. J., and Veto, I., 2001. Carbon isotope anomaly and other geochemical changes at the Triassic—Jurassic boundary from a marine section in Hungary. *Geology* 29: 1047–1050.
- Pálffy, J., Smith, P., and Mortensen, J., 2000. A U-Pb and $^{40}\text{Ar}/^{39}\text{Ar}$ time scale for the Jurassic. *Canadian Journal of Earth Sciences* 37: 923–944.
- Payne, J. L. and Kump, L. R., 2007. Evidence for recurrent Early Triassic massive volcanism from quantitative interpretation of carbon isotope fluctuations. *Earth and Planetary Science Letters* 256(1-2): 264–277.
- Payne, J. L., Lehrmann, D. J., Wei, J., Orchard, M. J., Schrag, D. P., and Knoll, A. H., 2004. Large Perturbations of the Carbon Cycle During Recovery from the End-Permian Extinction. *Science* 305: 506–509.

- Peters, K., Moldowan, J., McCaffrey, M., and Fago, F., 1996. Selective biodegradation of extended hopanes to 25-norhopanes in petroleum reservoirs. Insights from molecular mechanics. *Organic Geochemistry* 24(8-9): 765–783.
- Peters, K., Walters, C., and Moldowan, J., 2005. *The biomarker guide*, volume 2: Biomarkers in petroleum systems and Earth history. Cambridge University Press, Cambridge, 2nd edition.
- Phillips, J., 1840a. Organic remains. *Penny Cyclopaedia* 16: 487–491.
- Phillips, J., 1840b. Paleozoic series. *Penny Cyclopaedia* 17: 153–154.
- Phillips, J., 1841. *Figures and Descriptions of the Palaeozoic Fossils of Cornwall, Devon and West Somerset; Observed in the Course of the Ordnance Survey of that District*. Longman, London.
- Pilot, J., Rösler, H., and Müller, P., 1972. Zur geochemischen Entwicklung des Meereswassers und mariner Sedimente im Phanerozoikum mittels Untersuchungen von S-, O- und C-Isotopen. *Neue Bergbautech* 2(161-168).
- Primeau, F., 2005. Characterizing Transport between the Surface Mixed Layer and the Ocean Interior with a Forward and Adjoint Global Ocean Transport Model. *Journal of Physical Oceanography* 35(4): 545–564.
- Pujol, F., Berner, Z., and Stüben, D., 2006. Palaeoenvironmental changes at the Frasnian/Famennian boundary in key European sections: Chemostratigraphic constraints. *Palaeogeography Palaeoclimatology Palaeoecology* 240(1-2): 120–145.
- Raab, M. and Spiro, B., 1991. Sulfur isotopic variations during seawater evaporation with fractional crystallization. *Chemical Geology* 86: 323–333.
- Raup, D. and Sepkoski, J., 1982. Mass extinctions in the marine fossil record. *Science* 215(4539): 1501–1503.
- Renne, P. and Basu, A., 1991. Rapid eruption of the Siberian traps flood basalts at the Permo-Triassic boundary. *Science* 253: 176–179.
- Renne, P., Melosh, H., Farley, K., Reimold, W., Koeberl, C., Rampino, M., Kelly, S., and Ivanov, B., 2004. Is Bedout an impact structure? Take 2. *Science* 306: 610–611.
- Renne, P. R., Black, M. T., Zichao, Z., Richards, M. A., and Basu, A. R., 1995. Synchrony and Causal Relations Between Permian-Triassic Boundary Crises and Siberian Flood Volcanism. *Science* 269(5229): 1413–1416.

- Retallack, G., 1999. Postapocalyptic greenhouse paleoclimate revealed by earliest Triassic paleosols in the Sydney Basin, Australia. *Geological Society of America Bulletin* 111(1): 52–70.
- Romein, A. and J., S., 1981. The Cretaceous-Tertiary boundary - Calcareous nannofossils and stable isotopes. *Proceedings of the Koninklijke Nederlandse Akademie van Wetenschappen Series B - Paleontology Geology Physics Chemistry Anthropology* 84(3): 295–314.
- Schopf, J. W., 2006. Fossil evidence of Archaean life. *Philosophical Transactions of the Royal Society B - Biological Sciences* 361(1470): 869–885.
- Seifert, W. and Moldowan, J., 1986. Use of biological markers in petroleum exploration. In: Johns, R., ed., *Methods in Geochemistry and Geophysics*, volume 24, pages 261–290. Elsevier.
- Sharpton, V., Dalrymple, G., Marín, L., Ryder, G., Schuraytz, B., and Urrutia-Fucugauchi, J., 1992. New links between the Chicxulub impact structure and the Cretaceous/Tertiary boundary. *Nature* 359: 819–821.
- Sheehan, P., 2001. The Late Ordovician Mass Extinction. *Annual Review of Earth and Planetary Sciences* 29: 331–364.
- Shimoyama, A. and Yabuta, H., 2002. Mono- and bicyclic alkanes and diamondoid hydrocarbons in the Cretaceous/Tertiary boundary sediments at Kawaruppu, Hokkaido, Japan. *Geochemical Journal* 36(2): 173–189.
- Smith, W., 1816. *Strata Identified by Organized Fossils*. W. Arding, London.
- Smith, W., 1835. Deductions from established facts of Geology. *The Literary Gazette* (969): 522.
- Speden, I. and McKellar, I., 1958. The occurrence of Aratauran beds South of Nugget Point, South Otago, New Zealand. *New Zealand Journal of Geology and Geophysics* 1: 647–652.
- Stevens, G., 2004. Hettangian-Sinemurian (Early Jurassic) Ammonites of New Zealand. *Institute of Geological and Nuclear Sciences Monograph* 23: 107.
- Strauss, H., 1997. The isotopic composition of sedimentary sulfur through time. *Palaeogeography Palaeoclimatology Palaeoecology* 132: 97–118.

- Summons, R. E. and Hayes, J. M., 1992. Principles of molecular and isotopic biogeochemistry. In: Schopf, J. W. and Klein, C., eds., *The Proterozoic Biosphere: A Multidisciplinary Study*, pages 83–93. Cambridge University Press, Cambridge.
- Summons, R. E., Jahnke, L. L., and Roksandic, Z., 1994. Carbon Isotopic Fractionation in Lipids from Methanotrophic Bacteria - Relevance for Interpretation of the Geochemical Record of Biomarkers. *Geochimica et Cosmochimica Acta* 58(13): 2853.
- Swisher, C., III, Grajales-Nishimura, J., Montanari, A., Renne, P., Cedillo-Pardo, E., Maurrasse, F., Curtis, G., Smit, J., and McWilliams, M., 1992. Chicxulub crater melt-rock and K–T boundary tektites from Mexico and Haiti yield coeval $^{40}\text{Ar}/^{39}\text{Ar}$ ages of 65 Ma. *Science* 257: 954–958.
- Tanner, L. H. and Lucas, S. G., 2007. The Moenave Formation: Sedimentologic and stratigraphic context of the Triassic–Jurassic boundary in the Four Corners area, southwestern U.S.A. *Palaeogeography Palaeoclimatology Palaeoecology* 244(1-4): 111–125.
- Tanner, L. H., Lucas, S. G., and Chapman, M. G., 2004. Assessing the record and causes of the Late Triassic extinctions. *Earth Science Reviews* 65: 103–139.
- Taylor, E., Taylor, T., and Cúneo, N., 1992. The present is not the key to the past: A polar forest from the Permian of Antarctica. *Science* 257: 1675–1677.
- Teichert, C., 1988. Crises in cephalopod evolution. In: Marois, M., ed., *L'évolution dans sa Réalité et des Diverses Modalités*, pages 7–64. Fondation Singer-Polignac.
- Thiel, V., Peckmann, J., Richnow, H. H., Luth, U., Reitner, J., and Michaelis, W., 2001. Molecular signals for anaerobic methane oxidation in Black Sea seep carbonates and a microbial mat. *Marine Chemistry* 73(2): 97–112.
- Thompson, P., Waite, A., and McMahon, K., 2003. Dynamics of a cyanobacterial bloom in a hypereutrophic, stratified weir pool. *Marine and Freshwater Research* 54: 27–37.
- Tipper, H. and Guex, J., 1994. Preliminary remarks on the Hettangian ammonite succession in Queen Charlotte Islands, British Columbia. *Geobios* M.S. 17: 477–483.
- Tipper, H., P.L., S., Carneron, B., E.S., C., Jakobs, G., and M.J., J., 1991. Biostratigraphy of the Lower Jurassic formations of the Queen Charlotte Islands, British Columbia. In: G.J., W., ed., *Evolution and Hydrocarbon Potential of the Queen*

- Charlotte Basin. British Columbia.*, number 90-10 in Geological Survey of Canada Paper, pages 203–236. Geological Survey of Canada.
- Twitchett, R. J., 2006. The palaeoclimatology, palaeoecology and palaeoenvironmental analysis of mass extinction events. *Palaeogeography Palaeoclimatology Palaeoecology* 232(2-4): 190–213.
- Valentine, J. and Moores, E., 1970. Plate-tectonic regulation of faunal diversity and sea level: a model. *Nature* 228: 657–659.
- van de Schootbrugge, B., Tremolada, F., Rosenthal, Y., Bailey, T., Feist-Burkhardt, S., Brinkhuis, H., Pross, J., Kent, D., and Falkowski, P., 2007. End-Triassic calcification crisis and blooms of organic-walled ‘disaster species’. *Palaeogeography Palaeoclimatology Palaeoecology* 244(1-4): 126–141.
- Vaughan, A. and Storey, B., 2007. A new supercontinent self-destruct mechanism: evidence from the Late Triassic-Early Jurassic. *Journal of the Geological Society* 164(2): 383–392.
- Vellutini, D. and Bustin, R., 1990. Organic maturation of Mesozoic and Tertiary strata, Queen Charlotte Islands, British Columbia. *Bulletin of Canadian Petroleum Geology* 38(4): 452–474.
- Verati, C., Bertrand, H., and Feraud, G., 2005. The farthest record of the Central Atlantic Magmatic Province into West Africa craton: Precise $^{40}\text{Ar}/^{39}\text{Ar}$ dating and geochemistry of Taoudenni basin intrusives (northern Mali). *Earth and Planetary Science Letters* 235: 391–407.
- Verati, C., Rapaille, C., Féraud, G., Marzoli, A., Bertrand, H., and Youbi, N., 2007. $^{40}\text{Ar}/^{39}\text{Ar}$ ages and duration of the Central Atlantic Magmatic Province volcanism in Morocco and Portugal and its relation to the Triassic–Jurassic boundary. *Palaeogeography Palaeoclimatology Palaeoecology* 244(1-4): 308–325.
- Wang, C., 2007. Anomalous hopane distributions at the Permian-Triassic boundary, Meishan, China – Evidence for the end-Permian marine ecosystem collapse. *Organic Geochemistry* 38: 52–66.
- Waples, D. and Machihara, T., 1990. Application of sterane and triterpane biomarkers in petroleum exploration. *Bulletin of Canadian Petroleum Geology* 38(3): 357–380.
- Ward, P., 1980. Comparative shell shape distributions in Jurassic-Cretaceous ammonites and Jurassic-Tertiary nautilids. *Paleobiology* 6(1): 32–43.

- Ward, P. and Brownlee, D., 2000. *Rare Earth: Why Complex Life is Uncommon in the Universe*. Springer.
- Ward, P., Garrison, G., Williford, K., Kring, D., Goodwin, D., Beattie, M., and McRoberts, C., 2007. The organic carbon isotopic and paleontological record across the Triassic-Jurassic boundary at the candidate GSSP section at Ferguson Hill, Muller Canyon, Nevada, USA. *Palaeogeography Palaeoclimatology Palaeoecology* 244(1-4): 281–289.
- Ward, P., Montgomery, D., and Smith, R., 2000. Altered river morphology in South Africa related to the Permian-Triassic extinction. *Science* 289(5485): 1740–1743.
- Ward, P. D., Botha, J., Buick, R., De Kock, M. O., Erwin, D. H., Garrison, G. H., Kirschvink, J., , and Smith, R., 2005. Abrupt and gradual extinction among Late Permian land vertebrates in the Karoo Basin, South Africa. *Science* 307: 709–714.
- Ward, P. D., Garrison, G. H., Haggart, J. W., Kring, D. A., and Beattie, M. J., 2004. Isotopic evidence bearing on Late Triassic extinction events, Queen Charlotte Islands, British Columbia, and implications for the duration and cause of the Triassic/Jurassic mass extinction. *Earth and Planetary Science Letters* 224: 589–600.
- Ward, P. D., Haggart, J. W., Carter, E. S., Wilbur, D., Tipper, H. W., and Evans, T., 2001. Sudden productivity collapse associated with the Triassic—Jurassic boundary mass extinction. *Science* 292: 1148–1151.
- Waterhouse, J., 1964. Permian stratigraphy and faunas of New Zealand. *New Zealand Geological Survey Bulletin* 72.
- Werne, J. P., Lyons, T. W., Hollander, D. J., Formoloc, M. J., and Damsté, J. S. S., 2003. Reduced sulfur in euxinic sediments of the Cariaco Basin: sulfur isotope constraints on organic sulfur formation. *Chemical Geology* 195(1-4): 159–179.
- White, R. V. and Saunders, A. D., 2005. Volcanism, impact and mass extinctions: incredible or credible coincidences? *Lithos* 79(3-4): 299–316.
- Whiteside, J. H., Olsen, P. E., Kent, D. V., Fowell, S. J., and Et-Touhami, M., 2007. Synchrony between the Central Atlantic magmatic province and the Triassic–Jurassic mass-extinction event? *Palaeogeography Palaeoclimatology Palaeoecology* 244(1-4): 345–367.

- Whitman, W. B., Coleman, D. C., and Wiebe, W. J., 1998. Prokaryotes: The unseen majority. *Proceedings of the National Academy of Sciences of the United States of America* 95(12): 6578–6583.
- Wignall, P. and Hallam, A., 1992. Anoxia as a cause of the Permian–Triassic mass extinction: facies evidence from northern Italy and the western United States. *Palaeogeography Palaeoclimatology Palaeoecology* 93: 21–46.
- Wignall, P., Thomas, B., Willink, R., and Watling, J., 2004. Is Bedout an impact structure? Take 1. *Science* 306: 609.
- Williamson, J., 1932. Te Kuiti Subdivision. *New Zealand Geological Survey 26th annual report* pages 5–8.
- Williford, K., Ward, P., Garrison, G., and Buick, R., 2007. An extended stable organic carbon isotope record across the Triassic–Jurassic boundary in the Queen Charlotte Islands, British Columbia, Canada. *Palaeogeography Palaeoclimatology Palaeoecology* 244(1–4): 290–296.
- Withjack, M. O., Schlische, R. W., and Olsen, P. E., 1998. Diachronous rifting, drifting, and inversion on the passive margin of central eastern North America: An analog for other passive margins. *AAPG Bulletin* 82(5): 817–835.
- Worden, R., Smalley, P., and Fallick, A., 1997. Sulfur cycle in buried evaporates. *Geology* 25: 643–646.
- Xiao, S., Zhang, Y., and Knoll, A., 1998. Three-dimensional preservation of algae and animal embryos in a Neoproterozoic phosphorite. *Nature* 391(553–558).
- Xie, S., Pancost, R. D., Ying, H., Wang, H., and Evershed, R. P., 2005. Two episodes of microbial change coupled with Permo/Triassic faunal mass extinction. *Nature* 434: 494–497.
- Yans, J., Corfield, R., Racki, G., and Preat, A., 2007. Evidence for perturbation of the carbon cycle in the Middle Frasnian punctata Zone (Late Devonian). *Geological Magazine* 144(2): 263–270.
- Young, S., Saltzman, M., and Bergstrom, S., 2005. Upper Ordovician (Mohawkian) carbon isotope ($\delta^{13}\text{C}$) stratigraphy in eastern and central North America: Regional expression of a perturbation of the global carbon cycle. *Palaeogeography Palaeoclimatology Palaeoecology* 222(1–2): 53–76.

Zhang, W. and Grant-Mackie, J., 2001. Late Triassic-Early Jurassic palynofloral assemblages from Murihiku strata of New Zealand, and comparisons with China. *Journal of the Royal Society of New Zealand* 31: 575–683.

Appendix A

SUMMARY OF $\delta^{13}\text{C}_{ORG}$ DATA FOR KENNECOTT POINT SECTION

Table A.1: Summary of $\delta^{13}\text{C}_{org}$ data for Kennecott Point section. $\delta^{13}\text{C}_{org}$ is the mean of replicate sample runs, where multiple runs were performed. Where no replicates were analyzed, no error is given. $\delta^{13}\text{C}_{ra}$ values are after double or triple HCl treatment. TOC values for QCI99 and QCI-M section were shown graphically in Ward et al. 2004, but absolute data could not be located for inclusion here.

section	ID	pos (m)	$\delta^{13}\text{C}_{org}$		$\delta^{13}\text{C}_{ra}$		TOC	
			(‰ VPDB)	±	(‰ VPDB)	wt. %	±	
QCIJ	263.3	249.8	-30.62	0.15		3.49	0.41	
QCIJ	258.1	248.7	-30.63	0.40		7.19	4.81	
QCIJ	254.7	247.8	-32.40	0.86		3.49	0.13	
QCIJ	252.2	246.9	-31.21	0.03		4.26	0.37	
QCIJ	250.5	246.3	-30.79	0.04		1.01	0.03	
QCIJ	250.0	246.1	-31.44	0.23		2.54	0.05	
QCIJ	246.0	244.5	-31.42	0.32		7.22	0.04	
QCIJ	243.0	243.1	-32.60	1.87		1.41	0.01	

Continued...

section	ID	pos (m)	$\delta^{13}\text{C}_{org}$		$\delta^{13}\text{C}_{ra}$		TOC	
			(‰ VPDB)	±	(‰ VPDB)	wt. %	±	
QCIJ	241.0	242.2	-31.05	0.10		2.63	0.15	
QCIJ	238.0	240.6	-31.44	0.02		4.54	0.07	
QCIJ	236.0	239.5	-31.02	0.03		2.18	0.23	
QCIJ	232.0	237.2	-31.29	0.03		1.91	0.11	
QCIJ	229.0	235.4	-31.07	0.00		3.10	0.00	
QCIJ	226.0	233.5	-31.19	0.12		3.74	0.04	
QCIJ	221.0	230.2	-31.60	0.20		2.51	0.02	
QCIJ	218.0	228.1	-30.91	0.15		2.75	0.04	
QCIJ	216.0	226.6	-31.13	0.65		2.02	2.03	
QCIJ	211.0	223.0	-31.21	0.08		4.03	0.07	
QCIJ	210.0	222.2	-31.50			4.43		
QCIJ	206.0	219.2	-31.39	0.14		1.48	1.72	
QCIJ	204.0	217.7	-30.70	0.07		0.58	0.01	
QCIJ	203.0	216.9	-31.27	0.27		2.40	0.77	
QCIJ	198.0	213.0	-30.50	0.04		0.53	0.07	
QCIJ	197.0	212.2	-31.54	0.08		3.64	1.74	
QCIJ	194.0	209.8	-31.24			2.09		
QCIJ	192.0	208.2	-31.43	0.04		2.73	0.17	
QCIJ	187.0	204.2	-31.30	0.07		4.15	0.03	
QCIJ	180.4	198.9	-30.90			1.94		
QCIJ	175.0	194.5	-31.05	0.21		1.37	0.14	
QCIJ	172.0	192.1	-31.45	0.21		1.96	0.34	
QCIJ	166.2	187.6	-31.06	0.08		2.11	0.05	

Continued...

section	ID	pos (m)	$\delta^{13}\text{C}_{org}$		$\delta^{13}\text{C}_{ra}$		TOC	
			(‰ VPDB)	±	(‰ VPDB)	wt. %	±	
QCIJ	163.0	185.1	-30.65	0.58	-32.36	4.80	2.27	
QCIJ	158.6	181.7	-30.51			0.72	1.06	
QCIJ	150.6	175.8	-30.22			0.52	0.10	
QCIJ	150.0	175.3	-31.30	0.07	-32.00	5.14	0.13	
QCIJ	144.0	171.1	-30.80	0.00		4.19	0.00	
QCIJ	137.6	166.8	-30.92	0.03		2.47	0.14	
QCIJ	129.7	161.7	-31.60	0.05	-32.36	4.21	0.10	
QCIJ	120.5	156.3	-30.13	0.08	-30.50	2.20	0.04	
QCIJ	116.0	153.9	-29.04	0.02	-29.41	2.40	0.14	
QCIJ	113.0	152.3	-26.13	0.04	-26.42	2.00	0.40	
QCIJ	109.0	150.3	-27.69		-28.31	1.73		
QCIJ	105.0	148.5	-28.38	0.02	-29.31	0.67	0.09	
QCIJ	99.5	146.0	-25.66	0.00	-26.99	2.51	0.00	
QCIJ	91.4	142.8	-25.11	0.00	-25.26	2.80	0.00	
QCIJ	87.4	141.4	-25.58	0.08	-25.76	1.68	0.14	
QCIJ	78.7	138.6	-27.04	0.00	-27.52	1.09	0.00	
QCIJ	76.4	138.0	-26.68		-27.02	0.44	0.19	
QCIJ	69.8	136.2	-25.07	0.00	-25.12	2.49	0.00	
QCIJ	68.0	135.7	-25.01	0.07		0.84	0.04	
QCIJ	62.0	134.3	-29.27		-29.39	2.12		
QCIJ	55.0	132.9	-28.58	0.07	-28.96	1.26	0.16	
QCIJ	52.7	132.4	-27.78	0.02	-27.80	0.55	0.03	
QCIJ	50.0	131.9	-28.89	0.10	-29.13	1.19	0.14	

Continued...

section	ID	pos (m)	$\delta^{13}\text{C}_{org}$		$\delta^{13}\text{C}_{ra}$		TOC	
			(‰ VPDB)	±	(‰ VPDB)	wt. %	±	
QCIJ	43	130.7	-28.25	0.10	-28.55	1.11	0.02	
QCIJ	39	130.0	-28.64	1.09	-28.66	3.82	2.63	
QCIJ	35	129.3	-27.78	0.04	-28.09	2.60	0.20	
QCIJ	30.6	128.5	-29.80	0.01	-30.01	3.95	0.54	
QCIJ	29.7	128.3	-29.90			2.48		
QCIJ	26.7	127.8	-30.00		-30.89	2.93		
QCIJ	19.4	126.4	-29.89	0.01		3.26	0.08	
QCIJ	13	124.9	-29.98	0.16		3.39	0.78	
QCIJ	12.5	124.8	-30.61	0.04	-31.57	3.50	0.29	
QCIJ	8.8	123.9	-29.42	0.12		0.78	0.06	
QCIJ	3.3	122.3	-30.15	0.10	-30.58	2.54	0.67	
QCI99	1	121.3	-29.48	0.09				
QCI99	3	120.6	-29.55	0.18				
QCI99	2	119.8	-30.14	0.30				
QCI99	4	116.5	-29.58	0.39				
QCI99	6B	116.3	-29.91	0.12				
QCI99	6	116.0	-29.91	0.05				
QCI99	5B	115.5	-29.90	0.09				
QCI99	5	115.5	-29.79	0.07				
QCI99	7	113.3	-31.16	0.01				
QCI99	8	112.8	-31.16	0.23				
QCI99	8B	112.3	-31.25	0.03				
QCI99	8C	111.3	-30.83	0.54				

Continued...

section	ID	pos (m)	$\delta^{13}\text{C}_{org}$ (‰ VPDB)	±	$\delta^{13}\text{C}_{ra}$ (‰ VPDB)	TOC wt. %	±
QCI99	9	110.3	-31.29	0.16			
QCI99	9B	109.8	-31.06	0.08			
QCI99	10	108.3	-29.42	0.13			
QCI99	10B	107.3	-30.12	0.12			
QCI99	10C	106.8	-30.04	0.00			
QCI99	11	106.3	-29.75	0.08			
QCI99	11B	105.8	-28.50	0.15			
QCI99	12	105.3	-28.50	0.14			
QCI99	13	104.3	-29.47	0.08			
QCI99	13B	103.3	-29.42	0.27			
QCI99	13C	102.3					
QCI99	14	101.3	-30.06	0.12			
QCI99	15	100.3	-29.59	0.21			
QCI99	15B	99.8					
QCI99	15BC	99.3					
QCI99	16	98.8	-29.21	0.21			
QCI99	16B	97.7	-29.43	0.07			
QCI99	17	95.8	-29.24	0.17			
QCI99	17B	95.0					
QCI99	18	93.8	-29.96	0.21			
QCI99	19	92.3	-29.79	0.13			
QCI99	20	90.3	-30.15	0.13			
QCI99	21	88.3					

Continued...

section	ID	pos (m)	$\delta^{13}\text{C}_{org}$		$\delta^{13}\text{C}_{ra}$		TOC	
			(‰ VPDB)	±	(‰ VPDB)	wt. %	±	
QCI99	23	86.3	-29.16	0.19				
QCI99	24	85.9	-29.81	0.32				
QCI99	25	84.8	-30.02	0.10				
QCI99	26	83.2	-28.96	0.05				
QCI99	27	81.9	-28.88	0.02				
QCI99	28	80.3	-29.62	0.16				
QCI99	29	78.3	-29.02	0.50				
QCI99	30	77.5	-29.35	0.10				
QCI99	31	73.0	-29.85	0.14				
QCI99	32	68.3	-29.92	0.14				
QCI99	33	66.0	-29.60	0.23				
QCI99	34	65.3	-29.00	0.19				
QCI99	35	62.3	-29.36	0.25				
QCI99	36	58.3	-29.78	0.17				
QCI99	37	53.5	-30.04	0.01				
QCI99	38	50.3	-29.11	0.11				
QCI99	39	46.8	-27.93	0.52				
QCI99	40	43.3	-29.69	0.08				
QCI99	41	40.8	-29.08	0.03				
QCI99	42	36.8	-29.38	0.06				
QCI99	43	32.8	-29.35	0.03				
QCI-M	31.0	31.0	-29.88	0.14				
QCI-M	30.5	30.5	-30.10	0.26				

Continued...

section	ID	pos (m)	$\delta^{13}\text{C}_{org}$		$\delta^{13}\text{C}_{ra}$		TOC	
			(‰ VPDB)	±	(‰ VPDB)	wt. %	±	
QCI-M	30.0	30.0	-28.96	0.60		2.29		
QCI-M	29.5	29.5	-29.46	0.13				
QCI-M	29.0	29.0	-29.66			3.06	1.46	
QCI-M	28.5	28.5	-29.16	0.44		1.48		
QCI-M	28.0	28.0	-29.17	0.20		2.69		
QCI-M	27.5	27.5	-28.86	0.14		1.93		
QCI99	44	27.3	-29.74	0.06				
QCI-M	27.0	27.0	-29.36	0.08		3.90	1.91	
QCI-M	26.5	26.5	-28.68	0.10		2.33	0.79	
QCI99	45	26.3	-29.38	0.18				
QCI-M	26.0	26.0	-29.68	0.10		1.14	1.12	
QCI-M	25.0	25.0	-29.62	0.35				
QCI-M	24.5	24.5	-29.76	0.21				
QCI-M	24.0	24.0	-29.04	0.23		1.59		
QCI-M	23.8	23.8	-29.21	0.18		2.01	0.50	
QCI-M	23.5	23.5	-29.31	0.17		2.90		
QCI-M	23.3	23.3	-28.98	0.50		2.94	0.12	
QCI-M	23.0	23.0	-29.67	0.12		0.71	0.73	
QCI-M	22.5	22.5	-29.05	0.17		3.13		
QCI-M	22.0	22.0	-29.89	0.19				
QCI-M	21.5	21.5	-29.68	0.37				
QCI-M	21.3	21.3	-29.09	0.26		4.73	2.19	
QCI-M	21.2	21.2	-29.77			3.28		

Continued...

section	ID	pos (m)	$\delta^{13}\text{C}_{org}$		$\delta^{13}\text{C}_{ra}$		TOC	
			(‰ VPDB)	±	(‰ VPDB)	wt. %	±	
QCI-M	21.1	21.1	-29.91	0.02		3.44	1.24	
QCI-M	21.0	21.0	-29.86	0.05		2.53	0.53	
QCI-M	20.6	20.6	-29.28	0.11		6.08	0.05	
QCI-M	20.6	20.6	-29.61	0.21		0.93		
QCI-M	20.5	20.5	-29.65	0.19		1.23	0.05	
QCI-M	20.0	20.0	-29.19	0.25		2.81	1.31	
QCI-M	20.0	20.0	-29.58	0.19		1.87	1.57	
QCI-M	19.5	19.5	-28.81	0.12		2.54	0.78	
QCI99	46	19.5	-29.16	0.00				
QCI-M	19.1	19.1	-28.52	0.15		5.93	2.71	
QCI-M	19.0	19.0	-28.08			2.00		
QCI-M	18.0	18.0	-29.25	0.37				
QCI-M	17.0	17.0	-29.67	0.40				
QCI-M	16.0	16.0	-29.22	0.04				
QCI99	47	15.6	-29.28	0.04				
QCI-M	15.0	15.0	-29.31	0.47				
QCI-M	14.0	14.0	-29.05	0.20				
QCI99	48	12.3	-29.39	0.09				
QCI-M	12.0	12.0	-29.20	0.31		5.61		
QCI-M	11.0	11.0	-29.08	0.05		1.79	1.16	
QCI-M	10.0	10.0	-28.92	0.37		1.73	0.12	
QCI-M	9.7	9.7	-29.03	0.08		2.18	0.13	
QCI99	50	9.3	-28.75	0.13				

Continued...

section	ID	pos (m)	$\delta^{13}\text{C}_{org}$ (‰ VPDB)	\pm	$\delta^{13}\text{C}_{ra}$ (‰ VPDB)	TOC wt. %	\pm
QCI-M	9.0	9.0	-29.26	0.07			
QCI-M	8.0	8.0	-28.62			7.85	
QCI-M	7.2	7.2	-29.23	0.32		2.02	0.63
QCI-M	7.0	7.0	-29.51	0.10		3.61	
QCI-M	6.9	6.9	-29.87	0.13		2.20	1.00
QCI-M	6.8	6.8	-29.65	0.33		2.05	1.15
QCI-M	6.4	6.4	-29.63	0.14		0.43	
QCI-M	6.0	6.0	-29.51	0.01		3.51	0.97
QCI-M	5.9	5.9	-29.24	0.29		0.69	0.06
QCI99	51	5.3	-29.39	0.09		5.00	
QCI-M	4.7	4.7	-29.20	0.08		2.58	0.47
QCI-M	4.3	4.3	-29.71	0.16		3.12	
QCI99	TD266	4.1	-28.92	0.02			
QCI-M	3.0	3.0	-28.71	0.56			
QCI-M	2.0	2.0	-30.59	0.64			
QCI-M	1.0	1.0	-29.94			0.27	
QCI-M	0.0	0.0	-29.70	0.05			
average			-29.65	0.18	-28.88	2.63	0.56

Appendix B

**SUMMARY OF $\delta^{34}\text{S}_{\text{ORG+PYRITE}}$ DATA FOR KENNECOTT
POINT SECTION**

Table B.1: Summary of $\delta^{34}\text{S}_{\text{org+pyrite}}$ data for Kennecott Point section. $\delta^{34}\text{S}_{bu}$ is from untreated rock powder, $\delta^{34}\text{S}_a$ is after HCl treatment, and $\delta^{34}\text{S}_{bl}$ is after HCl and bleach treatment.

section	ID	pos (m)	$\delta^{34}\text{S}_{bu}$	% S_{bu}	$\delta^{34}\text{S}_a$	% S_a	$\delta^{34}\text{S}_{bl}$	% S_{bl}	\pm	\pm	\pm	\pm
QCIJ	263.3	249.8			-34.24	0.70	1.10	0.04				
QCIJ	254.7	247.8			-33.69	0.38	0.87	0.05				
QCIJ	250.0	246.1			-29.14	0.38	0.46	0.10				
QCIJ	241.0	242.2			-25.59	0.29	0.93	0.01				
QCIJ	232.0	237.2			-30.25	0.92	0.53	0.04				
QCIJ	221.0	230.2			-21.46	0.61	0.32	0.09	-27.52	0.10		
QCIJ	218.0	228.1			-29.94		0.28					
QCIJ	216.0	226.6			-21.25	0.46	1.21	0.04				
QCIJ	204.0	217.7			-34.57	0.40	0.48	0.10	-36.14	0.37	0.26	0.02
QCIJ	203.0	216.9			-35.32		0.46					
QCIJ	198.0	213.0			-24.16	0.24	0.65	0.06				
QCIJ	197.0	212.2			-33.39		0.46					
QCIJ	192.0	208.2			-37.96	0.28	0.72	0.09				

Continued...

section	ID	pos (m)	$\delta^{34}\text{S}_{bu}$	$\%S_{bu}$	$\delta^{34}\text{S}_a$	\pm	$\%S_a$	\pm	$\delta^{34}\text{S}_{bl}$	\pm	$\%S_{bl}$	\pm
QCIJ	187.0	204.2			-35.94		0.63					
QCIJ	175.0	194.5			-25.68	0.78	0.60	0.05				
QCIJ	172.0	192.1			-30.21		0.56					
QCIJ	163.0	185.1			-39.38	0.22	1.13	0.01	-40.78	1.02	0.64	0.08
QCIJ	150.0	175.3			-31.42	0.03	0.71	0.02				
QCIJ	144.0	171.1			-33.45	1.23	1.31	0.08				
QCIJ	137.6	166.8			-20.93	0.36	0.53	0.03				
QCIJ	129.7	161.7			-19.29	0.72	0.66	0.01				
QCIJ	120.5	156.3			-3.48	0.56	0.89	0.09	-7.89		0.22	
QCIJ	116.0	153.9			3.86	0.51	0.00	0.02				
QCIJ	113.0	152.3			-4.55	0.12	0.99	0.01	-5.49		0.32	
QCIJ	109.0	150.3			-10.68	0.56	1.00	0.09				
QCIJ	105.0	148.5			7.56	1.80	0.67	0.07				
QCIJ	99.5	146.0			-7.20	0.15	1.73	0.06	-7.28	1.07	0.37	0.13
QCIJ	91.4	142.8			17.52	0.31	0.75	0.08				
QCIJ	87.4	141.4			8.32	0.08	1.35	0.05	6.74		0.17	
QCIJ	78.7	138.6			-9.38	0.41	0.73	0.08	-9.83	0.09	0.27	0.23
QCIJ	76.4	138.0			11.98	1.29	0.72	0.04				

Continued...

section	ID	pos (m)	$\delta^{34}\text{S}_{bu}$	$\%S_{bu}$	$\delta^{34}\text{S}_a$	\pm	$\%S_a$	\pm	$\delta^{34}\text{S}_{bl}$	\pm	$\%S_{bl}$	\pm
QCIJ	69.8	136.2			15.18	0.03	0.66	0.03				
QCIJ	68.0	135.7			20.55	0.09	0.93	0.01	14.27		0.18	
QCIJ	62.0	134.3			-3.34	0.59	0.59	0.04	-6.28		0.14	
QCIJ	55.0	132.9			-22.49	1.18	0.53	0.05				
QCIJ	52.7	132.4			-13.12	0.81	0.83	0.08				
QCIJ	50.0	131.9			-27.18	1.87	0.39	0.00				
QCIJ	43	130.7			-28.03	0.26	0.85	0.00				
QCIJ	39	130.0			-19.67	0.63	0.92	0.05				
QCIJ	35	129.3			-8.81	0.45	1.13	0.05				
QCIJ	30.6	128.5			-21.43	0.67	0.80	0.07				
QCIJ	26.7	127.8			-30.00	0.79	0.66	0.05				
QCIJ	19.4	126.4	-25.43	0.73	-29.09	0.65	0.45	0.01	-33.80	0.49	0.29	0.15
QCIJ	13	124.9			-28.81	0.09	0.72	0.03				
QCIJ	12.5	124.8			-21.29	0.28	1.52	0.13				
QCIJ	8.8	123.9			-21.14	0.88	0.25	0.03				
QCIJ	3.3	122.3			-32.91	0.36	0.30	0.01	-32.47	1.05	0.19	0.06
QCI99	1	121.3	-27.98	1.35	-30.21	0.47	0.89	0.01				
QCI99	2	119.8	-25.52	0.90	-29.73	0.18	0.53	0.00				

Continued...

section	ID	pos (m)	$\delta^{34}\text{S}_{bu}$	% S_{bu}	$\delta^{34}\text{S}_a$	\pm	% S_a	\pm	$\delta^{34}\text{S}_{bl}$	\pm	% S_{bl}	\pm
QCI99	6B	116.3	-30.38	1.15	-33.65	0.81	0.80	0.01				
QCI99	5B	115.5	-20.84	0.86	-24.37	0.10	0.54	0.01				
QCI99	5	115.5	-26.84	0.66	-29.88	0.07	0.52	0.00				
QCI99	8B	112.3	-20.85	1.48	-23.41	0.09	1.12	0.02				
QCI99	8C	111.3	-16.66	1.05	-18.67	0.37	0.69	0.07				
QCI99	13	104.3	2.67	1.10	6.81	0.97	0.82	0.12	13.83	0.37	0.67	0.18
QCI99	13B	103.3	-28.24	0.91	-30.61	0.98	0.54	0.02				
QCI99	13C	102.3	-33.85	0.99	-36.45	0.45	0.65	0.03	-29.17	0.07	0.31	0.15
QCI99	14	101.3	-31.37	0.93	-32.34	0.49	0.51	0.04				
QCI99	15B	99.8	-33.47	0.97	-35.15	0.31	0.60	0.02				
QCI99	15BC	99.3	-11.84	0.87	-11.94	0.61	0.46	0.07				
QCI99	17	95.8	3.34	1.23	1.59	0.10	0.76	0.07	4.62	1.05	0.56	0.01
QCI99	17B	95.0	-19.88	1.00	-30.90	1.05	0.55	0.04	-30.57		0.25	
QCI99	18	93.8	-26.82	1.22	-30.12	0.30	0.60	0.02	-31.78	1.51	0.41	0.27
QCI99	20	90.3	-23.08	1.26	-28.39	1.68	0.79	0.02				
QCI99	21	88.3	-30.78	1.12	-34.33	0.76	0.62	0.07				
QCI99	24	85.9	-26.91	1.39	-29.41	0.59	0.81	0.01				
QCI99	25	84.8	-17.41	1.98	-18.63	1.05	1.16	0.01	-27.18		0.38	

Continued...

section	ID	pos (m)	$\delta^{34}\text{S}_{bu}$	% S_{bu}	$\delta^{34}\text{S}_a$	±	% S_a	±	$\delta^{34}\text{S}_{bl}$	±	% S_{bl}	±
QCI99	26	83.2	-31.12	1.17	-35.88	0.25	0.69	0.04	-44.46	0.29	0.37	0.03
QCI99	28	80.3	-31.49	1.09	-36.19	1.74	0.54	0.02				
QCI99	30	77.5	-25.40	1.19	-31.73	1.48	0.78	0.02				
QCI99	31	73.0	-26.50	1.46	-28.79	0.18	0.81	0.10				
QCI99	32	68.3	-26.27	1.73	-30.13	1.40	1.06	0.05				
QCI99	33	66.0	-27.86	2.05	-33.25	0.86	1.29	0.07				
QCI99	34	65.3	-14.39	0.86	-25.60	0.66	0.41	0.02				
QCI99	36	58.3	-19.74	1.22	-21.39	2.87	0.86	0.21				
QCI99	37	53.5	-20.89	1.50	-24.20	0.72	0.95	0.02				
QCI99	38	50.3	-30.63	0.97	-32.43	0.13	0.81	0.12				
QCI99	39	46.8	-10.73	0.75	-13.31	0.02	0.46	0.05				
QCI99	40	43.3	-23.33	1.90	-26.43	0.63	1.09	0.01				
QCI99	41	40.8	-31.14	0.93	-37.11	0.09	0.54	0.02				
QCI99	42	36.8	-32.94	1.62	-35.59	0.65	1.02	0.02				
QCI99	43	32.8	-23.36	1.17	-28.63	1.12	0.80	0.01				
QCI99	44	27.3	-16.41	1.50	-19.72	0.80	1.05	0.15				
QCI99	45	26.3	-27.71	1.44	-29.00	0.01	0.99	0.02				
QCI99	46	19.5	-25.07	0.95	-27.64	0.14	0.58	0.04				

Continued...

VITA

Kenneth Hart Williford

ammon@u.washington.edu

Department of Earth and Space Sciences Box 351310

University of Washington

Seattle, Washington 98195-1310

206.612.6486

Education

2003 to 2007: University of Washington Seattle, Washington Ph.D., Department of Earth and Space Sciences Graduate Certificate, Astrobiology Thesis: Biogeochemistry of the Triassic-Jurassic boundary

2001 to 2003: Savannah College of Art and Design Savannah, Georgia partial M.F.A. Film/Video

1998 to 2000: University of Washington Seattle, Washington M.S. Geological Sciences Thesis: Sr/Ca thermometry in the Caribbean reef coral *Siderastrea siderea*

1994 to 1998: University of the South Sewanee, Tennessee B.S. Natural Resources, Biology concentration, *cum laude*

Employment History

Research Assistant 9/2003 to 9/2005

Paleontological and geochemical field sampling in Queen Charlotte Islands, British Columbia, Canada, Nevada, USA, and New Zealand. Continuous flow isotope ratio mass spectrometry, measuring stable carbon and nitrogen isotopes.

Information Architecture Consultant 12/2001 to 11/2007

Designed, built, and supported intranet portals for H.O. Systems, VeriSign, Inc., and currently as a consultant for Morris Multimedia, Inc.

Geologist 9/2001 to 12/2001

Hall, Blake and Associates. Nashville, Tennessee. Soil analysis for Tennessee Department of Transportation road projects.

Middle School Teacher 9/2000 to 6/2001

Good Hope School St. Croix, USVI

courses taught:

Earth Science, Life Science, Pre-calculus, Physical Education, Computers, Music

Teaching Assistant 9/1998 to 6/2000

University of Washington, Department of Geological Sciences

courses taught:

Physical Geology - Fall 1998: taught two laboratory sections, led multiple field trips

Invertebrate Paleontology - Winter 1998, Winter 1999: organized laboratory portion, concentrating on identification and functional morphology of the primary invertebrate fossil groups

Dinosaurs - Fall 1999: organized review sessions and extra credit projects for 500 students

Geobiology - Spring 1998, Spring 1999: taught and played a primary role in the development of the laboratory portion of this course for the first two times it was offered at the University of Washington.

Scientific Field Experience

Williston Lake, British Columbia, Canada (5/2007); New Zealand (2-3/2006, 3-4/2004); Hungary and Austria (9/2005); Muller Canyon, Nevada, USA (4/2005); Queen Charlotte Islands, British Columbia, Canada (6/2004); Bocas del Toro, Panama (8/1999); Montana, USA (7/1999); Cumberland Plateau, Tennessee, USA (4/1998)

Skills

Scientific Instrumentation

Electron Microprobe Microanalysis, Gas Chromatograph Mass Spectrometry, Accelerated Solvent Extractor, High Pressure Liquid Chromatography, Dual Inlet Isotope Ratio Mass Spectrometry, Continuous Flow Elemental Analyzer Isotope Ratio Mass Spectrometry, Inductively Coupled Plasma Atomic Emission Spectrophotometry, reflected and transmitted light microscopy

Laboratory Techniques

liquid chromatography, organic extraction, preparation of acids and standard solutions, cleaning/grinding/acidification of sedimentary rocks for isotopic analysis, extraction of foraminifera with Quaternary O, fossil preparation

Computer Applications

HP ChemStation, Finnigan Isodat, NIH Image-J, MATLAB, Final Cut Pro, Avid, ProTools, WaveLab, BIASPeak, Cubase, Microsoft SharePoint

Outreach and other Relevant Experience

Project AstroBio 6/2005 to present

Coordinated with middle school teacher to provide extracurricular, experiential learning in Astrobiology

Board Member, Savannah Science Seminar 9/2002 to 9/2003

Provided extracurricular, experiential training in scientific careers to selected 11th grade students in Savannah, Georgia.

Reporter 9/1998 to 6/2000

Wrote the SciTech science and technology column for the UW Daily student newspaper.

National Outdoor Leadership School 6/1996 to 8/1996

Summer Semester in the Rockies. 1 month wilderness travel, 1 month backcountry free climbing, 1 month river travel in Wyoming, Colorado, and Utah. Chosen to act as "small group expedition leader," leading four other students from the continental divide in the Wind River Mountains to a campground in the foothills over four days while fasting.

Outward Bound 4/1993

Backcountry sailing in the Florida Keys and the Everglades

Awards

NSF IGERT Astrobiology Fellowship 9/2005 to 9/2007
2 year tuition, stipend and travel allowance

UW Graduate Student Support Fund 7/1999
Competitive grant provided travel expenses for field work in Panama

Order of the Gown 9/1995 to 6/1998
Academic achievement and student government organization

Wilkins Scholarship 9/1994 to 6/1998
Half-tuition academic merit scholarship to the University of the South, Sewanee, Tennessee

David A. Saidel Memorial Scholarship 9/1990 to 6/1994
Half-tuition academic merit scholarship to the Miami Valley School, Dayton, Ohio

Peer-Reviewed Publications

Williford, K.H., Ward, P.D., Garrison, G.H., Buick, R., 2007. An extended stable organic carbon isotope record across the Triassic-Jurassic boundary in the Queen Charlotte Islands, British Columbia, Canada. *Palaeogeography, Palaeoclimatology, Palaeoecology* 244(1-4): 290-296

Ward, P.D., Garrison, G.H., **Williford, K.H.**, Kring, D., Goodwin, D., Beattie, M., McRoberts, C., 2007. The organic carbon isotopic and paleontological record across the Triassic-Jurassic boundary at the candidate GSSP section at Ferguson Hill, Muller Canyon, Nevada, USA. *Palaeogeography, Palaeoclimatology, Palaeoecology* 244(1-4): 281-289

Conference Publications

Williford, Kenneth H., Ward, Peter D., and Garrison, Geoff, 2005. Biogeochemistry of the Triassic-Jurassic boundary. *Geological Society of America Abstracts with Programs*, Vol. 37, No. 7, p. 186

Conference Presentations

Williford, K.H., 2007. Biogeochemistry of the Triassic-Jurassic Boundary. The Global Triassic, Official meeting of the IUGS Subcommittee on Triassic Stratigraphy, IGCP 467. New Mexico Museum of Natural History, Albuquerque, New Mexico, USA, May 2007.

Williford, K.H., Ward, P.D., Garrison, G.H., Buick, R., Wakeham, S.G., 2006. Records of stable organic carbon isotopes and biomarkers from the Triassic-Jurassic boundary. INTERRAD XI and Circum-Pacific Triassic Stratigraphy and Correlation. IGCP 467. Wellington, New Zealand. March 2006.

Williford, K.H., Ward, P.D., and Garrison, G.H., 2005. Biogeochemistry of the Triassic-Jurassic boundary. IGCP 458 5th Field Workshop: Triassic/Jurassic boundary events. Tata, Hungary to Puch bei Hallein, Austria. 5-10 September, 2005

Williford, Kenneth H., Ward, Peter D., and Garrison, Geoff, 2005. Biogeochemistry of the Triassic-Jurassic boundary. Geological Society of America Abstracts with Programs, Vol. 37, No. 7, p. 186

Williford, K.H. and Ward, P.D., 2005. Biogeochemistry of the Triassic-Jurassic boundary. Second Astrobiology Graduate Conference. Scripps Institution of Oceanography. La Jolla, California, USA. 17-21 August, 2005